Atmospheric boundary layer height from ground-based remote sensing: a review of capabilities and limitations

Simone Kotthaus[1], Juan Antonio Bravo-Aranda[1,2,9], Martine Collaud Coen[3], Juan Luis Guerrero-Rascado[2,9], Maria João Costa[4], Domenico Cimini[5,6], Ewan J. O'Connor[7], Maxime Hervo[3], Lucas Alados-Arboledas[2,9], María Jiménez-Portaz[2,9], Lucia Mona[5], Dominique Ruffieux[3], Anthony Illingworth[8], and Martial Haeffelin[1]

[1]Institut Pierre Simon Laplace (IPSL), CNRS, École Polytechnique, Institut Polytechnique de Paris, 91128 Palaiseau Cedex, France
[2]University of Granada, Granada, Spain
[3]Federal Office of Meteorology and Climatology, MeteoSwiss, Payerne, Switzerland
[4]Earth Remote Sensing Laboratory (EaRSLab), Institute of Earth Sciences (ICT) and Physics Department, University of Évora, Évora, Portugal
[5]National Research Council of Italy, Institute of Methodologies for Environmental Analysis (CNR-IMAA), Potenza, Italy
[6]CETEMPS, University of L'Aquila, L'Aquila, Italy
[7]Finnish Meteorological Institute, Helsinki, Finland
[8]Department of Meteorology, University of Reading, Reading, United Kingdom
[9]Andalusian Institute for Earth System Research, Granada, Spain

Correspondence: Simone Kotthaus (simone.kotthaus@ipsl.fr)

Abstract. The atmospheric boundary layer (ABL) defines the volume of air adjacent to the Earth's surface for the dilution of heat, moisture and trace substances. Quantitative knowledge on the temporal and spatial variations of the heights of the ABL and its sublayers is still scarce, despite their importance for a series of applications (including, e.g., air quality, numerical weather prediction, greenhouse gas assessment and renewable energy production). Thanks to recent advances in ground-based remote sensing measurement technology and algorithm development, continuous profiling of the entire ABL vertical extent at high temporal and vertical resolution is increasingly possible. Dense measurement networks of autonomous ground-based remote sensing instruments, such as microwave radiometers, radar wind profilers, Doppler wind lidars or automatic lidars and ceilometers are hence emerging across Europe and other parts of the world. This review summarises the capabilities and limitations of various instrument types for ABL monitoring and provides an overview on the vast number of retrieval methods developed for the detection of ABL sublayer heights from different atmospheric quantities (temperature, humidity, wind, turbulence, aerosol). It is outlined how the diurnal evolution of the ABL can be monitored effectively with a combination of methods, pointing out where instrumental or methodological synergy are considered particularly promising. The review highlights that harmonised data acquisition across carefully-designed sensor networks as well as tailored data processing are key to obtaining high-quality products, which are essential to capture the spatial and temporal complexity of the lowest part of the atmosphere in which we live and breathe.

1 Introduction

The Atmospheric Boundary Layer (ABL) is the lowest part of the atmosphere where most of the interactions between the Earth's surface and the atmosphere take place (Seibert et al., 1998). It plays a crucial role for the exchange of momentum, heat, humidity, aerosols, as well as greenhouse and other atmospheric gases (Palmén and Newton, 1969; Garratt, 1994; Stull, 1988). Improved process-understanding and quantitative knowledge of ABL dynamics are hence crucial for a wide range of applications with high societal, economic and health impacts, including the assessment of air quality (e.g., Han et al., 2009; Stirnberg et al., 2021; Sujatha et al., 2016) or greenhouse gases (e.g., Lauvaux et al., 2016), generation of renewable energy (e.g., Peña et al., 2016), numerical weather prediction (NWP; e.g., Illingworth et al., 2019), sustainable urban planning (Barlow et al., 2017, e.g.,), and all aspects of transportation such as aviation, shipping, or road safety (e.g., Vajda et al., 2011).

Sampling the ABL vertical profile has historically been mostly achieved using radiosondes. While these balloon ascends provide indispensable information, their temporal resolution is usually insufficient to capture the full diurnal evolution of the ABL dynamics and the significant horizontal drift of the balloon during the ascent means observations are affected by spatial variations in ABL dynamics which can be challenging for data analysis and interpretation. In recent decades, ground-based remote sensing has started to close this gap, providing high-resolution information, initially with a focus on the lowest kilometre of the atmosphere (see reviews by Wilczak et al., 1997; Emeis et al., 2008). Significant advances in ground-based remote sensing measurement technology and algorithm development now allow for continuous profiling of the entire ABL vertical extent (ranging from a few tens of metres to >3 km, or even higher, depending on geographic settings and synoptic conditions) at high temporal and vertical resolution (Illingworth et al., 2019; Cimini et al., 2020) and automatic detection of ABL sublayer heights from different atmospheric quantities (Collaud Coen et al., 2014; Duncan et al., 2022).

With dense ground-based remote sensing networks emerging in Europe and other parts of the world, it is vital to recap capabilities and limitations of the various instruments and analytical approaches to support careful network design, algorithm implementation, and sound interpretation of the results. In their recent review Zhang et al. (2020) stress that interpretation of ABL height data should always take into account the specifics of both the retrieval algorithm (e.g. which atmospheric variable is analysed?) and the input data (e.g. characteristics of the sensor used for data acquisition).

The objective of this review is to provide a general overview on the latest ABL profiling techniques while making relevant details easily accessible. The sections hence offer multiple entry points (Figure 1) catering to a range of user backgrounds. The different atmospheric variables routinely analysed to gain insights on the ABL are presented in Section 1.1. Sensor types commonly used for ABL profiling are introduced in Section 2, highlighting their respective capabilities and limitations as well as their deployment in organised sensor networks. The wide range of ABL height retrieval methods is then reviewed in Section 3, linking potential retrieval errors to uncertainties inherent in the observed atmospheric quantity where appropriate. Quantification of layer height uncertainties is challenging, particularly due to the absence of an 'absolute truth' concept that could serve as the reference standard. Section 4 outlines how the various layer height retrievals based on different atmospheric quantities compare throughout the ABL diurnal evolution and depending on atmospheric stability or cloud conditions. This is to support a data users' assessment of how well a certain layer height product may characterise their process of interest.
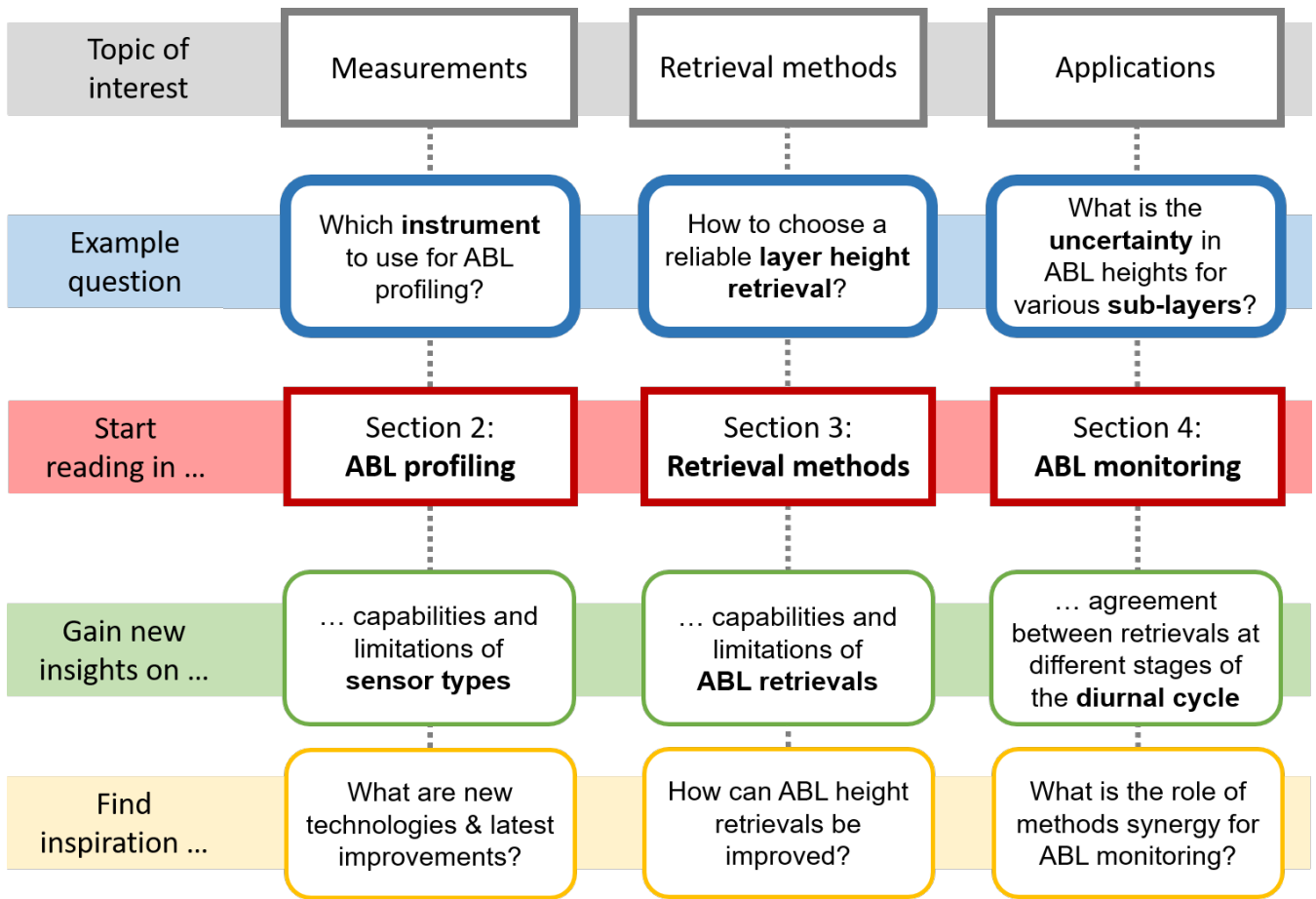
Figure 1. Entry points to this manuscript. The reader is invited to consult the respective section(s) related to their field of interest.

Ground-based profile remote sensing is a powerful tool to enhance our understanding of the atmospheric boundary layer. With careful, harmonised measurement network operations and processing procedures, increasingly detailed information can be collected that is very powerful to support many high-impact applications. The conclusions (Sect. 5) emphasise which aspects of data acquisition, algorithm development, data analysis and applications require additional attention to best advance this area of scientific research, sensor development, and environmental monitoring operations.

1.1 The atmospheric boundary layer and its sub-layers

The ABL[1] is the lowest part of the troposphere where direct interactions with the Earth's surface (land and sea) take place (Seibert et al., 2000). It responds directly to surface forcing at time scales of less than one hour (Garratt, 1994) while indirect effects (e.g. in the residual layer) can extend to daily time scales. Exchange mechanisms include the transfer of momentum, radiation, heat, moisture, particles and gases. The ABL defines the volume in which heat, moisture and trace substances are primarily dispersed following either the release at the surface or some altitude within the ABL or the entrainment from the free troposphere (FT) above. Exchanges with the FT takes place via entrainment and ejection processes (Stull, 1988). Horizontal variations in ABL dynamics stem from a combination of synoptic atmospheric conditions (e.g., atmospheric stability, wind shear, cloud dynamics) and surface forcings (driven by contrasts in e.g., surface cover, roughness, topography) (Garratt, 1994; Seibert et al., 2000).

The height of the ABL ($ABLH$) is here considered the height above ground where the surface influence becomes low, i.e. the transition to the FT. Different sub-layers occur within the ABL depending on atmospheric stability. If surface-driven processes dominate over synoptic flow conditions on a warm, cloud-free day, the ABL tends to follow a textbook evolution (Figure 2) with a *convective boundary layer* (CBL) forming in the morning in response to solar heating of the ground and resulting turbulent heat fluxes. The height of the CBL ($CBLH$) increases during the morning and reaches its peak in the early afternoon when it extends over the whole ABL ($ABLH = CBLH$). Around sunset, radiative cooling of the surface induces the growth of a new layer near the ground, the *stable boundary layer* (SBL). At this time of reduced solar input and decaying buoyancy, the CBL breaks down and decouples from the surface, whereby converting into the *residual layer* (RL), now located above the SBL top ($SBLH$). The height of the RL top now coincides with the $ABLH$ ($ABLH = RLH$). On the following day again, the RL is usually entrained into the newly forming CBL during morning growth. While neutral atmospheric stability usually dominates the RL, it is less frequent near the surface (Collaud Coen et al., 2014) but may still occur when shear production of atmospheric turbulence is strong (Nieuwstadt and Duynkerke, 1996).

In response to surface-atmosphere exchanges, cloud processes or synoptic-scale dynamics, the ABL sub-layers often deviate from this idealised concept. For example, over complex terrain, multiple layers often form in response to different mechanisms driving the ABL dynamics (De Wekker and Kossmann, 2015; Serafin et al., 2018). In cold seasons or over cold surfaces (such as snow and ice), the SBL can also dominate during daytime leading to an absence of the RL and consequently $ABLH = SBLH$ during both day and night. In the presence of a low-level jet (LLJ), the jet core (peak wind speed) defines the top of the surface-based shear layer acting as an upper bound for turbulent transport (Banta et al., 2006; Mahrt et al., 1979). The vertical profile of air temperature in the SBL often shows a characteristic surface-based temperature inversion (SBI), whose height ($SBIH$) can be very meaningful in restricting vertical dilution. While vertical mixing mainly occurs in the lower levels of the temperature inversion, a combination of potential other processes such as radiative cooling, subsidence or horizontal advection shapes the depth and the magnitude of the SBI.

---

[1]synonymous with the term *planetary boundary layer* (PBL), also commonly used

But also unstable conditions may persist at night where the surface remains relatively warm even after sunset (e.g., urban areas; (Barlow, 2014; Barlow et al., 2015; Pal et al., 2012)). In this case, no SBL is present at night. Still, a shallow mixing layer may form around sunset (decoupled from the RL) as the nocturnal surface buoyancy is now only driven by storage and anthropogenic heat fluxes and is hence weaker than the mixing during daytime. The term *mixing boundary layer* (MBL) generally refers here to the ABL sublayer closest to the ground. Its height ($MBLH$) may indicate either $CBLH$ or $SBLH$, whichever is present at the given moment. The $MBLH$ terminology is applied when no information on atmospheric stability is available to differentiate between SBL and CBL.

Exchange between the CBL and the FT (or the RL) occurs via the penetration of the CBL thermals into the air aloft and the entrainment of warm and (in the absence of clouds) dry air into the CBL. As horizontal wind speeds are usually lower in the CBL compared to the FT or RL (Figure 2), wind shear at the $CBLH$ further generates mechanical turbulence that contributes to the entrainment. The *entrainment zone* (EZ) refers to this region of interaction around the $CBLH$ and its depth (EZD) is related to the contrasts between the air in the CBL and the above FT (or RL), respectively. The EZ is associated with temporally intermittent turbulence and a vertical decline in intensity of the turbulence (Gryning and Batchvarova, 1994). The ABL transition to the FT is marked by a strongly positive temperature lapse rate, the *capping inversion* (CI). EZD is greater when the temperature difference between ABL and FT is weak (AMS, 2017). The CI often coincides with a sharp vertical decrease in specific humidity and significant vertical wind shear (Figure 2). The ABL-FT exchanges become more increasingly important over heterogeneous surfaces or complex topography (Lehning et al., 1998).

The interaction of clouds and ABL dynamics depends on the cloud type (Harvey et al., 2013). Cumulus clouds (Cu) forming at the CBL top can be understood as generating a deep EZ and thus, the $ABLH$ is located above the cloud base height, i.e. somewhere within the Cu. Radiative cooling in stratocumulus clouds (Sc) induces top-down mixing from the cloud layer toward the surface during day and night (Hogan et al., 2009; Wood, 2012) so that $ABLH$ rather coincides with the cloud top. If deep convective clouds are present, e.g., cumulonimbus (Cb) before the occurrence of precipitation, the ABL may present higher relative humidity, greater instability, stronger temperature inhomogeneity and less wind shear (Zhang and Klein, 2010) so that it becomes challenging to define the $ABLH$.

Layers of gaseous species or aerosols (e.g., dust, smoke, ash) can be present in the FT, e.g., through long-range transport, volcanic eruptions or pyrocloud convection (Fromm et al., 2010; Lareau and Clements, 2016). The lofted layer may remain decoupled from the local ABL but can also be (partially) entrained (Granados-Muñoz et al., 2012; Bravo-Aranda et al., 2015).
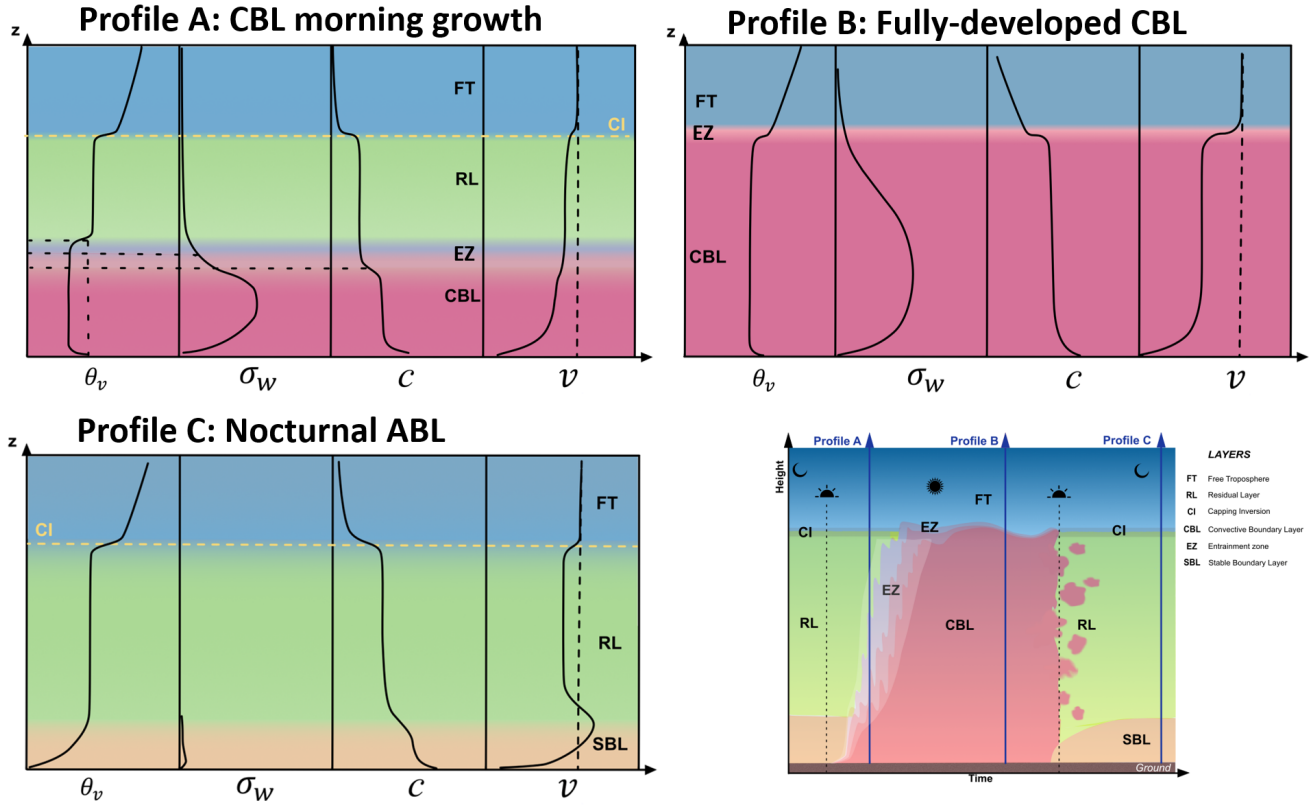
Figure 2. Idealised vertical profiles of exemplary atmospheric variables that are used to characterise thermodynamics (mean virtual potential temperature θ_v), dynamic and turbulent processes (vertical velocity variance σ_w, mean horizontal wind speed v), and resulting distributions of atmospheric tracers (mean atmospheric constituent c) during the idealised diurnal evolution of the atmospheric boundary layer (ABL), which is illustrated in the time-height sketch for an ABL over flat terrain on a cloud-free day. Dashed vertical lines in the v-panels represent the geostrophic wind reference. Selected profiles are shown at three distinct moments, with Profile A: the morning growth of the convective boundary layer (CBL; pink shading), Profile B: early afternoon with a fully-developed CBL, and Profile C: nocturnal conditions with a residual layer (RL; green shading) above the stable boundary layer (SBL; orange shading) near the surface. A capping inversion (CI) separates the ABL from the free troposphere (FT; blue shading) above. the entrainment zone (EZ) is a region of enhanced exchange between the CBL and the RL or FT, respectively. As the morning growth of the CBL (Profile A) is associated with high temporal variability of temperature, turbulence, and atmospheric constituents in the EZ, the temperature inversion, the reduction in vertical turbulent activity, and the vertical decrease in atmospheric constituents concentration may not always be located at the same height above ground, which is indicated by slightly changing colours and horizontal dashed lines. Idealised profiles and ABL sub-layer evolution adapted from De Wekker and Kossmann (2015); Beyrich (1997); Stull (1988).

2 Atmospheric boundary layer profiling

As stated by Beyrich (1997), profile observations should fulfill a series of requirements to adequately support the assessment of ABL dynamics and the detection of layer heights. Namely, they should (i) cover the full extent of the ABL (from the ground to the FT), (ii) have high vertical resolution of about 10-30 m, (iii) high temporal resolution of $\leq$1 h, and (iv) describe either the mixing itself or a result of mixing processes. We add that data with high temporal coverage (e.g., long time series) are necessary to determine variations in ABL dynamics at different temporal scales (synoptic, seasonal, annual, inter-annual) and measurements at multiple geographic locations enable horizontal variations to be assessed. Adequate atmospheric profiles (Sect. 2.1) can be captured by a series of different technologies (Sect. 2.2) that are increasingly operated in coordinated measurement networks (Sect. 2.3).

2.1 Profile variables characterising the atmospheric boundary layer structure

Different quantities provide insights into ABL dynamics and can be analysed to derive the heights of the various sublayers
(Sect. 1.1). While *thermodynamic variables* capture atmospheric stability conditions at a given moment, *dynamic variables*
describe the mixing processes induced by this stratification and *tracer variables* may portray the result of recent mixing
processes (Table 1). Figure 2 indicates how vertical profiles of selected exemplary atmospheric variables evolve throughout the
idealised evolution of the ABL on a cloud-free day.

These variables can either be *measurement variables* that are somewhat defined by the observation technology and setup
(e.g., radial velocity obtained by a Doppler wind lidar along its laser line-of-sight; Sect. 2.2.3) or *atmospheric variables* that
describe a physical process or characteristic of the air rather independently of the observation technique. Some atmospheric
variables are output directly by a certain sensor (e.g., air temperature measured with an in-situ thermometer of a radiosonde;
Sect. 2.2.1), while others are retrieved during post-processing following methods of various complexity. Certain variables are
calculated as a combination of multiple variables (e.g., potential temperature calculated from air temperature and atmospheric
pressure, colour ratio determined from backscatter coefficient observed at two different wavelengths) or by applying higher
order statistics (e.g., variance of vertical velocity) or both (e.g., turbulent kinetic energy calculated from variances of the
three wind velocity components). Other variables require more complex retrieval algorithms, with a series of assumptions
(e.g., retrieval of wind speed components from Doppler radial velocity) and even auxiliary information (e.g., retrieving air
temperature from microwave radiometer brightness temperature).

Both atmospheric variables and measurement variables can be exploited for ABL height detection (Sect. 3). Those most
commonly utilised, can be grouped by their physical relation to ABL dynamics (Table 1).

Physical meaning	Measurement variables	Atmospheric variables
thermodynamic processes		brightness temperature (T_b), air temperature (T), potential temperature (θ), virtual potential temperature (θ_v), relative humidity (RH), water vapour mixing ratio (r)
dynamic and turbulent processes	radial velocity (v_r)	refractive index structure parameter ($C_n{}^2$), horizontal wind speed (U), velocity components of the wind vector (u, v, w), variances of the velocity components ($\sigma_u{}^2$, $\sigma_v{}^2$, $\sigma_w{}^2$), turbulent kinetic energy (TKE), eddy dissipation rate (ϵ)
tracers	signal-to-noise ratio (SNR), carrier-to-noise ratio (CNR)	mass or number concentration of particles and gases (ρ or c), attenuated backscatter coefficient (β_{att}), particle backscatter coefficient (β_p), particle extinction coefficient (α_p), volume depolarisation ratio (δ), particle depolarisation ratio (δ_p), colour ratio

Table 1. Atmospheric variables analysed for detection of ABL heights are relevant for thermodynamic and dynamic processes or act as atmospheric tracers. Measurement variables provide information on the probed atmosphere but are strongly dependent on sensor characteristics or measurement setup. Depending on the measurement technology, variables are directly observed, retrieved from measurements or calculated. Note: humidity can also be interpreted as an atmospheric tracer but is here grouped with air temperature due to its importance for thermodynamic processes. Based on the variables listed here, other higher-order variables or parameters can be calculated (such as turbulent fluxes or Richardson numbers) that are valuable for characterising the ABL, especially where observations from multiple systems are available for synergy applications.

2.2 Measurement principles

A range of technologies (Table 2) is available to measure the quantities (Sect. 2.1) analysed for layer detection (Sect. 3). Atmospheric profile measurements can be achieved using tower-based or airborne in-situ sensors (Sect. 2.2.1) or with remote sensing techniques that again can be airborne, space-borne or ground-based, respectively. Ground-based remote sensing profilers generally provide data at high temporal and vertical resolution and good sensitivity in the ABL. In the following, sensors are briefly introduced, grouped according to their characteristic output variables into profilers for thermodynamic variables or atmospheric trace gases (Sect. 2.2.2), wind and turbulence profilers (Sect. 2.2.3), as well as aerosol profilers (Sect. 2.2.4). For further technical details, the reader is referred to relevant textbooks (e.g., Emeis, 2010; Foken, 2021).

While some passive radiometer technologies capture thermodynamic profiles (Sect. 2.2.2), most approaches actively emit a signal which is then recorded after its interaction with the probed atmospheric volume. Probably the most widely applied approach for ground-based atmospheric remote sensing is using laser technology. Depending on the instrument specifics, lidars can be used to measure profiles of meteorological properties such as wind and turbulence (e.g. Doppler lidars), temperature (e.g. Raman lidar), humidity (e.g. differential absorption lidars), atmospheric gases (e.g. other inelastic lidars), or atmospheric aerosol particle characteristics (e.g. aerosol backscatter lidars). For all lidar systems, the incomplete optical overlap between the field of view of the receiver telescope and the emitted laser beam (Freudenthaler et al., 2018; Simeonov et al., 1999) can significantly increase the uncertainty in the first range gates. The part of the profile affected often extends over several hundred meters, but this varies significantly with instrument design (Haeffelin et al., 2012; Caicedo et al., 2020). And also the maximum range from which the signal is recorded depends on the instrument specifics (e.g. laser power, optics). In general, there is an inverse relation between the near-range and far-range capabilities of lidar systems. While high-power systems have a monitoring range of many kilometers (some reaching the stratosphere), they require an increasingly large telescope which then increases the blind-zone near the sensor. Low-power systems tend to have better performance in the near-range but with a more limited vertical extent. While also the vertical resolution of the recorded profile used to increase with laser power and vertical range extent, manufacturers increasingly apply oversampling procedures to the data products whereby increasing the number of range gates. Thick water clouds fully attenuate the lidar signal, so that the recorded information reduces to noise at some depth inside the cloud. Noise levels further increase due to the background signal induced by solar radiation.

While ground-based techniques are focus of this review, some ABL information can be gathered by space-borne technologies, including aerosol lidars (e.g., Cloud-Aerosol Lidar and Infrared Pathfinder Satellite Observations (CALIPSO); Jordan et al., 2010; Liu et al., 2015a; Zhang et al., 2016), Doppler wind lidars (e.g., Atmospheric Laser Doppler Instrument (Aeolus-ALADIN); Straume et al., 2020; Flamant et al., 2016), or radio-occultation systems (Global Navigation Satellite System Radio Occultation (GNSS-RO); von Engeln et al., 2005; Ao et al., 2012; Xie et al., 2012; Chan and Wood, 2013; Basha and Ratnam, 2009). Satellite microwave and near-infrared passive observations also allow for the quantification of boundary layer water vapor even beneath uniform marine clouds (Millán et al., 2016). Following the success of COSMIC, the promising COSMIC-2 mission was launched in 2019 to provide radio occultation data at even higher resolution through deeper tropospheric penetration (50% within 200 m of Earth's surface). These observation enable improved detection of the $ABLH$ and superrefraction at

the top of the ABL (Ho et al., 2020; Schreiner et al., 2020). Satellite observations are less applicable for the detection of very shallow layers (e.g., Aeolus-ALADIN is not suitable for the monitoring of shallow layer conditions, Abril-Gago et al., 2021) or sublayer heights (such as $SBLH$ and RLH) given the degradation of profiles at low altitudes above the surface (Seidel et al., 2010; Xie et al., 2012) and the relatively coarse horizontal resolution (e.g., $\sim$200 km for GNSS-RO and $\sim$87 km for Aeolus). The latter introduces additional uncertainty over coastal regions as well as in presence of complex terrain (Ao et al., 2012). Still, satellite-based ABL layer heights are very valuable, as they provide globally consistent estimates (Ho et al., 2015) whose seasonal cycle constitutes an important constraint on the behaviour of global atmospheric models (Chan and Wood, 2013; Liu et al., 2015a).

In the following sections the emphasis is placed on in-situ platforms and ground-based remote sensing instruments that are to-date commonly used to observe the ABL and can be considered the most promising candidates for extensive measurement network operations (Sect. 2.3). These are radiosoundings for in-situ profiling (Sect. 2.2.1; note that significant advances are expected for network operations of uncrewed areal systems), passive radiometers for temperature profiling (Sect. 2.2.2), Doppler wind lidars for profiling of wind and turbulence (Sect. 2.2.3), and finally automatic lidars and ceilometers for aerosol profiling in the ABL (Sect. 2.2.4).

During the discussion of respective sensor capabilities, it is obviously of interest to assess the agreement of observations obtained from different sensors in terms of absolute values. However, it should be kept in mind that layer height retrieval methods (Sect. 3) tend to exploit relative changes (such as vertical gradients) which means aspects such as sensor response time of in-situ measurements, or vertical resolution are generally also critical to consider.

2.2.1 In-situ profiling

In-situ sensors are attached to various kinds of platforms to gather atmospheric profile measurements. Instruments operated at multiple levels on **tall towers** are capable of capturing conditions in the lowest few hundred metres of the atmosphere based on profiles of temperature, humidity, wind, turbulence or atmospheric composition (Bosveld et al., 2020; Ramon et al., 2020; Neisser et al., 2002), often continuously at very high temporal and vertical resolution. A similar range of the atmospheric column can be probed by instruments hosted on **tethered balloons** (Keller et al., 2011; Spirig et al., 2004), however, the latter are still mostly operated manually during dedicated field campaigns only.

Other airborne measurements of meteorological variables and atmospheric composition tend to reach higher atmospheric levels, including in-situ sensors attached to radiosonde balloons or on board of airplanes. **Radiosondes** are probably the most common data source used to derive $ABLH$ operationally. In-situ measurements of air temperature and humidity are taken by sensors that are being lifted up by a helium-inflated aerostatic balloon while atmospheric pressure, wind speed and direction are derived along the flight path via satellite tracking (e.g. GPS). The balloon ascent allows profiles to be recorded up to $\sim$35 km above ground level (a.g.l.) with high and nearly constant vertical resolution at the order of tens of meters. The sounding takes 1.5-2.0 h to reach the maximum altitude before the balloon bursts (usually in the lower stratosphere). Typical uncertainties in radiosonde measurements are $\pm$0.2-0.6 K for air temperature, 6 % for relative humidity, and 0.4-1.0 m s^{-1} for horizontal wind speed (Bian et al., 2011; Dirksen et al., 2014; Renju et al., 2017). Lightweight sondes attached to smaller balloons (Elie

Table 2. Instrument types used to gather vertical profiles of atmospheric and measurement variables (Sect. 2.1; Table 1) in the atmospheric boundary layer. These observations are increasingly organised in national and international monitoring networks (see Sect. 2.3 for further details). Acronyms: ACTRIS (Aerosols, Clouds and Trace gases Research Infrastructure), ADnet (Asian Dust and aerosol lidar observation network), AMDAR (Aircraft Meteorological Data Relay), ARM (Atmospheric Radiation Measurement), EARLINET (European Aerosol Research Lidar Network), EUMETNET E-PROFILE (European Profile of the European Meteorological Network), IAGOS (In-service Aircraft for a Global Observing System), IGRA (Integrated Global Radiosonde Archive), LALINET (Latin America Lidar Network), MPLnet (NASA Micro-Pulse Lidar Network), MWRnet (Microwave Radiometer Network), NDACC (Network for the Detection of Atmospheric Composition Change), NYS Mesonet (New York State Mesonet).

Instrument type	Measurement and atmospheric variables	Network operations
Airborne in-situ meteorological sensors	$T, \theta, \theta_v, RH, u, v, U$	AMDAR, ARM, IGRA
Airborne in-situ chemistry sensors	ρ, c	IAGOS, ARM
Microwave radiometer (MWR), infrared spectrometer (IRS)	T_b, T	EUMETNET E-PROFILE, ACTRIS/Cloudnet, MWRnet, NYS Mesonet, ARM
Differential absorption lidar (DIAL)	r, ρ, c	ACTRIS/NDACC
Radio acoustic sounding system (RASS)	T	
Raman lidar	$T, r, \rho, c, \beta_{att}, \beta_p, \alpha_p, \delta, \delta_p$, colour ratio	ACTRIS/EARLINET, ACTRIS/Cloudnet, ARM, NDACC
Doppler wind lidar (DWL)	$v_r, u, v, w, U, \sigma_w, \sigma_u, \sigma_v, TKE, \epsilon$	ACTRIS/Cloudnet, EUMETNET E-PROFILE, NYS Mesonet, ARM
Radar wind profiler (RWP)	$c_n^2, v_r, u, v, w, U, \sigma_w, \sigma_u, \sigma_v, TKE$	EUMETNET E-PROFILE, ARM
Sodar	$c_n^2, v_r, u, v, w, U, \sigma_w$, TKE	ARM
Automatic lidars and ceilometers (ALC)	β_{att}, δ	ACTRIS/EARLINET, ACTRIS/Cloudnet, EUMETENET E-PROFILE, ARM
Aerosol lidar	$\beta_{att}, \beta_p, \alpha_p, \delta, \delta_p$, colour ratio	ACTRIS/EARLINET, NDACC, LALINET, MPLnet, ADnet, ARM

210 Quentin Bessardon et al., 2019) are not always able to profile the entire troposphere, however, they usually ascend to heights above the $ABLH$. As they are technically easier to operate and may not require the same level of security clearance they are particularly useful for ABL profiling in populated environments such as cities.

The main advantages of radiosonde data are: (i) observations of temperature, humidity, air pressure, wind speed and direction are collected simultaneously using the same measurement system; (ii) coordinated radiosonde ascents are available at a high 215 number of launch sites worldwide (Sect. 2.3); (iii) data are transmitted via international communication networks with very short time delay which makes them well-suited for operational use; and (iv) time series extend for decades, making radiosondes

especially valuable for climatology studies. It should be noted however, that only 177 sites worldwide (status 2021) meet the stringent requirements for climate monitoring (CIMO-TECO, 2018; Thorne et al., 2017; WMO, 2010).

The main shortcoming of radiosondes is their low temporal frequency. Most operational sites only launch the balloons twice daily at specified synoptic times (00 UTC, 12 UTC), with some up to four times daily. While these coordinated launches at synoptic times are required to take the extremely valuable *global snapshot* of the atmosphere, they generally limit the representation of the ABL diurnal evolution at a given place. Where the launch times occur e.g. during morning growth and/or evening decay of the CBL, diurnal minima or maxima may not be captured. Even during special field campaigns, 1.5-3.0 h is typically the closest interval between launches. This low temporal resolution hampers the investigation of the diurnal cycle of ABL sublayer heights and the comparison of $ABLH$ maxima at different locations. Note that some radiosonde data products of routine ascents limit the vertical information to standard, significant pressure levels for real-time dissemination and archiving. This often means details of the ABL structure are obscured.

Other specific problems that can result in systematic errors in derived ABL characteristics include humidity sensor uncertainties in cold and dry or cloudy conditions (Seidel et al., 2010; Wang and Wang, 2014) and significant horizontal displacement of the balloon during the ascent (Schween et al., 2014). This drift means observations are affected by spatial variations in ABL dynamics which can be challenging for data analysis and interpretation. Some stations operate automatic launch systems that can introduce temperature and humidity uncertainties in the lowest altitudes (< 200 m) as sondes are located in climate–controlled chambers before being released into ambient air (Madonna et al., 2020). Site-dependent radar tracking uncertainties (Seibert et al., 2000) that have caused errors in the wind profiles at low altitudes are no longer a concern as GPS tracking is now used instead. Careful removal of discontinuities induced by changes to the operating system helps to harmonise long-term records (Madonna et al., 2022).

Uncrewed aerial systems (UAS) can gather data at very high temporal and vertical resolution often covering the full vertical extend of the ABL, however, they can not (yet) be operated fully autonomously and temporal coverage is often limited. Similarly, data from research aircraft flights (e.g., Guimarães et al., 2019) are scarce. The air volume sampled by both UAS and research aircraft flights can be restricted by air traffic control regulations. **Networks of commercial passenger airplanes** gather atmospheric profile information more continuously. The initiatives Aircraft Meteorological Data Relay[2] (AMDAR) and In-service Aircraft for a Global Observing System[3] (IAGOS) collect several atmospheric variables (such as temperature, humidity, wind speed, wind direction, or various atmospheric constituents, depending on the measurement system) during their flights whereby gathering vertical ABL profile data near the airports during start and landing. Observation accuracy is generally similar to that of radiosondes (Berkes et al., 2017), however, the vertical resolution is lower and systematic biases have been reported (e.g., AMDAR air temperature bias of up to 0.5-1.0 K; Ballish et al., 2008). Further, the airplane flight paths are associated with a much greater horizontal displacement ($\sim$10 km km^{-1}) than radiosondes ($\sim$ 1 km km^{-1}; Rahn and Mitchell, 2016). Naturally, the temporal resolution of IAGOS and AMDAR profiles depends on the frequency of reporting airplanes starting or landing in the region of interest. AMDAR data have been applied successfully to study the ABL in regions

---

[2]https://public.wmo.int/en/programmes/global-observing-system/amdar-observing-system
[3]https://www.iagos.org/

250 with multiple busy airports in close vicinity, such as Los Angeles, USA, (Rahn and Mitchell, 2016), London, UK, (Kotthaus and Grimmond, 2018a) or Paris, France, (Kotthaus et al., 2020), while Petetin et al. (2018) derive generalised ABL profiles for Northern hemisphere mid-latitudes from a climatology of IAGOS profiles.

2.2.2 Profiling of thermodynamic variables and atmospheric gases

Different ground based remote-sensing technologies are available to obtain vertical profiles of thermodynamic variables (tem-
255 perature, water vapour) and/or other atmospheric gases. These include Raman lidars, differential absorption lidars (DIAL), radio-acoustic sounding systems (RASS), and radiometers.

Raman lidar systems transmit at one or multiple wavelengths and detect the Raman-shifted scattering by molecular excitation at other wavelengths, enabling the determination of the constituent of interest (Table 2), such as the water vapour mixing ratio (Wulfmeyer et al., 2010), the particle extinction coefficient (Ansmann et al., 1992) or air temperature using the
260 rotational Raman technique (Behrendt et al., 2015). Raman lidars widely use Nd:YAG lasers at tens Hz typical repetition rates, with extremely high pulse energy of >1 J at the fundamental wavelength (1064 nm) and up to hundreds of mJ at the second (532 nm) and third (355 nm) harmonics. Depending on the laser repetition rate and pulse energy, temporal resolution ranges from seconds to minutes. Range resolution is defined by the speed of the data acquisition system (e.g., a 100 ns laser pulse length has a 15 m folded scattering length; Weitkamp, 2005), with very high resolution (7.5 m or even higher) possible. The
265 most prominent limitation in the exploitation of Raman lidars is their limited temporal coverage. These systems are generally not operated continuously because Raman channels only provide usable results when the natural background light is low, i.e. at night. In addition, consumables of high-power lidars are expensive, so that most operators limit measurements to times when no low-level liquid-water clouds are present as these extinguish the lidar signal at very low altitudes. As a consequence, Raman lidars are rarely used to monitor ABL dynamics and studies focus on atmospheric layers at greater altitudes instead.
270 A differential absorption lidar (**DIAL**) transmits laser beams at two wavelengths exploiting the differential attenuation (Lammert and Bösenberg, 2006) to derive vertical profiles of water vapour (Behrendt et al., 2007) or trace gases such as CO_2 (Gibert et al., 2008), CH_4 (Robinson et al., 2015), ozone (Banta et al., 1998; Ravetta and Ancellet, 1998), or NO_2 (Piters et al., 2012). Thanks to recent developments, compact DIAL systems are becoming increasingly available that allow for continuous water vapour profiling of the ABL, using a significantly lower pulse energy compared to the Raman lidar (Newsom et al.,
275 2020).

RASS systems either combine a radar wind profiler with a source of acoustic signals (e.g., sodar) or a sodar system with a source of electromagnetic signals (Emeis, 2010; Foken, 2021). From the Doppler shift of the respective Bragg-scattered radar signal the speed of sound is measured as a function of altitude, from which the profile of virtual temperature can be deduced. The uncertainty in temperature can be < 0.5 K, provided a number of careful corrections are applied (Görsdorf and Lehmann,
280 2000). Temporal resolution depends on the application with 10 minutes averaging being typical. The vertical resolution of the profile depends on the length of the pulse transmitted, with RASS systems usually configured to have a resolution of 30-60 m. As for many ground-based remote sensing instrument types, the capabilities to capture information in the near-range or greater altitude, respectively, depends on the specific RASS system characteristics. While sodar-based RASS or 1-GHz radar wind

profilers with RASS capability reach their maximum range at about 500 m, measurements well above 1 km can be obtained
with RASS systems using a radar wind profiler at about 500 MHz.

Two types of ground-based profiling radiometers measure the downwelling radiance naturally emitted by the atmosphere at selected band channels: microwave radiometers (**MWR**) and infrared spectrometers (**IRS**). The measured radiance is internally converted to atmospheric brightness temperature (Table 1). As T_b holds information on atmospheric thermodynamic conditions, further atmospheric variables (e.g., temperature, humidity, liquid water path and integrated water vapour content) can be derived, using retrieval methods aided by some *a priori* knowledge. The atmospheric variables obtained from MWR and IRS depend on the number and spectral range of the channels utilised by a given sensor.

In the 20-60 GHz frequency (0.5-1.5 cm wavelength) range, the atmospheric thermal radiance is mostly emitted by atmospheric gases (primarily oxygen and water vapour) and hydrometeors (mainly liquid water droplets). MWR operating at several channels in the 20-30 GHz and 50-60 GHz frequency bands observe temperature and humidity profiles, respectively. Vertical resolution of the obtained temperature profiles is higher in the lowest 2 km where most of the information content resides. For humidity profiles the information is spread along the vertical range with generally coarser resolution. Most common MWR profilers provide information on tropospheric temperature and specific humidity and the column-integrated liquid water content (Solheim et al., 1998; Westwater et al., 2004; Rose et al., 2005) at high temporal resolution ($\sim$1 min). When compared to nearby radiosonde ascents, MWR retrievals agree within 0.5-2.0 K root mean square deviation (RMSD) for temperature (decreasing from surface upwards) and 0.2-1.5 g m^{-3} for absolute humidity. The mean RMSD value within the boundary layer is $\sim$0.8 K for the temperature retrievals (Liljegren et al., 2005; Cimini et al., 2006; Löhnert et al., 2009; Löhnert and Maier, 2012). Bias values between MWR and Raman lidar are within $\pm$0.4 g kg^{-1} (or $\pm$20 %) for water vapor mixing ratio measurements with RMSD < 1 g kg^{-1} (25-55 %) and within 0–1.2 K for temperature measurements with RMSD $\sim$0.6-1.8 K (at 5 min integration time; Di Girolamo et al., 2020). Bianco et al. (2017) find lower statistical differences against radiosonde data for RASS than for MWR.

IRS exploit high spectral resolution radiances measured in the thermal infrared spectrum to retrieve temperature and water vapor profiles in cloud-free air. The Atmospheric Emitted Radiation Interferometer (AERI) is a Fourier transform IRS operating in the thermal infrared range (3000-520 cm^{-1} wavenumber, 3.3–19 μm wavelength; Knuteson et al., 2004a, b). It is specifically designed to record downwelling radiance at high spectral resolution (0.5 cm^{-1}). The observed radiance is processed to retrieve temperature and water vapour profiles up to cloud base, and in addition cloud properties and trace-gas concentrations (Feltz et al., 2003; Turner and Löhnert, 2014; Turner and Blumberg, 2018), with a temporal resolution of 30 s. When compared to nearby radiosonde ascents, IRS retrievals agree within $\sim$1 K RMSD for temperature and $\sim$0.8 g kg^{-1} for water vapor mixing ratio (e.g., Blumberg et al., 2015; Wulfmeyer et al., 2015; Weckwerth et al., 2016).

MWR and IRS techniques both measure atmospheric natural radiation that is then inverted to estimate thermodynamic variables. Thermodynamic profiles from MWR or IRS have been demonstrated to be useful to estimate $ABLH$ (Cimini et al., 2013) and atmospheric stability indices (Feltz and Mecikalski, 2002; Wagner et al., 2008; Cimini et al., 2015). However, despite their similarities they provide partially complementary information. In general, IRS data have greater information content than MWR, resulting in higher vertical resolution for temperature and humidity profiles, and sensitivity to trace gases and cloud

particle size. IRS also provides higher sensitivity to low-cloud liquid water path, though the signal saturates above $\sim$40 g m^{-2}.

320 MWR again are only slightly affected by liquid water, which gives them an advantage in capturing profiles even within or above clouds (unlike IRS, which is limited to cloud base). Further can MWR be used within light precipitation (Cimini et al., 2011; Bianco et al., 2017) because the antenna is protected by a radome with hydrophobic coating and a continuous tangential air flow. Still, the above measures are generally not be sufficient under moderate to heavy precipitation when the quality of retrieved profiles is degraded and hence usually excluded from analysis.

325 The most prominent limitation of ground-based radiometric profiling is its low-to-moderate vertical resolution. The information content of ground-based radiometry on the vertical distribution of atmospheric thermodynamics resides in the differential absorption of multi-frequency and multi-angle observations. However, contributions from different layers to the observed T_b (i.e. the weighting functions, Westwater et al., 2004) show significant overlap, leading to substantial redundancy in the observations. Although the retrievals of atmospheric profiles from passive instruments like MWR and IRS are usually provided on

330 fine vertical grids (e.g., $\sim$50, 100, and 250 m at $<$500 m, 500–2000 m, and $>$2000 m, respectively), this spacing should not be confused with the actual vertical resolution, which by definition is the minimum distance at which differences in the vertical profile are resolved. Several methods are used to quantify the vertical resolution of radiometric profiling, including, e.g., the degrees of freedom for signal (Löhnert et al., 2009), the inter-level covariance (Liljegren et al., 2005), and or averaging kernels (Blumberg et al., 2015). Using the latter, temperature profiles show a vertical resolution varying linearly with height as by a

335 factor of $\sim$2 for MWR and $\sim$1.4 for IRS, respectively. The vertical resolution for the water vapor mixing ratio is less regular, but still roughly linearly with height ($\sim$z+1 [km]).

To summarise, passive radiometers provide better coverage of temperature and humidity profiles compared to Raman lidars because they can gather data continuously. But also DIAL systems increasingly provide continuous profiles of water vapour or other gases in the ABL. Vertical resolution is greater for IRS between 0.5-2.0 km and greater for MWR above 4 km; IRS and

340 MWR provide partially complementary information despite their substantial similarities, given the higher vertical information content of IRS in the ABL and the capability of the MWR to gather information within and above clouds and during light precipitation. Synergy of MWR and/or IRS with active remote sensing technologies such as DIAL or Raman lidar can improve data quality (e.g., Turner and Löhnert, 2021; Djalalova et al., 2022), e.g. achieving a more accurate representation of the moisture gradient across the entrainment zone (Smith et al., 2021).

345 ### 2.2.3 Wind and turbulence profiling

Several technologies allow for the vertical profiles of mean wind speed, direction and turbulence to be captured (Foken, 2021), including sodars, radar wind profilers (RWP) and Doppler wind lidars (DWL). Where profiles of both turbulence and temperature fluctuations (e.g., from RASS; Sect. 2.2.2) are observed, profiles of turbulent heat fluxes can be obtained (Engelbart and Bange, 2002; Behrendt et al., 2020).

350 **Sodars** send out pulses of sound to probe the atmosphere. The sodar technique is based on fluctuations in the refractive index of the air (Sect. 2.1) and the amplitude of the return signal is related to the refractive index structure parameter ($C_n{}^2$; Singal, 1997; Bradley, 2007). Based on these, turbulent structures in the ABL can be characterised (Emeis et al., 2008; Kramar

et al., 2014; Beyrich, 1997). Compared to most other remote sensing profiling systems, sodars have a particular advantage in being capable of sensing close to the instrument, typically within 20 m. Very shallow ABL can also be measured even in

355 challenging polar locations (Kouznetsov, 2009), especially when combined with sonic anemometers (Argentini et al., 2005). This good near-range capability goes along with a rather limited range extent to about 1 km which is linked to the absorption of sound in the air causing a considerable sensitivity of the system to environmental noise. Wind and turbulence derived from sodar observations are severely affected by precipitation as the fall speed of the precipitation disturbs the signal but also water on the antenna tends to increase retrieval uncertainty. Another disadvantage is that the sound signal can often be a disturbance

360 for humans and animals which makes it difficult to operate sodars continuously in many environments.

RWP operate on Doppler technology, either in the the very-high frequency (VHF) domain (20-300 MHz) or ultra-high frequency (UHF) domain (0.4-2 GHz) with boundary layer RWP usually around 1 GHz (*L-Band*). UHF RWP are better suited for probing the ABL thanks to their higher vertical resolution and lower cost. An electromagnetic pulse is emitted towards the zenith and 2-4 off-zenith directions (15°-tilted). The angle can be achieved with different antennas or with a single phased-array

365 antenna. In the UHF band, the return signal intensity depends mainly on humidity and temperature gradients in the atmosphere. It is recorded and analyzed in real-time by the system: a succession of coherent averaging and noise filtering steps are followed by a fast Fourier transform (FFT). The frequency spectrum obtained for each range gate is characterized by four moments: noise level, signal power, spectral width and Doppler shift. By combining the Doppler shift of the three beams, mean wind speed and wind direction are calculated at each range gate (Ecklund et al., 1988). Vertical resolution is at the order of 100-400 m,

370 depending on the measurement setup. The main advantage of RWP is their capability to operate under all weather conditions at moderate cost. They even provide useful information inside cloud or fog layers and when aerosol concentrations are very low, an advantage over most lidar systems. Large errors in RWP profile data are mostly caused by larger objects, such as birds (Lehmann and Teschke, 2008). Provided suitable scan patterns, averaging strategies and quality control, the uncertainties and biases in RWP profiles are comparable to DWL observations. With less than 100 RWP operated worldwide (Sect. 2.3), their

375 limited number is a clear disadvantage when it comes to spatial coverage.

There are two types of **DWL**: one uses the molecular backscatter component and applies narrow-band spectral filters to measure the frequency shift while the other type (*heterodyne* Doppler lidar) uses the aerosol-particle backscatter component and coherent mixing with a reference beam to detect the slight Doppler shift in frequency between the emitted pulse and backscattered return. All DWL exploit the Doppler shift along the line-of-sight, or *radial*, to measure the *radial Doppler*

380 *velocity*. Given their negligible terminal fall velocities, backscattering aerosol particles and cloud droplets are ideal tracers to track the wind motion. Ground-based commercial DWL capable of probing the full depth of the ABL typically use the heterodyne principle. They generally operate at wavelengths between 1.5-2.0 μm, taking advantage of components developed for the telecommunication industry. Note that attenuated backscatter (Sect. 2.1) can also be retrieved from DWL observations, if the instrument telescope function is accounted for (Pentikäinen et al., 2020).

385 Heterodyne DWL work with continuous-wave technology or by emitting short-laser pulses. The maximum range for continuous-wave DWL systems is limited to about 250 m as the range-weighting function becomes very broad beyond this distance (Kavaya and Suni, 1991). Pulsed DWL systems emit very short pulses of radiation and the range information is obtained from the round

trip time between the transmitted pulse and the received signal. Their maximum unambiguous range depends on the pulse repetition frequency (e.g. 15 kHz pulse repitition frequency corresponds to a maximum range of ∼10 km.) and is greater than for continuous-wave systems. Pulsed DWL are available at different frequencies, with some providing high-resolution data only over a few hundred meters.

Pointing to nadir (zenith), the radial Doppler velocity observed from aerosol or cloud droplets is the vertical air motion w; for larger particles the observed radial Doppler velocity is the sum of the vertical air motion speed w and the fall velocity of the particles. For beams tilted away from zenith, the radial Doppler velocity contains components of both the horizontal wind and the vertical motion. Combining scans from multiple directions permits the horizontal wind components to be derived using trigonometry under the assumption of horizontal homogeneity of the wind field in the observed volume (Banta et al., 2013; Päschke et al., 2015; Teschke and Lehmann, 2017). Where multiple DWL are deployed to sample the same volume of air, direct retrievals of the three-dimensional wind vector and its fluctuations can be obtained (Sathe and Mann, 2013). Comparisons with sonic and cup anemometers on towers or masts show that winds can be derived from DWL with sufficient accuracy for wind energy applications (Peña et al., 2008; Pichugina et al., 2012). Under ideal conditions, the DWL precision is within the uncertainty of the anemometer measurements used as a reference (Gottschall et al., 2012).

If winds are sampled at very high temporal frequency, higher order moments, such as velocity variances (Sect. 2.1) and even skewness, kurtosis, turbulent kinetic energy (TKE) or eddy dissipation rate (ϵ) can be determined (e.g., Cohn, 1995). Being direct measures of turbulence, TKE and ϵ are best suited for fair site and instrument inter-comparisons and can be obtained from various scan strategies, including vertical stare, multi-beam, conical scanning (Banakh and Smalikho, 1997; Banakh et al., 2010; Sathe et al., 2015; Bonin et al., 2017; Smalikho and Banakh, 2017; Yang et al., 2020), or a combination of scan types (Bonin et al., 2018). TKE can also be obtained by scanning at the specific elevation angle of $35.5°$ (Eberhard et al., 1989). These methods usually include measurements of the wind profile to provide the horizontal length scales required (O'Connor et al., 2010). Instrument noise can play a role when measuring turbulence statistics if high-frequency variations are introduced into the signal (Tucker et al., 2009; Lenschow et al., 2000). Gravity waves and other larger-scale atmospheric motions can hamper the simple interpretation of velocity fluctuations as a proxy for turbulent motion. Methods are under development to diagnose and account for such situations (Banakh and Smalikho, 2016; Bonin et al., 2018). In general, it is crucial to assess the implications of noise filtering, sampling frequency, integration time, and measurement volume on turbulence observations (Bonin et al., 2017; Pichugina et al., 2008). Also physical quantities describing atmospheric turbulence derived from DWL observations have been successfully evaluated against data gathered by sonic anemometers on masts (Bonin et al., 2016; Bodini et al., 2018; Bonin et al., 2018), tethered-balloons (Frehlich et al., 2008; O'Connor et al., 2010), radiosondes (Tucker et al., 2009), or a combination of these (Wildmann et al., 2019). For a review on pulsed DWL including descriptions of the various scan strategies, the reader is referred to e.g., Liu et al. (2019b).

The intrinsic uncertainty in the measured Doppler radial velocity is directly related to the DWL carrier-to-noise ratio (Rye and Hardesty, 1993; O'Connor et al., 2010). As the latter depends on both the lidar system and the aerosol load of the atmosphere, uncertainty estimates should take into account the sampling strategy and potential instrument-specific corrections (Manninen et al., 2016; Vakkari et al., 2019). Increased uncertainties have been reported in pristine conditions such as the

Arctic (e.g., Hirsikko et al., 2014). As for all lidar systems, the incomplete optical overlap of DWL usually means data in the lowest range gates need to be treated with caution and are often discarded from analysis. For DWL that are able to gather profiles up to several kilometres range and are hence able to capture $ABLH$ peaks during deep afternoon convection this *blind zone* may hinder the assessment of very shallow ABL sublayers. Here *mini*DWL systems that focus on the very near range at high vertical resolution offer valuable sensor synergy. The issue of incomplete optical overlap in the near range can also be somewhat overcome by scanning DWL systems because a combination of low-level scanning strategies to higher elevation scan patterns means wind profiles are sampled throughout the entire ABL extent (Banta et al., 2006; Pichugina and Banta, 2010; Vakkari et al., 2015).

DWL can operate under all weather conditions at high temporal (<1 min) and vertical (<100 m) resolution, however, thick water clouds usually fully attenuate the signal so little information can be obtained above the cloud base. Precipitation can cause significant uncertainties in the wind and turbulence retrievals since rapid variation in terminal fall velocities for different sizes of large precipitation particles (drizzle, rain drops, ice particles) manifest themselves as vertical velocity fluctuations that resemble turbulence. This imparts biases if not accounted for. Methodologies using the associated variations in the signal backscattered from precipitation particles are being developed to identify such cases. Also, rainfall on the telescope window reduces measurement accuracy.

The resolution, spatial extent, and accuracy of the retrieved wind information depends on the instrument model, the scan strategy, and the state of the atmosphere. As for aerosol lidars (Sect. 2.2.4), the strength of the backscattered signal increases with aerosol load and relative noise levels can be high were little aerosol is present. A major advantage of DWL with scanning capabilities is that a series of different measurement setups can be alternated to gather optimised sampling strategies for several advanced data products simultaneously. This proves valuable not only for the detection of ABL sublayer heights but also for in-depth characterisation of ABL dynamics (Sect. 4).

2.2.4 Aerosol profiling

Ground-based lidar systems available for the profiling of aerosols differ greatly in laser power and wavelengths utilised (Foken, 2021). It can be generally differentiated between high-power lidar systems and the comparatively low-power automatic lidars and ceilometers (ALC). The latter is a collective term that refers to both ceilometers which traditionally focused on cloud base height estimation and those backscatter lidars primarily designed to continuously provide aerosol profile information (such as micro pulse lidars; MPL). Capabilities and limitations of high-power aerosol lidars have been outlined for the Raman lidar (see description in Sect 2.2.2), a research-grade lidar which is able to sample water vapour and at times temperature, in addition to aerosol properties (Table 2).

ALC are compact, simple backscatter lidars which operate at wavelengths mostly in the infrared or visible spectral region (e.g. 532 nm, 808 nm, $\sim$910 nm, 1064 nm are common wavelengths). ALC record the attenuated backscatter (Sect. 2.1) signal, which often needs to be absolutely calibrated during post-processing (Wiegner and Geiß, 2012; Hopkin et al., 2019). While most ALC are monochromatic, few models with multiple wavelengths do exist and first sensors with depolarisation capabilities

start to emerge. CBH is the standard output variable for all ALC in addition to the attenuated backscatter profiles. Retrievals of ABL sublayer heights are also increasingly incorporated by the manufacturers.

The most striking disadvantage of ALC compared to high-power lidars is their comparatively low SNR. Given the latter not only depends on atmospheric composition but is largely determined by the laser power and optics of the lidar system (Heese et al., 2010), data from high-power lidars are often able to capture more details of the atmosphere vertical structure and high-quality information can be obtained over a greater vertical extent. ALC performance is reduced in pristine environments where aerosol load is low or at elevated heights above the sensor. But also among ALC the SNR capabilities vary greatly (Caicedo et al., 2020; Kotthaus et al., 2016) due to the wide range of models available from various manufacturers. It can be generally differentiated between ALC that provide high-SNR observations and those with rather low-SNR (Kotthaus et al., 2020). While data from high-SNR ALC can usually be analyzed at the recorded temporal resolution, averaging was found to improve the SNR of low-SNR ALC (e.g., Markowicz et al., 2008; Stachlewska et al., 2012; Lee et al., 2019; Mues et al., 2017; Min et al., 2020; Caicedo et al., 2020; Tsaknakis et al., 2011). It should be noted that some instrument-related artifacts have been detected that may be associated with specific hardware or firmware versions (Kotthaus et al., 2016; Kotthaus and Grimmond, 2018a).

High-power lidars have a significant blind zone while ALC usually reach full optical overlap at lower levels, giving them an advantage in monitoring shallow ABL sublayers. Although most ALC manufacturers supply optical overlap correction functions (at times specific to the individual sensor) more complex correction models can be necessary to dynamically account for variations in the overlap function (e.g., dependent on the instrument internal temperature; Hervo et al., 2016; Geiß et al., 2017).

ALC are usually operated continuously as they work autonomously under all weather conditions with very low maintenance. Their data have a much greater temporal coverage than those collected by high-power lidars that are mostly limited to specific research infrastructures (Sect. 2.3) and usually do not operate continuously (as mentioned for the Raman lidar; Sect. 2.2.2), although the number of systems with 24 h-operation is increasing. A clear strength of ALC is their unprecedented spatial distribution (Sect. 2.3). Aerosol profile information obtained from lidar systems can be analysed to obtain heights of the ABL and its sublayers (Sect. 3.3).

2.3 Profiling Sensor Networks

Profile data of the atmospheric boundary layer (Table 1) gain value when gathered by coordinated and harmonised measurement networks as these add information on variations in the horizontal spatial domain. High-quality ABL network data not only provide unprecedented details for process studies but also show great potential for the advancement of NWP via data assimilation (Illingworth et al., 2019; Martinet et al., 2020; Tangborn et al., 2021). Mobile platforms equipped with multiple instruments can be a powerful addition during intensive observation periods (Wagner et al., 2019).

While radiosonde stations have been organised in coordinated networks for decades, collaborative measurement networks of RWP, DWL, MWR and ALC are now also emerging (Figure 3) as off-the-shelf commercial instruments can now be deployed for unattended, continuous operations, providing atmospheric profile observations in nearly all-weather conditions (Sect. 2.2). DIAL and Raman lidars are mostly organised in research networks, such as ACTRIS/EARLINET[4] (Pappalardo et al., 2014), NDAAC[5], or PollyNet (Baars et al., 2016), providing observations of the full troposphere and even lower stratosphere. However, as these sensors are less autonomous compared to MWR, RWP, DWL, or ALC, spatial coverage tends to be lower for these networks. Other ground-based remote sensing profiling technologies (e.g. sodar) are to-date operated less continuously and at fewer stations for the reasons outlined above (Sect. 2.2).

Worldwide there are ∼1300 **radiosonde** launch sites (Figure 3a, WMO, 2017), with ∼800 stations making observations at least once but mostly twice daily. A subset of upper-air stations (∼170) comprises the global climate observing system (GCOS) upper-air Network (GUAN, WMO, 2014). The GUAN Monitoring Centre is hosted at the European Centre for Medium-range Weather Forecasts (ECMWF). Analysis of GUAN data is optimised by the U.S. National Oceanic and Atmospheric Administration (NOAA) National Climatic Data Center (NCDC). NOAA/NCDC archives all GUAN data and makes them available through the Integrated Global Radiosonde Archive[6] (IGRA). A subset of GUAN has been selected to establish the GCOS reference upper-air network (GRUAN; WMO, 2013), providing radiosonde data from reference-quality stations with traceable uncertainty estimates (Bodeker et al., 2016). Higher vertical resolution radiosonde data, but spatially and temporally more limited, are provided by the Stratospheric-tropospheric Processes And their Role in Climate data center[7] (SPARC) through the U.S. High Vertical Resolution Radiosonde Data[8] (HVRRD).

For both MWR and DWL, networking at national and international level is still in its infancy (Hirsikko et al., 2014; Thobois et al., 2018), meaning MWR and DWL data could be exploited more effectively in the future. The U.S. ARM program[9] runs a network of several MWR (Cadeddu et al., 2013) and also IRS, though still at a limited number of stations. A first attempt at MWR network operation in Europe was the LUAMI (Lindenberg Upper-Air Method Intercomparison) campaign funded by the German Meteorological Service (DWD) to demonstrate the capabilities of MWR profiler systems for use in operational meteorology. A test network of eight MWR profilers supplied quality-checked data in near real-time to a network

---

[4] https://www.earlinet.org
[5] https://www.ndsc.ncep.noaa.gov/
[6] https://www.ncdc.noaa.gov/data-access/weather-balloon/integrated-global-radiosonde-archive
[7] http://www.sparc-climate.org/
[8] http://www.sparc-climate.org/data-center/data-access/us-radiosonde/
[9] www.arm.gov/capabilities/instruments/mwrp
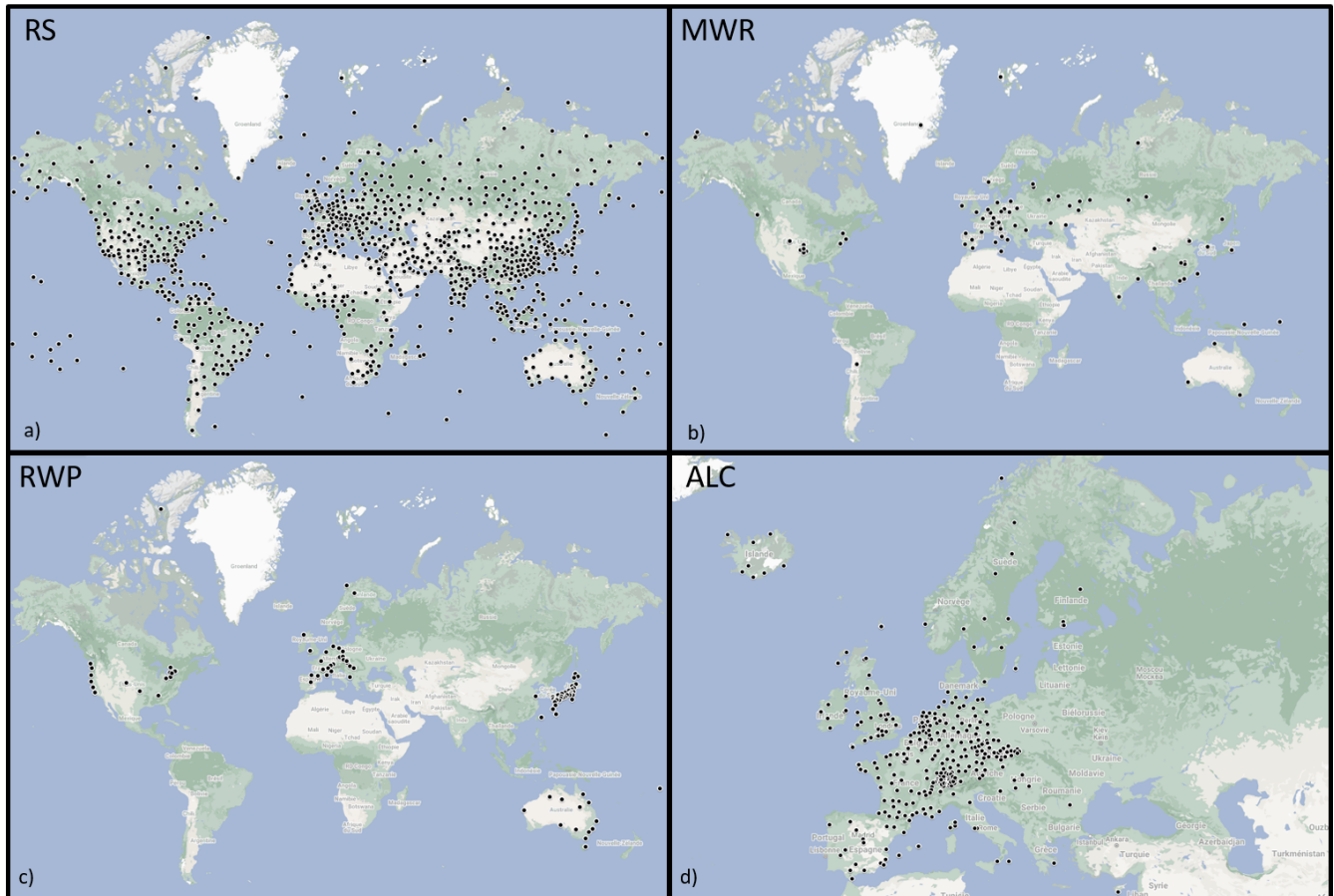
Figure 3. Selected operational networks of profiling stations (status December 2021): a) global distribution of radiosonde stations (RS) [WMO], b) global distribution of microwave radiometers (MWR) [MWRnet,MTP-5, RPG], c) global distribution of radar wind profilers (RWP) [JMA, NOAA, E-PROFILE], and d) European distribution of Automatic Lidars and Ceilometers (ALC) [E-PROFILE]. Note that this is by no means a complete representation of all profiling instruments being operated. Additional networks do exist but meta data, such as station locations are not always easily accessible. Background map © Google Maps 2022.

510 hub (Güldner, 2013, and references therein). Several European COST[10] actions taking place over the last fifteen years have worked towards the establishment of an international network of MWR: MWRnet[11] is a bottom-up network of users, currently grouping more than 100 MWR of different types worldwide (Figure 3b), with 25 profilers located in Europe. MWRnet activities demonstrate the potential of MWR observations for data assimilation (Caumont et al., 2016) and the maturity of these sensors for network deployment (Illingworth et al., 2019). As a consequence, the European national meteorological services network

515 (EUMETNET) accepted the business case for a European MWR network as part of the Composite Observing System (EUCOS) service E-PROFILE[12] which will be implemented until 2023 (Rüfenacht et al., 2021).

National **RWP** networks are operated worldwide (Figure 3c) utilising various frequencies, i.e. in Australia (14 systems), China (128, Liu et al., 2020), Japan (33, JMA[13]), Canada (7), United States (9, NOAA[14]), and in several European countries (32). EUMETNET E-PROFILE coordinates the RWP network operations in Europe, Canada and Australia. However, many

520 RWP are not yet integrated in such coordinated networks but are rather operated individually by national hydrological and meteorological services (NHMS), airports, private companies, or research institutions (Ruffieux, 2014).

In Europe, many of the **DWL** dedicated to meteorological applications are located at stations that also serve the Aerosol, Cloud and Trace gases Research Infrastructure[15] (ACTRIS). The US ARM program operates a network of several DWL alongside their MWR and cloud radars (Mather and Voyles, 2013). Operational DWL are incorporated in the urban meteorological

525 observation system (UMS-Seoul) designed and installed in Seoul, South Korea (Park et al., 2017), the 3DREAMS network in Hong Kong, China (Yim, 2020), and DWL are a major component of the New York State Mesonet[16] (Thobois et al., 2018; Brotzge et al., 2020; Shrestha et al., 2021). There is now a significant number of DWL deployed in commercial networks for wind energy applications mostly dedicated to observe winds at turbine level (around 50-150 m altitude) rather than the full extent of the ABL, and the data may be commercially sensitive.

530 **ALC** are the most widely used instruments in ground-based profile remote sensing networks. There are several network initiatives coordinating ALC measurements globally, such as the NASA-led Micro-Pulse Lidar Network[17] (MPLnet; Welton et al., 2018), the U.S. Environmental Protection Agency (EPA) network for Photochemical Assessment Monitoring Stations[18] (PAMS; Caicedo et al., 2020), or the Asian Dust and aerosol lidar observation network (ADnet; Shimizu et al., 2016), amongst others. With more than 370 units (status 2021) transmitting data in near real-time (Figure 3), EUMETNET E-PROFILE com-

535 bines the majority of ALC networks established across Europe (Figure 3d). E-PROFILE ALC data partly coincide with operations of ACTRIS, which has two topical centres (Center for Aerosol Remote Sensing (CARS); Center for Cloud Remote Sensing (CCRES)) developing services to enhance the quality of ALC measurements and also the European research infrastruc-

---

[10]Cooperation in Science and Technology; https://www.cost.eu/

[11]http://cetemps.aquila.infn.it/mwrnet/

[12]https://e-profile.eu/

[13]https://www.jma.go.jp/jma/en/Activities/windpro/windpro.html

[14]https://psl.noaa.gov/data/obs/datadisplay/

[15]https://www.actris.eu/

[16]https://www2.nysmesonet.org/

[17]https://mplnet.gsfc.nasa.gov/

[18]https://www.epa.gov/amtic/photochemical-assessment-monitoring-stations-pams#sites

ture Integrated Carbon Observing System[19] (ICOS), which is increasingly monitoring ABL sublayer heights for the support of greenhouse gas assessments.

---

[19]https://www.icos-cp.eu/

3 ABL height retrievals

Layer boundaries both within and at the top of the ABL (Sect. 1.1) constitute zones of transition between air of different characteristics. The various physical quantities (Sect. 2.1) derived from profile measurements (Sect. 2.2) each capture some aspects of the ABL development determining these layer heights (Figure 2). The most common methods developed to retrieve the ABL sublayer heights from profiles of temperature and humidity (Sect. 3.1), wind and turbulence (Sect. 3.2), or aerosol characteristics (Sect. 3.3) are outlined in this section. Certain approaches (such as the bulk-Richardson method here described in Sect. 3.1) are in fact not only associated with only one of those categories as they exploit a combination of atmospheric variables. While some measurement systems capture multiple variables simultaneously (e.g. radiosondes), the synergy between measurements from different ground-based remote sensing profilers (e.g. combining the temperature profile from MWR and wind profile from DWL) is a promising approach as it allows for multi-variable parameters to be calculated.

Limitations and uncertainties are discussed and where possible linked to the characteristics of the sensors used for data collection. Two prominent effects reducing the capability of many active ground-based remote sensing instruments are a) a potential blind zone that reduces the capability of observing shallow layers in the near range and b) insufficient signal-strength at higher altitudes. Profilers with a certain blind zone (many lidars or radar wind profilers) do not provide information in the first range gates near the sensor which means, when the signal is send upwards (e.g., DWL vertical stare or high elevation angles), the first reliable measurement level may be located above a shallow $MBLH$. In such a case, the derived heights should be interpreted as an 'upper limit' of the true $MBLH$. Similarly, observations obtained under low SNR conditions (e.g., due to low aerosol load) may not capture the full extent of the ABL (Liu and Liang, 2010) in which case derived layer heights should be considered a lower limit (Bonin et al., 2018; Krishnamurthy et al., 2021).

It is generally challenging to objectively quantify the performance of a method used for layer height detection, mainly because there is no absolute reference for ABL heights against which the derived product could be verified. Instead, evaluation is usually based on inter-comparisons, both between methods using the same quantity and between results obtained from different atmospheric variables. During interpretation it is hence key to consider that discrepancies not only reflect the errors of the respective height retrieval methods and the uncertainties in the atmospheric profiles analysed but may further be affected by a series of methodological aspects.

- A potential mismatch can be introduced by the representation of the analysed profile linked to data acquisition or processing (e.g., profile vertical and temporal resolution (averaging), horizontal displacement of the sensor).

- Atmospheric processes portrayed by the observations may differ (e.g., when comparing thermodynamic layer estimates to aerosol-based layer estimates).

- All layer *heights* in reality relate to a transition *zone* between two atmospheric layers, so that the specific signature in the atmospheric profile associated with the respective layer height is relevant (e.g., is $CBLH$ located at the bottom, middle or top of EZ?; Helmis et al., 2012).

Due to the lack of a better alternative, thermodynamic layer heights (Sect. 3.1) derived from radiosonde profiles (Sect. 2.2.1) are most commonly used as a reference (Seibert et al., 2000). However, comparing balloon ascends and ground-based remote sensing data can be prone to some systematic discrepancies connected to horizontal and temporal variations in ABL dynamics.

- The horizontal drift of the balloon during the ascent means vertical profiles derived from radiosondes may be influenced by spatial variations in ABL dynamics and do not necessarily represent the ABL structure just above the launch site. This impacts the comparison especially where ABL dynamics respond to surface heterogeneities (e.g., Tang et al., 2016; Peng et al., 2017). But also the synoptic flow plays a role given radiosonde balloons are drawn into regions of convergence so that their profiles are more likely to trace convective activities (Schween et al., 2014).

- Spatial displacement between balloon ascends and the ground-based profile can be further altered if the remote sensing instrument is operating on a moving platform (e.g., ship-based observation; Tucker et al., 2009).

- At the EZ, convective plumes can cause variations of $ABLH$ at the order of several hundred metres ($\sim$150-250 m; Hennemuth and Lammert, 2006; Granados-Muñoz et al., 2012) within a few minutes. While some ground-based profiling sensors operate at very high resolution and can hence capture such temporal variations, the radiosondes only monitor the layer boundary at one given instance.

- The agreement between layer heights detected by methods based on different atmospheric quantities varies with atmospheric conditions (such as stability, cloud dynamics, etc.; Sect. 4.4). As these usually change through the course of a day, the timing of radiosonde ascents relative to the diurnal cycle of the ABL dynamics can affect the comparison statistics.

- *Standard* sounding data (i.e. radiosonde profiles reduced to significant pressure levels; Sect. 2.2.1) yield higher $ABLH$ than data at high vertical resolution which can introduce structural uncertainties of a few hundred meters in long-term statistics.

- Systematic performance errors of the radiosonde humidity sensors (Sect. 2.2.1) lead to reduced accuracy of humidity-based detection methods (Sect. 3.1) in the presence of clouds.

All these aspects should be considered when interpreting limitations and uncertainties of the various methods. In general, uncertainties in layer height detection vary with time of day and differ between the layer targeted. Uncertainty increases when multiple ABL sublayers are present given not only the detection of a layer boundary is required but rather a second step, the so-called *layer attribution*, is required. Particularly at times with significant temporal variations in ABL dynamics (e.g., morning growth and evening decay of the CBL, formation of a low-level jet, advection of air masses, formation of clouds or fog), multiple layer boundaries need to be interpreted with care.

Beyrich and Leps (2012) developed a scheme that utilises the agreement between different methods (in their case thermodynamic and wind-based detection applied to radiosonde profiles) to quantify the uncertainty of the layer heights at a given

moment and assign quality flags accordingly. This is a promising approach that could be further extended where data from multiple systems are available simultaneously that allow for a range of detection methods based on different atmospheric variables to be applied in synergy.

3.1 Methods based on temperature and humidity

Detection methods for ABL heights based on temperature and/or humidity profiles rely on thermodynamic effects. They allow for the identification of daytime and nighttime layer heights, namely $CBLH$, $SBIH$, $SBLH$, and RLH (Sect. 1.1; Seibert et al., 2000; Seidel et al., 2010, 2012, and references therein). While some methods are directly applied to the profiles of air temperature, others utilise the potential temperature that considers atmospheric stability or the virtual potential temperature which accounts for atmospheric humidity effects in addition (Figure 2). Computation of θ (θ_v) requires atmospheric pressure (and humidity) which are at times obtained from external data sources (e.g., other sensors, reanalysis). Some methods directly explore profiles of relative humidity or specific humidity (Beyrich and Leps, 2012). Alternatively to air or potential temperature, the brightness temperature (Sect. 2.1) observed by radiometer profilers (Sect. 2.2.2), can be used as an input for layer height retrievals, as this physical quantity holds information on both temperature and humidity (similarly to the virtual potential temperature).

Temperature and humidity methods can be applied to profile data from in-situ measurements (Sect. 2.2.1), radiometers, DIAL or Raman lidars (Sect. 2.2.2) but are also very commonly implemented in numerical modelling when ABL heights are provided as a diagnostic variable determined from the model output (e.g., Cohen et al., 2015).

3.1.1 Methods

The two most commonly applied temperature-based approaches for the detection of $CBLH$ are the parcel method (Holzworth, 1964) and the bulk-Richardson method (Hanna, 1969; Vogelezang and Holtslag, 1996; Zilitinkevich and Baklanov, 2002). The parcel method defines $CBLH$ as the height to which an air parcel with ambient surface air temperature can rise adiabatically from the ground by convection and is obtained by following the dry adiabat from the surface up to its intersection with the temperature profile. While the parcel method is only applicable under unstable atmospheric conditions, the bulk-Richardson method takes into account the implications of wind shear contribution to turbulence generation and is hence applicable in all stability regimes. The bulk-Richardson number Ri_b represents the ratio of turbulence induced by thermal buoyancy and wind shear, respectively, and profiles of both temperature and horizontal wind are required to calculate Ri_b. It is essentially a synergy approach that combines thermodynamic and dynamic effects and could as well be grouped into dynamic retrieval methods (Sect. 3.2). Both $CBLH$ and $SBLH$ can be determined as the altitude where Ri_b exceeds a critical threshold. Typical values of this thresholds are around 0.10-0.40 (Sørensen et al., 1996) or 0.25-0.50 (Seibert et al., 2000) with the value 0.25 used to estimate layer heights provided in the ERA-Interim re-analysis data (von Engeln and Teixeira, 2013). The exact threshold value has a relatively modest impact on the layer detection accuracy if remaining < 0.5 (Seidel et al., 2012; Guo et al., 2016; Beyrich and Leps, 2012; Cimini et al., 2013). As the bulk-Richardson method and the parcel method are identical if the threshold value is set to 0, layer estimates from the former are greater by definition. This increment was found to be about 20 m on average for the $CBLH$ (Collaud Coen et al., 2014). As moisture lightens the air and allows it to rise convectively to greater altitudes, using θ_v instead of θ (Sect. 2.1) in both methods results in slightly greater layer heights (by 3–8%; Collaud Coen et al., 2014).

Both the parcel and bulk-Richardson method highly depend on the accuracy of the ambient air temperature at the surface.
640 A temperature excess corresponding to the strength of convective thermals can be added to θ_v at the surface under unstable conditions (Holtslag and Nieuwstadt, 1986; Seibert et al., 2000). This excess temperature is usually applied when the surface air temperature is measured at a height exceeding the standard 2 m, as in e.g., radiosoundings or NWP model data (Stohl et al., 2005).

In addition to the commonly used parcel and bulk-Richardson methods, several other thermodynamic methods are available
645 to detect heights of ABL sublayers, including:

- $SBIH$ and $SBLH$ under stable conditions

    - As a clear indicator of a stable boundary layer, $SBIH$ is diagnosed from air temperature profiles (Bradley et al., 1993; Seidel et al., 2010).

    - At the transition between the SBL and the neutral residual layer, $SBLH$ is marked by a vertical gradient of θ equal
650   to zero, that corresponds to the theoretical lapse rate (Collaud Coen et al., 2014) or equal to a critical lapse rate determined by the maximum variance of the gradient (Min et al., 2020).

    - Liu and Liang (2010) refine $SBLH$ detection by choosing the first height above ground that either shows a minimum in the potential temperature gradient or local maximum in horizontal wind speed if a LLJ is present. The method uses surface classification (land, ocean, ice) to determine critical thresholds.

655 It should be noted that the accuracy of $SBLH$ (and to some extend $SBIH$) detection highly depends on the vertical resolution of the analysed temperature profile. In contrast to the parcel method or the Ri_b method, no vertical interpolation or smoothing of the profile data can be performed.

- $CBLH$ under unstable conditions

    - The *Heffter method* determines $CBLH$ as the minimum height where the vertical gradient of θ exceeds $0.005 \, \mathrm{K \, m^{-1}}$
660   while θ changes by more than 2 K across the inversion layer (Heffter, 1980).

    - The minimum height where θ reaches a certain increment compared to its ABL minimum can mark the $CBLH$ (Nielsen-Gammon et al., 2008).

    - The maximum negative vertical gradient of refractivity (Sect. 2.1) or humidity was found to mark the $CBLH$ (Seidel et al., 2010).

665 - Schmid and Niyogi (2012) improve the detection of $CBLH$ by allocating heights where a change in the vertical θ_v gradient coincides with a dew point temperature inversion.

- $MBLH$ independent of atmospheric stability

    - To derive the $MBLH$ from temperature profiles, both the base of an elevated temperature inversion (Seidel et al., 2010) and the height of the maximum positive θ gradient (Stull, 1988; Seidel et al., 2010) have been applied. As

670   vertical mixing can already be reduced for a certain region below a positive vertical gradient in air temperature, the latter criterion can be a more accurate indicator for $MBLH$. However, the profile data of atmospheric pressure required to calculate θ may not always be available.

- Cimini et al. (2013) apply a multivariate statistical regression method trained with real observations to derive $MBLH$ directly from T_b. This method exploits all the information in the MWR observations and is independent
675   of uncorrelated retrieval errors in the temperature and humidity profiles (Sect. 2.2.2) as both systematic and random errors are inherently accounted for.

- To ensure continuous layer detection, different temperature-based methods can be combined depending on atmospheric stability as the most applicable method may vary during the course of the day and between land cover types. Maybe the most common method synergy is the combination of the parcel method ($CBLH$) and the $SBIH$
680   at night.

- Some disagreement between temperature- and humidity-based methods stems from the presence of clouds, which create a complex vertical ABL structure (Sect. 4.6). While humidity-based methods tend to respond to the layer boundary at the cloud top (large negative humidity gradient), the maximum gradient of θ usually occurs in the middle of the EZ above the cloud. To overcome this issue, $ABLH$ can be assigned to the level where all of the
685   above variables exhibit pronounced variations simultaneously, rather than looking for the strongest change in one specific profile variable only.

3.1.2   Capabilities and limitations

Long-term, multi-site comparisons reveal some systematic differences between the various temperature- and humidity-based methods (e.g., Seidel et al., 2010; Beyrich and Leps, 2012). The Heffter method often overestimates $MBLH$ and the definition
690 of thresholds was found challenging (see discussion in Caicedo et al., 2020, and references therein). Sinclair et al. (2022) find agreement and sign of systematic biases depend on atmospheric stability. The T_b regression method (Cimini et al., 2013) provides height estimates that are mostly consistent with the bulk-Richardson approach. Methods based on finding extreme vertical gradients are in better agreement with each other than those based on locating elevated temperature inversions (Seidel et al., 2010).

695   It is generally concluded that uncertainties in layer detection are closely linked to uncertainties in the atmospheric profiles analysed (e.g., errors in surface wind speed, vertical interpolation and vertical resolution; Seidel et al., 2012). Given such errors are much more pronounced (10-80 %) for low layer heights (<1-2 km), relative uncertainties of the layer detection can be large (>50 %) for shallow layers but usually remain below 20 % for layer heights >1 km (Seidel et al., 2012; Aryee et al., 2020; Guo et al., 2016). Uncertainties are usually greatest during the evening decay (Sect. 4.4) of the CBL as this is a time of significant
700 non-stationarity. Methods agree better when applied to radiosonde profiles at midday compared to midnight conditions (Beyrich and Leps, 2012), which further highlights that the $CBLH$ layer boundary is often well-defined while detection of $SBLH$ is more ambiguous.

Both the parcel method and the bulk-Richardson method are sensitive to surface-level data (Sect. 3.1.1). For example, a change in surface temperature by ± 0.5 K leads to uncertainties at the order of ± 50-150 m for the maximum $CBLH$ in the early afternoon at a mid-latitude continental site (Collaud Coen et al., 2014). Careful quality control of the measurements is hence required to ensure physically reasonable coupling of the surface air temperature value to the first values of the temperature profile (Beyrich and Leps, 2012). Horizontal and/or vertical separation between the site of the surface measurements and the radiosonde launch site can cause artificially large vertical gradients in the combined temperature profile which may result in significant average differences in the derived $ABLH$ of up to several hundred metres (Seidel et al., 2010). In such a case, it is preferable to initialise the layer detection with the first reported upper air level instead of surface observations.

From an analysis using MWR data, Collaud Coen et al. (2014) found the parcel method to be more robust and hence better suited for automatic real-time detection of the $CBLH$ compared to the bulk-Richardson method because the latter requires more input data. In addition to the temperature (and pressure) data, wind profile observations are needed which introduces additional measurement uncertainties and missing values from a second system. Such issues are slightly reduced when the methods are applied to e.g. radiosonde data, as here both wind and temperature are gathered by the same measurement system. Due to the simplicity of the parcel method it is more likely to capture shallow layer heights. Seidel et al. (2010) conclude that diurnal and seasonal variations based on this method generally tend to have a greater amplitude and can be considered more consistent than those derived from other approaches. This is in agreement with the analysis by Collaud Coen et al. (2014).

The presence of clouds increases uncertainty in $CBLH$ retrievals for all methods (Sect. 4.6), so that temperature-based methods applied to radiosondes and MWR profile data show better agreement during clear-sky days (Cimini et al., 2013). When the parcel method is applied to temperature profile data obtained from radiosondes and MWR, the latter tend to significantly under-estimate the $MBLH$ (Cimini et al., 2013). Up to now, no quantitative, comparison analysis has been performed regarding $MBLH$ estimates from different MWR types, although there have been field campaigns where multiple commercial MWR were operated side-by-side, such as the Joint CALibration experiment (JCAL; Pospichal et al., 2016) or the recent Field Experiment on submesoscale spatio-temporal variability in Lindenberg[20] (FESSTVaL).

The method using T_b regression analysis (Cimini et al., 2013) relies on "independent training data". Given there is no absolute reference when it comes to ABL heights, the choice of training data and potential systematic differences in the physical representation of ABL dynamics by the observed quantity analysed and the respective detection approach can affect the performance of this method. Still, even when trained with aerosol-derived layer estimates (Sect. 3.3), the T_b regression method shows better agreement with layer estimates from the bulk-Richardson method applied to radiosonde profiles compared to the parcel method and θ_v-gradient method applied directly to temperature and humidity data from the MWR.

---

[20]https://fesstval.de/

3.2 Methods based on wind or turbulence

Methods exploiting wind profile observations to detect ABL heights can generally be grouped into those using components of the mean wind and those based on turbulence indicators. The objective of these methods is to identify the height of the turbulent layer connected to the surface. The mixing is either caused by buoyancy-driven turbulence or shear-driven turbulence, or a combination of the two. Intermittent turbulence in the residual layer can affect the performance of layer detection algorithms (Pichugina and Banta, 2010) but wind and turbulence methods are usually not applied to detect RLH.

3.2.1 Methods

Using mean wind profiles (Figure 2), the most commonly applied layer detection approach is the bulk-Richardson method (see Sect. 3.1). Looking at the relation between thermally-induced buoyancy and shear-induced turbulence, this synergy method is applicable under all stability conditions (i.e. for detection of both $SBLH$ and $CBLH$). Alternatively, $SBLH$ can be identified as the height of a local maximum in horizontal wind speed or a local minimum in vertical wind speed or wind shear, respectively (Balsley et al., 2006; Banta et al., 2006; Pichugina and Banta, 2010; Lemone et al., 2014). Johansson and Bergström (2005) find significant changes in the mean ascent rate of radiosonde balloons indicate the transition from turbulent to non-turbulent regimes, whereby exploiting a mean quantity to diagnose turbulence indicators indirectly (Lemone et al., 2014).

Due to advances in high-resolution ground-based profiling, direct measures of atmospheric turbulence can be determined quantitatively with increasing accuracy (Sect. 2.2.3). Turbulence can be diagnosed from the refractive index structure parameter (Sect. 2.1) observed by sodar and RWP (Sect. 2.2.3). The peak in the vertical profile of the refractive index structure parameter caused by small-scale buoyancy fluctuations across the entrainment zone has been found to coincide with the $MBLH$ (White, 1993; Angevine et al., 1994; Wilczak et al., 1997). Given these fluctuations are associated with relatively high SNR in sodar and RWP observations, some methods assign $CBLH$ to a local peak in RWP SNR (Liu et al., 2019a; Collaud Coen et al., 2014). RLH can also be detected by analyzing profiles of C_n^2, but only for specific (mostly cloud-free) weather conditions. $ABLH$ is diagnosed from space-borne GNSS-RO observations as the strongest negative gradient in refractivity (Ao et al., 2012; Chan and Wood, 2013), that is associated with the strong moisture and temperature gradients usually present at the top of the ABL (Xie et al., 2012).

Estimates of atmospheric turbulence can also be obtained from temporal and/or spatial fluctuations in high-resolution wind profiling data. The most commonly exploited turbulence variables derived from high-frequency wind components are the variance of vertical velocity, variance in horizontal velocity, turbulent kinetic energy and the eddy dissipation rate (Sect. 2.1). To ensure layer detection relies on the measurement of turbulence intensity, it is important to remove non-turbulent fluctuations from the wind field components (Bonin et al., 2018). Applying a high-pass filter was found to be a simple but effective means to sufficiently reduce the influence of sub-mesoscale motions, drainage flows, and gravity waves (Bonin et al., 2017, 2018), with frequencies on the order of minutes to tens of minutes (Finnigan et al., 1984). Berg et al. (2017) chose to detect layer heights based on the normalised vertical velocity variance to reduce the impact of coherent vertical motions above the ABL.

During convective atmospheric conditions, the vertical velocity variance from vertically pointing profile observations is the most direct measure of the instantaneous mixing within the CBL. The $CBLH$ is commonly assigned to the height above ground where the vertical velocity variance (Figure 2) falls below a set threshold, with both absolute (0.04-0.16 $\mathrm{m^2\,s^{-2}}$; Tucker et al., 2009; de Arruda Moreira et al., 2018; Barlow et al., 2011; Huang et al., 2017; Vakkari et al., 2015; Theeuwes et al., 2019) and relative values (e.g., 10 % of profile maximum; Barlow et al., 2011) implemented successfully. Given the gradual decay of turbulence in the afternoon and evening CBL, Schween et al. (2014) find $CBLH$ detection to be particularly sensitive to the threshold value during this period. The choice of threshold value can depend on the ABL structure (Tucker et al., 2009; Huang et al., 2017) and the scanning-strategy dependent noise levels (Bonin et al., 2018). When shear-driven turbulence dominates, horizontal velocity variance becomes a better indicator for the layer boundaries. The vertical profile of horizontal velocity variance depends on atmospheric stability, with a near-surface peak under slightly stable conditions, a rather constant vertical distribution under medium stable conditions, and a maximum aloft near the core of the LLJ under strongly stable conditions (Banta et al., 2006). Tucker et al. (2009) use the same threshold values as for the vertical velocity variance to determine shallow layer heights from horizontal velocity variance.

Turbulent kinetic energy or eddy dissipation rate are other quantitative measures of turbulence useful for layer detection. Lemone et al. (2014) find a relative value of 5% of the profile maximum TKE most suitable for the detection of $SBLH$ while LeMone et al. (2013) apply fixed values (0.101 and 0.200 $\mathrm{m^2\,s^{-2}}$) to determine $CBLH$ from model data. Vakkari et al. (2015) assign $CBLH$ to the height where the eddy dissipation rate falls below 10^{-4} $\mathrm{m^2\,s^{-3}}$ while Frehlich et al. (2006) examine the strongest negative gradient of this quantity. For specific scan patterns, the variance of radial velocity (i.e. the native variable obtained form Doppler wind lidar measurements) is directly related to TKE (Sect. 2.2.3) and is hence also exploited for layer detection. Pichugina and Banta (2010) determine the $SBLH$ as the height of the first significant local minimum in the vertical profile of the radial velocity variance.

Under well-mixed, convective conditions, i.e. when $CBLH$ coincides with $ABLH$, turbulence-based detection methods can be supported by applying SNR requirements (Moreira et al., 2015; Pearson et al., 2010; Singh et al., 2016). Lothon et al. (2006) evaluate the total velocity variance from DWL observations for layer detection, which inherently includes the SNR information as the recorded signal responds to both atmospheric variations and instrument-related noise (Tucker et al., 2009).

To cover the full range of $MBLH$ at a given measurement location, wind or turbulence measurements from multiple data sources can be combined (e.g., sodar and RWP; Beyrich and Görsdorf, 1995; Beyrich, 1997; Angevine et al., 2003). The great advantage of scanning DWL systems is that a series of wind and turbulence variables can be obtained within a rather short time interval by a single sensor (Sect. 2.2.3). For example, vertical stare measurements can be alternated with range-height indicator (RHI) scans (Tucker et al., 2009) to capture convection or plan position indicator (PPI) scans at low elevation angles (Vakkari et al., 2015) to capture shallow layers. To facilitate the composition of layer information from various atmospheric variables (mean wind fields, different turbulence indicators, SNR), fuzzy logic algorithms (Bianco and Wilczak, 2002; Bianco et al., 2008; Allabakash et al., 2017) or machine learning (Krishnamurthy et al., 2021) are increasingly implemented. Recent advanced approaches (Bonin et al., 2018; Krishnamurthy et al., 2021) combine a diverse combination of atmospheric variables which enables reliable layer detection under nearly all atmospheric conditions. To enhance agreement with aerosol-derived

layer heights (Sect. 3.3), Bonin et al. (2018) give less weight to the vertical velocity variance during layer height retrieval whereby moving the focus towards those indicators that portray the resulting 'mixed conditions' instead of the mixing process itself. Where the ABL responds to significant surface heterogeneities (Banks et al., 2015; Haid et al., 2020; Vakkari et al., 2015), site-specific design of DWL scanning strategies is recommended to best capture the variability in $MBLH$.

3.2.2 Capabilities and limitations

The altitude range of the atmospheric profile captured by the measurements and the accuracy of wind and turbulence data from ground-based remote sensing systems depends on instrument capabilities and measurement setup (Sect. 2.2.3). The ability to detect shallow layers generally depends on how large the blind zone of the sensor is, while observing the full depth of deeper convective conditions is dependent on SNR. Turbulence-based $MBLH$ estimation is particularly applicable in daytime convective conditions (Bianco et al., 2008; Collaud Coen et al., 2014). Decaying turbulence in the residual layer can be a source of added uncertainty (Lemone et al., 2014).

Rainfall can be a significant source of uncertainty for automatic layer detection from profiles of wind and turbulence. It is possible to diagnose from the vertical velocity profile based on the terminal fall speed of rain drops (e.g., using column averaged vertical velocity $< -1 \mathrm{~m~s}^{-1}$; Bonin et al., 2018), but such filters will not detect precipitation conditions with lower fall speeds (such as drizzle or snow) and can miss precipitation that evaporates before reaching the surface (virga).

3.3 Methods based on attenuated backscatter

815 The distribution of aerosols and moisture usually results from a complex combination of processes, including emission, formation, accumulation, deposition, transport (advection), and also mixing. Profiles of attenuated backscatter (Sect. 2.1) hence trace some aspects of the recent history of ABL dynamics. Layer boundaries can be detected if aerosol properties differ between the atmospheric layers examined. The most pronounced layer edge is usually the $ABLH$ because aerosol concentrations and humidity tend to be significantly higher in the ABL than in the FT (Figure 2). But also within the ABL, mixing dynamics can

820 lead to contrasting aerosol properties between different layers. During night and early morning, the lowest layer is considered the $MBLH$ ($SBLH$ under stable conditions) while the layer above defines RLH (Sect. 1.1). During unstable daytime conditions, the aerosol-based $MBLH$ forms in response to recent CBL mixing processes. Vertical and temporal changes recorded at high resolution allow for EZ characteristics to be examined. Decoupled, elevated aerosol layers above the ABL can be identified if they possess distinct aerosol characteristics. Lidars that capture additional information (such as e.g., depolarisa-

825 tion, colour ration; Sect. 2.1) can provide valuable insights that allow for boundary layer aerosols to be better distinguished from lofted layers (e.g., Bravo-Aranda et al., 2017).

The physical quantity of attenuated backscatter is most commonly observed by ALC or aerosol research lidars (Sect. 2.2.4) but can also be derived from DWL (Sect. 2.2.3). Layer heights derived from different systems can be combined to overcome instrument-related limitations, e.g. results from more powerful lidars can be combined with those from ALC observations (e.g.,

830 Wang et al., 2020). As the majority of layer detection algorithms does not rely on absolute values in attenuated backscatter but rather assess relative variations of this quantity in time and height, the range-corrected signal is often used as an alternative input. Also profiles of SNR (from e.g. ALC, DWL or RWP; Compton et al., 2013; Molod et al., 2015, 2019) can be used as input under the assumption that this variable is directly related to the distribution of scatterers in the atmosphere. While the discussion here focuses on ground-based profilers, it should be noted that aerosol-based techniques can also be used for

835 the analysis of airborne lidar profiles (e.g., Scarino et al., 2014), satellite data (CALIOP; Zhang et al., 2016), or output from numerical simulations.

3.3.1 Methods

Aerosol-based retrievals of ABL heights detect layer boundaries based on regions of significant vertical (and at times temporal) change in attenuated backscatter. Where multiple layers are present within the ABL, the role of the respective layers needs to

840 be examined carefully. Hence, two steps are required to determine the ABL heights from aerosol backscatter observations: (1) *detection of layer boundaries* within and at the top of the ABL, and (2) *layer attribution* to distinguish between simultaneous layers (e.g., $MBLH$ and RLH). Methods that predominantly address the task of layer detection are here considered *first-generation* aerosol-based retrievals, while those with a special focus on the more challenging aspect of layer attribution are grouped into *second-generation* aerosol-based retrievals.

845 To detect heights (or regions) of potential layer boundaries from attenuated backscatter profiles, a range of indicators has proven useful (see reviews by e.g., Emeis et al., 2008; Dang et al., 2019). These include negative vertical gradients and

inflection points (e.g., Sicard et al., 2006; Emeis et al., 2008; Münkel, 2007; Schäfer et al., 2004; Lee et al., 2019), 2D-edge detection (e.g., Canny, 1986; Parikh and Parikh, 2002; Haeffelin et al., 2012), wavelet covariance transform (WCT; e.g., Cohn and Angevine, 2000; Morille et al., 2007; Baars et al., 2008; de Haij et al., 2006; Gan et al., 2010; Granados-Muñoz et al., 2012; Lewis et al., 2013; Caicedo et al., 2020), the cubic root gradient which takes into account the influence of gravity waves (Yang et al., 2017), and spatio-temporal variance (e.g., Menut et al., 1999; Martucci et al., 2007; Lammert and Bösenberg, 2006; Piironen and Eloranta, 1995; Hooper and Eloranta, 1986). For example, $ABLH$ is derived from CALIPSO satellite observations as the maximum in vertical and horizontal variance (Jordan et al., 2010).

Many layer detection methods show varying reliability at different stages of the diurnal ABL evolution. $ABLH$ is usually marked by the strongest negative gradient in attenuated backscatter. The mixing between moist ABL air and dry FT air across the EZ results in an area of strong spatio-temporal variance (e.g., Menut et al., 1999). But also entrainment of RL air into the CBL during morning growth can cause distinct variance signatures (e.g., Lammert and Bösenberg, 2006). While some methods (such as the wavelet approach) are less affected by noise, the simple method of vertical gradient detection can be advantageous in capturing layers at low ranges (Di Giuseppe et al., 2012).

Several approaches have been developed to accomplish the second task of layer attribution. First-generation retrieval methods apply attribution criteria either on the respective indicator (e.g., strongest negative vertical gradient) and/or simply based on height (e.g., first significant negative gradient above ground) to assign the layer of interest. Second-generation retrieval algorithms again can broadly be grouped into the following categories:

– Methods based on general layer characteristics: These methods group aerosol data along the vertical profile into categories. To differentiate between the ABL with high aerosol load and the FT with low aerosol signal, an idealised profile can be fitted to the observations (e.g., Steyn et al., 1999; Eresmaa et al., 2006, 2012; Li et al., 2017; Peng et al., 2017). Further do recent artificial intelligence (AI) approaches analyse the profile across the whole layer, incl. extended Kalman filters (Lange et al., 2013; de Arruda Moreira et al., 2018; Kokkalis et al., 2020), *K-means* cluster analysis applied to either the attenuated backscatter profile (KABL; Toledo et al., 2014; Rieutord et al., 2021; Min et al., 2020) or layer candidates derived from first-generation methods (ISABL; Min et al., 2020), or a supervised *AdaBoost* algorithm (ADABL; Rieutord et al., 2021).

– Combination of identification techniques: Given that the various layer-detection techniques can be sensitive to slightly different layer boundaries, a combination of indicators can help to distinguish between layers. For example, Martucci et al. (2010a) combine the height of maximum negative gradient and height of maximum variance to detect $MBLH$ both during day and night together with lofted, decoupled aerosol layers. STRAT-2D (Morille et al., 2007; Haeffelin et al., 2012) uses the variance field to determine which wavelet-detected layer boundary is likely associated with $MBLH$ by analysing the location of the EZ. pathfinderTURB (Poltera et al., 2017) and STRATfinder (using advantages of STRAT+ and pathfinderTURB; Kotthaus et al., 2020) combine gradient and variance field diagnostics before tracing $MBLH$. COBOLT (Geiß et al., 2017) uses a combination of gradients, variance statistics and WCT, varying with solar angle to identify the $MBLH$. Applying Gradient Boosted Regression Trees, de Arruda Moreira et al. (2022) combine

an $MBLH$ first-estimate derived using the gradient method with several meteorological variables to retrieve $MBLH$ values that are comparable to those derived from a microwave radiometer, discriminating between $CBLH$ and $SBLH$. The profile-fit approach is combined with WCT by Sawyer and Li (2013) and with the negative gradient detection in the proprietary Vaisala BLview software (Münkel, 2016), respectively. It should be noted that the BLview algorithm provides several layer candidates so that some post-processing is required to select the appropriate $MBLH$. This has been achieved using, e.g., the provided quality flags (Geiß et al., 2017), gradient thresholds (Haman et al., 2012), manual screening (Caicedo et al., 2017), or a combination of time-tracking and height criteria (Mues et al., 2017; Lotteraner and Piringer, 2016).

– A priori assumptions based on ancillary observations: Where climatology statistics are available from independent measurements (e.g., radiosondes) limits can be prescribed that may vary by season. For example, in pathfinderTURB and STRATfinder absolute limits for $MBLH$ and morning transition growth rate are specified by the user. Some studies set time-specific coefficients (morning, afternoon, and night, respectively) for the WCT (Gan et al., 2011; Caicedo et al., 2020). STRAT+ (based on STRAT-2D; Pal et al., 2013) uses radiosonde profiles and turbulent surface sensible heat flux measurements to derive stability information that aid interpretation of the variance field.

– A priori assumptions from model results: Simple models describing general ABL dynamics or output from NWP models representing varying synoptic conditions have been used to guide layer attribution. For example, Di Giuseppe et al. (2012) use a bulk model (Tennekes, 1973) based on surface sensible heat flux data to define times of morning and evening transition.

– Temporal layer tracking: Temporal consistency is a powerful criterion for layer attribution (Angelini et al., 2009) as it reduces physically unreasonable height fluctuations and growth rates. For example, the temporal-height-tracking method (THT; Martucci et al., 2010a) uses the $MBLH$ estimate at a previous time step to define the search window for the subsequent detection. A similar approach is implemented in COBOLT (Geiß, 2016) and by Wang et al. (2012) or Caicedo et al. (2020). The MIPA algorithm (Vivone et al., 2021) uses morphological and object-based image processing techniques to improve temporal consistency of the detected $MBLH$. A recent family of algorithms (pathfinder, pathfinderTURB, STRATfinder) apply a graph theory approach to trace the path of $MBLH$ through the day. In CABAM (Kotthaus and Grimmond, 2018a), points of significant negative gradients are connected to layers which are then traced through the day following growth and decay criteria in a dynamic decision tree. The extended Kalman filter applied by Kokkalis et al. (2020) uses information from past profile analysis to inform $ABLH$ detection, which generally improves temporal consistency but can also lead to errors when air with different aerosol load is advected. Also the supervised ADABL algorithm (Rieutord et al., 2021) considers temporal consistency.

– Additional lidar profiles: The POLARIS algorithm analyses the depolarisation ratio in connection with the WCT approach (Bravo-Aranda et al., 2017). The MDS method (Liu et al., 2018) determines $ABLH$ by adding information on the particle size by calculating the degree of difference in aerosol characteristics between observations from two ad-

jacent lidar range gates as a combination of aerosol backscatter and the color ratio (Sect. 2.1). As research lidars and
some novel ALC (Sect. 2.2.4) increasingly provide additional profile information on top of the attenuated backscatter,
promising developments are expected from algorithms that exploit more than one aerosol variable to differentiate layer
characteristics.

While most of these retrieval algorithms output one layer height (usually either $MBLH$ or $ABLH$), simultaneous identification of several layers is possible provided the layer attribution step does account for it (Kotthaus et al., 2020; Milroy et al., 2012; Caicedo et al., 2020; Toledo et al., 2017). Elevated aerosol layers can be traced in addition to ABL heights. For example, Poltera et al. (2017) detect a continuous aerosol layer above the ABL using pathfinerTURB while Pandolfi et al. (2013) track a decoupled aerosol layer above the ABL at a coastal site and Gan et al. (2010) derive RLH and elevated aerosol layers using the WCT approach.

In the absence of clouds, aerosol-derived $ABLH$ is usually located somewhere in the centre of the EZ, where vertical negative gradients and spatio-temporal variance are strongest due to the exchange of aerosols and moisture between the ABL and FT (Menut et al., 1999). Where observations at very high temporal resolution in the order of minutes are available and SNR is sufficient, temporal variations in $ABLH$ permit the estimation of EZD (e.g., Cohn and Angevine, 2000) and entrainment velocities (Träumner et al., 2011). Martucci et al. (2010a) performed spectral analysis on high-resolution $ABLH$ observations to characterize entrainment processes under different atmospheric stability conditions. Alternatively, the transition zone concept, based on the difference between high attenuated backscatter values in the ABL and low values in the FT (Steyn et al., 1999) can be used to determine the EZD. Statistical concepts capturing temporal, spatial and small-scale turbulence variations can differ significantly from the transition zone estimates given the latter is mostly limited to small-scale turbulence effects (Träumner et al., 2011).

3.3.2 Capabilities and limitations

Both the detection and the attribution step of aerosol-based layer retrievals highly depend on the quality of the attenuated backscatter profiles analyzed (de Haij et al., 2006; Milroy et al., 2012). $MBLH$ and $ABLH$ retrievals based on attenuated backscatter have seen significant improvements due to recent advances in ALC measurement technology (Illingworth et al., 2019; Cimini et al., 2020) and detailed correction procedures (Hervo et al., 2016; Kotthaus et al., 2016) as both improve data quality and availability. An important variable describing the information content of a measurement at a certain time and range is the SNR (Sect. 2.1). Any combination of high instrument-related noise, low aerosol (and moisture) load, or very deep convection reduces the SNR which can lead to both under- and over-estimation of peak $ABLH$ (Kotthaus et al., 2020). Applying an SNR filter can improve layer detection (Poltera et al., 2017; Min et al., 2020), however, care must be taken in pristine environments (Boy et al., 2019), where atmospheric scatterers are scarce and the recorded signal may not necessarily exceed instrument and background noise significantly. While SNR-limitations mostly lead to uncertainties in the detection of layer boundaries at elevated heights above ground, the detection of shallow layers (nocturnal $MBLH$ and $SBLH$) can be

affected by the incomplete optical overlap and near-range artefacts (Schween et al., 2014; Kotthaus et al., 2020; Caicedo et al., 2020).

In addition to instrument-related uncertainties, discrepancies in layer results arise from the choice of retrieval algorithm. Haeffelin et al. (2012) compared five $MBLH$ detection techniques applied to observations from three different ALC at two contrasting measurement sites. While layer detection methods (first derivative, WCT, and two-dimensional derivative) often agree, the greatest uncertainty in final products was associated with the step of layer attribution, even when considering simple categories only. Second-generation algorithms (Sect. 3.3.1) hence put a special focus on the interpretation of the ABL sublayers. Comparing different second-generation methods, it appears that those including criteria on temporal consistency of layer estimates tend to perform slightly better (de Bruine et al., 2017; Knepp et al., 2017).

Agreement between retrieval methods varies with the complexity of the ABL structure. Provided sufficient SNR, results from different methods and sensors tend to agree best in the afternoon during peak convective activity (Milroy et al., 2012) when the CBL extends over the whole ABL leaving essentially no sublayers to confuse the algorithms (Toledo et al., 2017). Layer attribution is challenged when several aerosol layers are present simultaneously, such as during night and early morning. If MBL and RL aerosols have similar characteristics, the $MBLH$ may not be characterised by a particularly strong gradient (Granados-Muñoz et al., 2012). Highest uncertainty generally occurs during the evening transition (Geiß et al., 2017) when new aerosol gradients start to form gradually and decaying turbulence may not be traced successfully by backscatter variance methods in case of homogeneous aerosol distributions (Poltera et al., 2017). In addition to ABL-internal sublayers, elevated aerosol layers add complexity and hence layer retrieval uncertainty. Any aerosol-based method is challenged when temporal variations of gradients (or variances) are dominated by advection of aerosols (e.g., due to strong sea breezes or dust transport; Tang et al., 2016; Bravo-Aranda et al., 2017; de Arruda Moreira et al., 2020; Diémoz et al., 2019b; Caicedo et al., 2019). Advances in measurement technology (such as depolarisation information becoming increasingly available; Sect. 2.2.4) and continued algorithm development (including AI methodologies; Rieutord et al., 2021) are expected to further improve layer attribution efforts.

The lidar signal is strongly attenuated by liquid clouds, so that the signal is often completely extinguished at a few hundred meters above cloud base (depending on the system characteristics; O'Connor et al., 2004). As a consequence, the profile of attenuated backscatter yields little information above the altitude of such thick water clouds. Where clouds form within the ABL, aerosol-derived layer heights can severely underestimate $CBLH$ (Hennemuth and Lammert, 2006). Advanced detection algorithms hence increasingly take into account the presence of boundary layer clouds (Poltera et al., 2017; Caicedo et al., 2020). Where the cloud base height variable provided by the ALC is used, it should be noted that this product can show systematic differences between internal algorithms from various manufacturers (Martucci et al., 2010b; Pattantyús-Ábrahám et al., 2017) and even between models from the same brand (Liu et al., 2015b). Most methods naturally struggle with reliable layer detection and attribution during precipitation or the passage of synoptic fronts (de Bruine et al., 2017; Yang et al., 2017) as the ABL is generally poorly defined during those times when surface-atmosphere interactions play a minor role compared to larger-scale processes.

980 Some studies assign a quality flag to the derived layer heights based on the magnitude of the attenuated backscatter vertical gradient (e.g., de Haij et al., 2006; Ketterer et al., 2014). For $ABLH$, such indicators can be suitable given the strong contrasts in aerosol content between the ABL and the FT. However, the strength of the vertical gradient does not necessarily reflect the uncertainty in $MBLH$ detection at night or during morning growth as the contrast between the layer coupled to the surface and the RL is often weaker than to the FT. Careful quality control during post-processing (e.g., based on physically reasonable

985 temporal variations in layer heights) can help focus inter-comparison or evaluation efforts (Kotthaus et al., 2020; Caicedo et al., 2020).

Aerosol-based retrievals for ABL heights are most commonly evaluated against thermodynamic retrievals (Sect. 3.1) applied to radiosonde profile data (Sect. 2.2.1). When comparing aerosol-derived layers to thermodynamic results, the differences of the underlying physical processes need to be taken into account during interpretation (Hennemuth and Lammert, 2006).

990 Naturally, comparison statistics vary with the retrieval method applied on the radiosonde data (Haman et al., 2012). Compared to thermodynamic estimates, aerosol-derived $CBLH$ can have a negative bias (e.g., de Haij et al., 2006; Bravo-Aranda et al., 2017; de Bruine et al., 2017; Liu and Liang, 2010) as the atmospheric quantities of temperature and aerosol show different EZ characteristics (see discussion in Sect. 4.2). Best agreement between the temperature- and aerosol-based layer height detection is again found in the early afternoon, when the CBL extends over the whole ABL (de Bruine et al., 2017). Given the impact

995 of advection on ABL complexity, agreement between the different approaches can vary with synoptic conditions or local circulations induced by surface cover heterogeneities (Pandolfi et al., 2013; Hennemuth and Lammert, 2006). Liu et al. (2018) find agreement between several aerosol-based $ABLH$ results and the bulk-Richardson method applied to daytime radiosonde profiles clearly improves with increasing atmospheric instability.

At night, thermodynamic detection of the height of the CI from radiosondes or AMDAR profiles (Sect. 2.2.1) were found

1000 to coincide well with aerosol-derived RLH (Martucci et al., 2007; Kotthaus et al., 2020; Milroy et al., 2012). The few studies showing direct $SBLH$ comparisons between aerosol-derived and thermodynamic results generally suggest a good agreement between the layer estimates, with small biases reported in either direction (Pal et al., 2013; Haman et al., 2012; Tang et al., 2016). Still, substantial systematic biases may occur, with aerosol-derived $MBLH$ remaining below $SBIH$ (Marsik et al., 1995). Mismatches are explained by the contrasting physical processes that are being traced, such as when radiative cooling

1005 leads to the formation of a surface-based temperature inversion which is not necessarily associated with any contrasts in aerosol characteristics (Milroy et al., 2012).

Due to the lack of suitable reference data and the physical difference between aerosol-based and thermodynamic layer detection, a few studies applied manual or semi-automatic layer detection for the evaluation of aerosol-based retrievals (de Bruine et al., 2017; Poltera et al., 2017; Kotthaus and Grimmond, 2018a). Although manual detection can be a very valuable tool, it is

1010 labour-intensive and not necessarily objective (Poltera et al., 2017).

4 Monitoring ABL heights

As ground-based remote sensing profilers have different capabilities (Sect. 2.2) and algorithm uncertainties depend on a variety of atmospheric characteristics, the performance of the various sublayer height retrieval methods (Sect. 3) changes throughout the diurnal evolution of the ABL (de Arruda Moreira et al., 2018). The following section summarises the most important strengths and weaknesses of the methods when monitoring the height of the boundary layer at night or during stable conditions (Sect. 4.1), morning growth (Sect. 4.2), peak CBL development (Sect. 4.3), and evening decay (Sect. 4.4). Further, capabilities are discussed that are relevant for the characterisation of the entrainment zone (Sect. 4.5) and the cloud-topped ABL (Sect. 4.6).

The few available synergy applications are highlighted to indicate possible future pathways of ground-based remote sensing implementation. Where observations from multiple profilers are available simultaneously, analyses suggest a synergistic interpretation of results from different methods could lead to an enhanced description of the ABL, including the detection of sublayer heights (Saeed et al., 2016) and the description of the processes shaping the ABL development (Manninen et al., 2018). In addition, combining observations from several sensor systems provides crucial information for the assessment and quantification of layer detection uncertainties (e.g., Cohen et al., 2015) and could be exploited to assign quality flags for the derived layer heights (as has been done for various retrievals from radiosonde profiles by Beyrich and Leps, 2012).

It should be noted that studies directly inter-comparing ABL height retrievals based on different atmospheric quantities are still rare, especially those covering extended time periods. Given their impact on layer height uncertainty, measurement setup (such as MWR calibration, DWL focal setting and scan strategy, aerosol lidar optical overlap, amongst others; Sect. 2.2), data processing, and quality control (Sect. 3) should all be carefully evaluated when comparing results from various methods.

4.1 Nocturnal and/or stable boundary layer heights

At night, the $MBLH$ is rather shallow, with stable conditions being more likely. For the detection of shallow layers, a low first measurement level and high vertical resolution of the profile data are beneficial. In-situ data obtained on e.g., tall towers, tethered balloons or using UAS usually provide very detailed information, however, some lack temporal coverage. For radiosondes launched with automatic systems, measurement uncertainties in the lowest part of the profile can pose challenges for the assessment of very shallow layer heights or stability conditions.

For ground-based remote sensing instruments, the near-range capabilities are critical (Sect. 2.2). Layer heights can only be detected if they exceed a potential blind zone of the instrument and they are not obscured by sensor-related uncertainties. MWR are very suitable for shallow layer height detection given their sensitivity is maximal near the sensor (Sect. 2.2.2). High-power research lidars often do not provide information in the lowest few hundred meters (Sect. 2.2.4), meaning that ALC can be more suitable for the detection of shallow layers from aerosol profiles. Improved monitoring of the lowest few hundred metres of the atmosphere at high vertical resolution can be achieved by operating active remote sensing profilers at a low elevation angle (e.g., ALC; Poltera et al., 2017). Scanning DWL (Sect. 2.2.3) can alternate scans at low and high elevation angles, whereby the associated wind and turbulence retrievals have to assume spatial homogeneity of the atmosphere across the sampled volume.

Where both temperature and wind information are available (e.g. from in-situ observations, or through instrument synergy), $SBLH$ can be derived from the profile of the bulk Richardson number. While results of this method are particularly sensitive to the first-level air temperature observations in the in-situ profile, uncertainty may increase in general when combining results obtained from two sensor types (e.g. DWL and MWR). $SBLH$ can also be approximated from various features in the temperature profile, that also allows for the detection of $SBIH$. In the presence of a LLJ (Sect. 3.2), wind and turbulence profile data not only allow for the retrieval of $SBLH$ but also help interpret its effects on mixing and advection of moisture, heat and pollutants (Hu et al., 2013; Reitebuch et al., 2000; Bennett et al., 2010). The relation of $SBIH$ to the position of the LLJ changes over time, with $SBIH$ increasing over the course of the night often to exceed the height of the LLJ maximum at some point (Mahrt et al., 1979). In general, discrepancy between temperature-based methods and those analysing vertical wind profiles can be profound (Beyrich and Leps, 2012). Aerosol-based methods can track shallow $MBLH$ if quality observations in the near-range are available and careful layer attribution is performed to reduce confusion with the residual layer height.

Some systematic differences in nocturnal $MBLH$ are reported between results from the various methods available (Sect. 3), with discrepancies between layers detected based on the same or different atmospheric quantities, respectively, at the same order of magnitude. On average, uncertainty in $SBLH$ detection is estimated around 30-40% (Steeneveld et al., 2007). Since turbulence in the SBL is usually not uniform (Beyrich, 1997), the diagnosed layer heights can differ systematically from thermodynamic or aerosol-based methods. While Schween et al. (2014) find turbulence-based nocturnal $MBLH$ exceeds aerosol-based layer heights by about 300 m on average during stormy winters in rural Germany, average nocturnal $MBLH$ differences between turbulence and aerosol-based methods in London, UK, are mostly at the order of their day-to-day variability (Barlow et al., 2011; Kotthaus et al., 2018). More studies are needed to assess the impact of ABL dynamics and atmospheric stability on the relative agreement of the various methods for nocturnal layer height detection.

At night (and early morning), the detection and layer attribution of the $MBLH$ ($SBLH$) can be challenged by the presence of the RL. Layer detection becomes more uncertain if atmospheric characteristics are similar within the MBL and the RL above. As aerosol-based methods are particularly challenged by the presence of a RL, most second generation algorithms (Sect. 3.3) aim to specifically address this source of error. Further, aerosol characteristics (e.g., size distributions) and intermittent turbulence can cause signatures in attenuated backscatter and turbulence fields, respectively, that may appear as additional layer boundaries within the RL. For the turbulence analysis, layer detection can be improved by distinguishing between surface-driven processes in the MBL and the decoupled mixing above (Sect. 4.7). Temperature-based layer heights (Sect. 3.1) derived from MWR profiles (Sect. 2.2.2) are less likely to mistake elevated layer boundaries for $MBLH$ as these profilers are more reliable in the near range and respond less to RL signatures.

The RL is a remnant of the previous day's CBL (Sect. 1.1), so that aerosols and moisture remaining in this elevated layer above the $MBLH$ present very suitable atmospheric tracers. While some turbulent exchange between the RL and the FT can be picked up (Fochesatto et al., 2001), the RLH can be tracked most reliably using thermodynamic retrievals (Sect. 3.1) of the CI applied to airborne in-situ sensors or by aerosol-based methods (Sect. 3.3) because the contrasts at the $ABLH$ are usually striking. As MWR profiles are generally less sensitive to contrasts near the RLH (Sect. 2.2.2) algorithms are usually not applied to radiometer profiles for the detection of this RLH. Uncertainty in RLH detection can be increased by various

atmospheric processes, such as low aerosol load (reducing SNR for lidar systems; Sect. 2.2.4), the presence of shear layers (generated by e.g., orography, LLJ) or the advection of air with different aerosol or humidity content.

Instrument synergy has been identified as a promising means to better characterise the nocturnal boundary layer. Exploiting a combination of attenuated backscatter and turbulence variables derived from DWL profiles, Manninen et al. (2018) present a synergy approach to characterise the RL as the non-surface-connected region of the ABL where the turbulence activity is intermittent or absent. Collaud Coen et al. (2014) and de Arruda Moreira et al. (2020)

Several studies highlight that synergy analysis of MWR and aerosol lidar data is particularly promising for nocturnal layer assessment given the respective strengths in observing $SBLH$ and RLH features (Collaud Coen et al., 2014; de Arruda Moreira et al., 2020; Da Silva et al., 2022). Saeed et al. (2016) use information on temperature inversion heights derived from MWR profile data to constrain an aerosol-based $SBLH$ retrieval.

4.2 Morning growth

The time of $CBLH$ morning growth is characterised by substantial temporal variations (Halios and Barlow, 2017), especially where the surface energy balance exhibits a pronounced diurnal cycle. For the detection of the $CBLH$ from radiosonde profiles, again the bulk Richardson method is available but also its simplified version based on temperature profile data alone, i.e. the Parcel method, is applicable (amongst others; Sect. 3.1).

Compared to the limited temporal coverage of radiosonde ascents (Sect. 2.2.1), the continuous monitoring enabled by remote sensing profilers is a clear advantage for the assessment of this period characterised by significant seasonal but also day-to-day variability. Approaches based on high-frequency variations of wind (Sect.3.2) or aerosol (Sect. 3.3) often reveal pronounced signals near the $CBLH$ during this time of day. Given their ability to capture turbulence even in the near range (Sect.2.2), sodar systems are particularly valuable for the monitoring of the growth (onset) of the $CBLH$ (Beyrich, 1995). Turbulence-based $CBLH$ from RWP usually requires longer integration times (20-60 min) compared to DWL or ALC that both range in the order of minutes.

As for nocturnal conditions (Sect. 4.1), the presence of a RL can affect the detection of $CBLH$ during morning growth as entrainment of RL air (instead of air from the FT) can act to reduce the contrasts of measured quantities near the $CBLH$. Among aerosol-based approaches, detection methods that account for the potential presence of a RL in addition to $CBLH$ are more reliable (Sect. 3.3). The detection of $CBLH$ from RWP data during morning growth relies on the careful differentiation between the turbulent signature generated by the entrainment of RL air into the CBL and variations near the RLH (Bianco et al., 2022).

Based on selected case studies, turbulence- and aerosol-based $CBLH$ during morning growth are often very similar provided appropriate layer attribution is performed (Cohn and Angevine, 2000; Collaud Coen et al., 2014). However, several studies also report a temporal delay of aerosol-derived $CBLH$ morning growth both relative to temperature-derived $CBLH$ (Wang et al., 2012; Kotthaus et al., 2020) and turbulence-derived $CBLH$ results (Wiegner et al., 2006; Barlow et al., 2011; Kotthaus et al., 2018), with time lags of up to two hours. Presumably, it can require some time before aerosols emitted at the surface and transported upwards by turbulent mixing establish a clear layer boundary relative to the RL. In addition, entrainment

of RL air with lower humidity and aerosol load may delay morning growth of aerosol-based $MBLH$ (Gibert et al., 2007). Some studies found turbulence-derived $CBLH$ to not only start rising earlier but also to grow faster than layer heights from aerosol-based methods (Barlow et al., 2011; Schween et al., 2014). However, this may be partly linked to the response of the respective detection algorithms to the presence of clouds (Wiegner et al., 2006), as Kotthaus et al. (2018) found similar growth rates when looking at cloud-free conditions only. No clear picture has yet emerged on a potential time lag between the growth of temperature- and turbulence-derived layer heights (de Arruda Moreira et al., 2018, 2019). Due to advances in algorithm development (Sect. 3), multi-sensor analysis has the potential to better quantify the relation of layer heights based on thermodynamic, dynamic and aerosol-based retrievals, respectively, which is expected to provide valuable new insights into the understanding of ABL dynamics during CBL development.

4.3 Daytime Convective Boundary Layer

Most methods for $MBLH$ detection perform best during daytime, especially once the $CBLH$ coincides with $ABLH$ (Sect. 1.1). Provided sufficient SNR and careful data processing, $CBLH$ from all retrieval methods can agree within a few hundred metres or even less (Granados-Muñoz et al., 2012; Renju et al., 2017). If radiosonde ascends at noon are compared to ground-based remote sensing profile data, the CBL may not yet reach its full extent so that layer attribution (i.e. confusion of $CBLH$ and RLH) can be a general source of uncertainty. Sensors restricted by low SNR (such as, e.g., sodar, RASS, some ALC; Sect. 2.2), often fail to detect the fully-developed CBL in the afternoon, especially where boundary layer development is deep, aerosol load is low, or environmental noise levels are high (Boy et al., 2019).

Schmid and Niyogi (2012) highlight that a thick EZ, likely to occur during deep afternoon convection (> 3 km), can result in a weaker delineation at the $ABLH$, increasing uncertainty in layer detection for all methods. While turbulence-based algorithms are challenged in the presence of strong shear layers above the ABL (Marsik et al., 1995), elevated aerosol layers increase the likelihood of false layer attribution for aerosol-based techniques (Granados-Muñoz et al., 2012; Tang et al., 2016). Layers holding advected aerosol with characteristics differing from local emissions (e.g., long-range transport of desert dust) may further alter the air temperature profile (Guerrero-Rascado et al., 2009), whereby potentially inducing errors in the applied thermodynamic retrieval (Granados-Muñoz et al., 2012). Synoptic circulation or orography-induced flow patterns that are influencing cloud conditions or the advection of decoupled layers have hence been found to affect comparison statistics (Granados-Muñoz et al., 2012; Pandolfi et al., 2013; Tang et al., 2016; Pearson et al., 2010; de Arruda Moreira et al., 2019).

Daytime maxima of the layer estimates from temperature-, wind- or turbulence-, and aerosol-based methods are most similar in clear-sky conditions (Barlow et al., 2011; de Arruda Moreira et al., 2018). In accordance with the delayed morning growth of aerosol layers (Sect. 4.2), some studies find $CBLH$ from aerosol-based methods to peak up to 2 h later than layer heights diagnosed from turbulence (Barlow et al., 2011; Kotthaus et al., 2018) or temperature profiles (Renju et al., 2017). No clear relation has yet been established between peak daytime $CBLH$ from aerosol-based retrieals and either turbulence or thermo-dynamic methods, as negative (Barlow et al., 2011; Kotthaus et al., 2018), positive (Schween et al., 2014; Granados-Muñoz et al., 2012; de Arruda Moreira et al., 2019), as well as no bias (Collaud Coen et al., 2014; Wang et al., 2012) are reported. Similarly, both positive, negative, and negligible deviations were found when comparing turbulence-derived $CBLH$ based on

DWL data and temperature-based results obtained from MWR profiles (de Arruda Moreira et al., 2018, 2019). Further research is needed to assess which factors (including algorithm uncertainty, sampling strategy and atmospheric dynamics) best explain potential biases, accounting not only for cloud dynamics and the presence of elevated aerosol layers but also the presence of thermals overshooting the inversion at the ABL top which are inducing vast temporal variability (Renju et al., 2017; de Bruine et al., 2017) or atmospheric stability and moisture transport which can affect $CBLH$ growth rates (Helbig et al., 2021).

4.4 Evening decay

The daytime CBL transitions into the nocturnal boundary layer around sunset (Sect. 1.1). The decay in surface-driven buoyancy is directly monitored by the turbulence profiles obtained by sodars, DWL, or RWP (Sect. 2.2.3). Thermodynamic and turbulence-based $CBLH$ are in general agreement, showing a gradual decrease in the afternoon up to about sunset (Wang et al., 2012; Collaud Coen et al., 2014; Renju et al., 2017). Schween et al. (2014) illustrate the breakdown of turbulent exchange in the afternoon based on DWL profile data while Manninen et al. (2018) highlight elevated turbulence can occur during the evening transition as the RL decouples. Layer detection from RWP observations was found more uncertain in the presence of elevated shear layers (Ketterer et al., 2014).

In response to the vanishing buoyancy, aerosols start to settle in the afternoon whereby slowly forming new layer boundaries. As aerosol-based $MBLH$ is a record of the history of recent turbulence activity (Träumner et al., 2011), layer attribution is especially challenged during the time of evening CBL decay (Sect. 3.3.2). Where aerosol emissions at the surface are high (e.g., in cities), new shallow aerosol layers tend to become visible around sunset as the reduced vertical dilution increases low-level concentrations. If no clear aerosol gradient forms close to the surface around sunset (Sect. 4.1), the RLH may at times be misinterpreted as $MBLH$ in which case evening discrepancies between layer results from different methods can be at the order of magnitude of the $ABLH$. Reliable data in the near range, careful processing algorithms and high surface aerosol emission rates increase the likelihood of this transition time to be captured (accurately) by ALC (Sect. 3.3.2).

4.5 Entrainment zone

Characterising the entrainment zone (Sect. 1.1) around the $CBLH$ can greatly benefit interpretation of ABL dynamics, local climate conditions and air quality. The EZD can be estimated from temporal (or spatial) variations in $CBLH$ (Sect. 3) that are a direct measure of the entrainment process, provided observations are collected at very high temporal resolution. Aerosol profiles with sufficient SNR are rather suitable for the assessment of EZD. For example, de Bruine et al. (2017) report fluctuations of 100-500 m around an average, rather constant $ABLH$. Cohn and Angevine (2000) find EZD based on fluctuations of $ABLH$ from aerosol-derived methods to be more consistent than those from RWP observations, as the latter are associated with greater noise levels for the sensor used. Where turbulence-based $CBLH$ from DWL requires rather long integration times (Sect. 3.2), this is a disadvantage for the estimation of EZD (Träumner et al., 2011). For shallow CBL, also sodar observations have been successfully exploited to determine the EZD (Beyrich and Gryning, 1998).

Alternatively, the EZD can be approximated based on gradients of mean observed quantities between the CBL and FT (RL), derived from e.g. radiosonde data. The rather low range resolution of the MWR near the $ABLH$ (Sect. 2.2.2) can cause considerable uncertainty when studying the EZ based on remotely-sensed temperature profiles (Wang et al., 2012).

4.6 Cloud-topped boundary layer

While many studies focus on the analysis of clear-sky conditions, cloud-topped mixed layers are starting to receive increasing attention. Given the diverse capabilities and limitations of the remote sensing profilers for the observation of clouds (Sect. 3), the disagreement between layer estimates generally increases with cloud complexity (e.g., Cohn and Angevine, 2000; Collaud Coen et al., 2014; Cimini et al., 2013; Emeis et al., 2009). The strong attenuation of the lidar signal by water clouds causes a distinct signature in ALC and DWL profiles. Developed to record cloud base height, ALC inherently have built-in algorithms reporting this quantity. It should however be noted that cloud base height detection methods vary between manufacturers (Sect. 3.3) so that generalised algorithms may need to be applied during post-processing when consistent products are required across a diverse sensor network. High-power lidar systems are usually not operated under cloudy conditions (Sect. 2.2.2, 2.2.4). MWR and RWP can penetrate the layer of cloud droplets. RWP observations have been used to determine the cloud top but frequent false detection was linked to elevated layers of high humidity or turbulence (Collaud Coen et al., 2014).

Doppler cloud radars (DCR) can be used to characterize the vertical extent of boundary-layer clouds, such as shallow convective clouds, stratiform clouds (stratus or stratocumulus), and even fog. In the case of adiabatic fog, the fog layer (typically 50-400 m deep) is destabilized due to strong radiative cooling at the top coinciding with strong temperature inversion. Mixing then occurs between the fog top and the surface. Wærsted et al. (2017) combine measurements from MWR and DCR to retrieve the temperature profile in adiabatic fog layers, hence characterizing precisely the depth of the mixing.

Automatic ABL height retrieval algorithms are increasingly incorporating the presence of clouds into the layer detection and attribution process (Poltera et al., 2017; Caicedo et al., 2020). Both cloud cover and cloud type can be critical (Sawyer and Li, 2013; Kotthaus and Grimmond, 2018b), given convective clouds are associated with surface-driven turbulence and stratiform clouds initiate mixing by cloud dynamics (Hogan et al., 2009). Turbulence characteristics present useful information to differentiate between surface- and cloud-driven turbulence (Harvey et al., 2015). The cloud base height may be used as a reasonable proxy for $CBLH$ for shallow Cu clouds, where the convective nature of the cloud can be assessed by surface heat flux measurements (Schween et al., 2014; Wiegner et al., 2006) or derived from remote sensing data (Manninen et al., 2018). Depending on the retrieval applied to determine the cloud base height, potential biases may be introduced. For deeper Cu, the relation between cloud base and $CBLH$ is more ambiguous. In autumn and winter, the cloud base height is often related to the dissipation of Sc clouds or fog processes (Schween et al., 2014). The relation of cloud base and $MBLH$ is subject to ongoing research.

4.7 Atmospheric stability and ABL classification

ABL dynamics form in response to a complex combination of processes, including e.g., surface forcing, the synoptic flow (Shi et al., 2019), elevated sources of turbulence associated with clouds or winds (e.g., LLJ), local-scale circulations induced by

land cover contrasts (Moigne et al., 2013) or topography (Rotach and Zardi, 2007). To understand the relative importance of these drivers in defining ABL sublayer heights, automatic classification methods are increasingly developed.

A common ABL classification is the delineation between cloudy and cloud-free conditions, which can be accomplished using surface radiation data, the cloud information reported by an ALC (Sect. 2.2.4) or by exploiting any remotely sensed profile signal sensitive to clouds (Sect. 2.2). To account for differences in ABL heights associated with cloud dynamics, ALC data have also been used to automatically distinguish simple cloud types (Kotthaus and Grimmond, 2018a). Pal et al. (2013) classify ABL regimes using cloud cover (cloudy vs clear-sky) and atmospheric stability (from surface observations) to distinguish between days dominated by local surface-driven buoyancy and those dominated by larger scale events. Using airborne profile measurements, Mahrt (1991) find ABL humidity exchanges are generally either associated with an *entrainment-drying* regime characterised by a vertical divergence of the moisture flux or a *moistening* boundary layer dominated by surface evaporation fluxes.

Atmospheric stability indicators that account for both thermal buoyancy and wind shear (such as the Richardson number), can be obtained from suitable in-situ observations (Sect. 2.2.1) or a synergy of wind and temperature profiles observed by multiple systems. Based on temperature profiles alone, lapse rates and other indices of thermal atmospheric stability can be derived (Feltz and Mecikalski, 2002; Wagner et al., 2008; Cimini et al., 2015) and used to classify the ABL regime (Liu and Liang, 2010).

But also from wind- and turbulence alone, valuable characteristics can be determined, e.g. to differentiate between buoyancy- or shear-driven turbulence (Tucker et al., 2009), surface or elevated turbulence sources (Tonttila et al., 2015; Manninen et al., 2018; Huang et al., 2020; Harvey et al., 2015), and elevated turbulence sources associated with the flow (e.g., LLJ; Tuononen et al., 2017) or cloud dynamics (Marke et al., 2018; Harvey et al., 2013; Manninen et al., 2018). The sign of the vertical velocity skewness provides information on the source of turbulence, with positive values typical for surface-driven buoyancy in clear-sky CBL and negative values associated with cloud-topped boundary layers dominated by 'downwards convection' driven by radiative cooling at the cloud top (Hogan et al., 2009). The vertical velocity skewness further helps to determine whether clouds are coupled to the surface (e.g., shallow cumulus clouds) or decoupled from the surface (e.g., some nocturnal Sc; marine Sc). The SBL turbulence regime from velocity variance indicators was found consistent with stability indicators derived from AERI temperature profiles (Bonin et al., 2015) and useful for the characterisation of LLJ evolution (Bonin et al., 2019).

Building on the profile-based classification approach from Harvey et al. (2013), Manninen et al. (2018) developed a pixel-based ABL classification scheme that exploits several atmospheric quantities derived from DWL observations. An example of a clear-sky case (Fig. 4) illustrates the complexity in ABL dynamics with diurnal variations clearly detectable from the profile data (Manninen et al., 2018). Unstable atmospheric conditions drive the $CBLH$ morning growth in two stages (Fig. 4a,b), i.e. the slow increase of near surface convective conditions followed by a rapid growth phase (Halios and Barlow, 2017). The gradual decay of convective activity in the evening transition is clearly detected (Fig. 4a,b). A LLJ forms at some point after sunset (Fig. 4c,d).

1245   Based on profiles of the aerosol scattering ratio derived from ALC measurements, the complex ABL dynamics in an Alpine valley were classified which proved valuable for the assessment and understanding of local air quality conditions (Diémoz et al., 2019a, b). Studies that group aerosol or trace gas profile observations according to e.g. turbulence, stability, or LLJ regimes (e.g., Su et al., 2020; Klein et al., 2017, 2019; Dieudonné et al., 2013), characteristic features are starting to emerge that can be very valuable for the assessment of near-surface air pollution concentrations. The gained processes-understanding
1250   of such synergy applications that combine multiple atmospheric variables, means ABL classifications are increasingly able to account for the complex interactions of the processes that drive ABL dynamics and atmospheric composition.
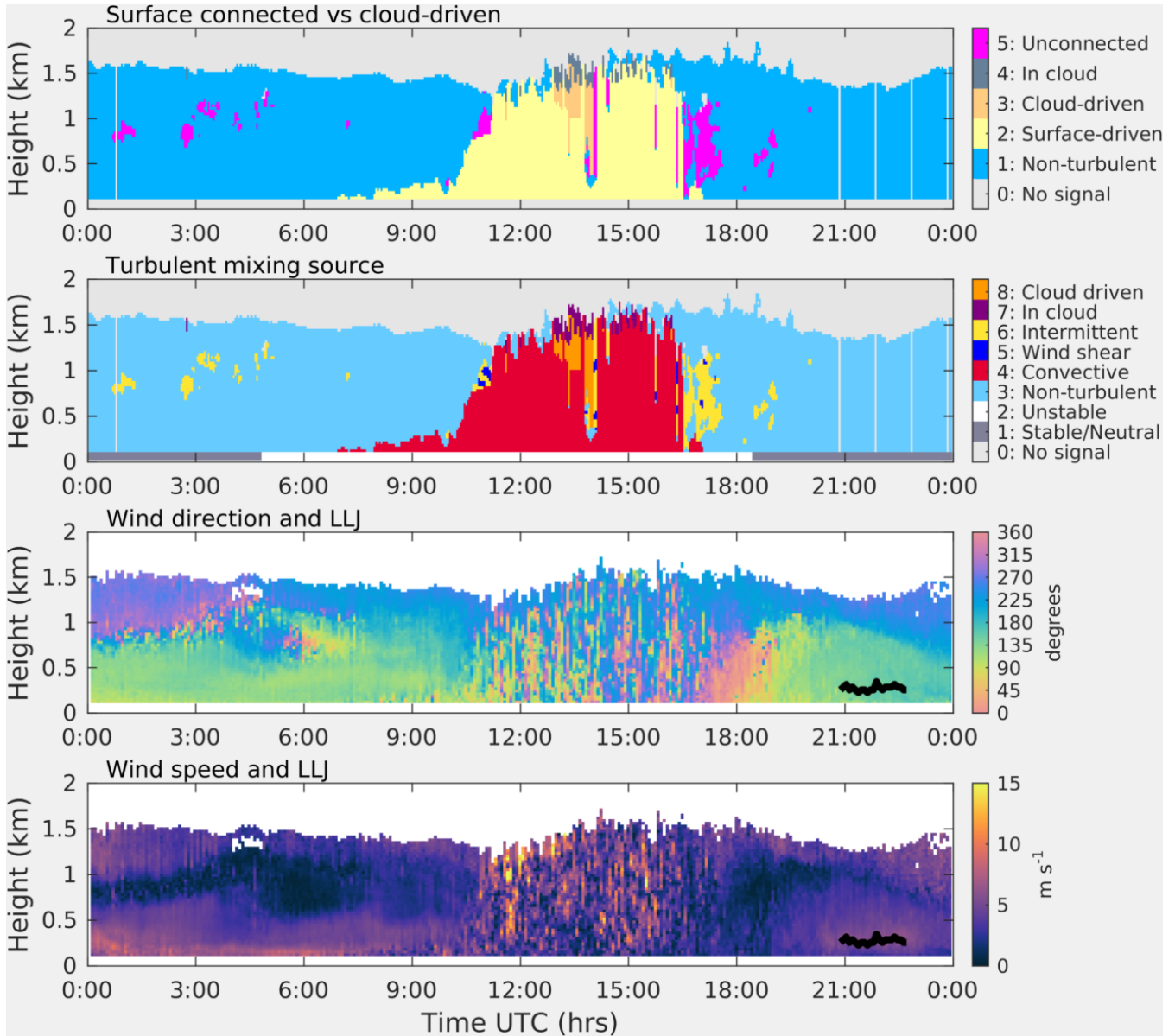
Figure 4. Time-height plots of atmospheric boundary layer classification using the Manninen et al. (2018) scheme showing (a) whether mixing is connected to the surface or cloud driven and (b) the turbulent mixing source, together with time-height plots of (c) wind direction and (d) wind speed on 28 August 2017 at Jülich, Germany. The black lines on the two lower panels show low-level jet (LLJ) altitude (Tuononen et al., 2017).

5 Conclusions

Despite the importance for a range of applications, quantitative knowledge on the temporal and spatial variations in atmospheric boundary layer (ABL) height is still scarce. While synchronised radiosonde data provide an immensely valuable assessment of conditions at the global scale now for decades, their comparatively low temporal resolution (amongst other limitations) means they often do not capture diurnal and seasonal variations of ABL dynamics at a given location. Thanks to advances in ground-based remote sensing, high-quality profile observations spanning the ABL extent at very high temporal resolutions are now increasingly collected by operational measurement networks. As these data start to resolve spatio-temporal variations in ABL dynamics even in complex environments such as mountainous terrain or cities, they provide valuable contributions to international research projects in these domains (e.g. the EU H2020 Green deal projects *RI-URBANS*[21] (ACTRIS) and *ICOS-cities*[22] (ICOS) or the WWRP-Endorsed Project *TEAMx*[23]).

As dense measurement networks are emerging across Europe and other parts of the world with high spatial coverage, harmonisation of operations, data processing and layer height retrievals are key. International operational networks (such as, e.g., E-PROFILE, ACTRIS, ICOS, ARM), not only collect and archive the observations but also strive to harmonise sensor settings and standardise file formats. Further does coordination between different sensor networks receive increasing attention as this clearly benefits synergy applications. Close collaborations with NHMS, academia and instrument manufacturers, are vital to formulate and implement standard operating procedures, to closely monitor house-keeping data, and to develop both detailed correction procedures and advanced data products, including the heights of the ABL sublayers. In Europe, several EU COST actions were paramount for the exchange of knowledge and best practices, including Action 710 (Harmonisation of the pre-processing of meteorological data for atmospheric dispersion models; Seibert et al., 2000), EG-CLIMET (European Ground-based observations of essential variables for CLImate and METeorology; Illingworth et al., 2015), and TOPROF (Towards Operational ground based PROFiling with ceilometers, Doppler lidars and microwave radiometers for improving weather forecasts; Illingworth et al., 2019). Following the progress made in this field over recent decades, the action PROBE[24] (PROfiling the atmospheric Boundary layer at European scale; 2019-2023; Cimini et al., 2020) focuses on the harmonisation of operational procedures which is necessary to ensure also higher-level products are comparable across Europe and even globally.

This review outlines how ground-based remote sensing methods are best exploited in order to gain a detailed understanding of ABL sublayer heights and dynamics. Firstly, the capabilities and limitations of various measurement technologies available to capture different atmospheric profile variables within the ABL are summarised. Choosing the appropriate technology for a given network not only needs to consider the physical information content of the atmospheric quantity observed (temperature, humidity, wind, turbulence, aerosol, or gas) but also whether the sensitivity, resolution, and capabilities of a given sensor are appropriate to monitor the layer(s) of interest. Such instrument characteristics not only differ between sensor types but also

---

[21] https://riurbans.eu/

[22] https://www.icos-cp.eu/projects/icos-cities-project

[23] http://www.teamx-programme.org/

[24] http://www.probe-cost.eu/

between models from different manufacturers and can depend even on firmware, hardware, instrument settings, instrument age, or sampling strategies.

Certain ground-based remote sensing instruments are especially suitable for the operation in automatic measurement networks as these systems are compact, tend to have comparatively lower costs and can be operated with low maintenance under all (or most) weather conditions. Namely, these are (i) microwave radiometers (MWR) and infrared spectrometers (IRS) for the profiling of temperature (and humidity), (ii) (scanning) Doppler wind lidars (DWL) or radar wind profilers (RWP) for the observation wind and turbulence profiles, and (iii) (high-SNR) automatic lidars and ceilometers (ALC) for aerosol profiling in the ABL. Further could the deployment of differential absorption lidars (DIAL) in organised sensor networks increase in the future, adding profile observations of humidity or trace gases.

Numerous methods are available to derive the height of the ABL and its most prominent sublayers, namely the mixing boundary layer height (MBLH) and the height of the residual layer (RLH). The MBLH represents the stable (SBLH) or convective boundary layer height (CBLH), respectively, depending on atmospheric stability conditions. In addition to layer height retrievals, methods are discussed which characterise the ABL according to atmospheric stability and turbulence, cloud dynamics, or aerosol distributions based on atmospheric profile observations. An overview is provided on the capabilities and limitations of the large number of layer height retrievals, including thermodynamic methods, wind and turbulence retrievals and those based on aerosol information. Retrievals based on temperature, turbulence or wind can take into account the atmospheric stratification of the probed layer and are hence able to specifically address either SBLH or CBLH. The height of the surface-based temperature inversion (SBIH) can further be determined from temperature profile data while a low-level jet can be diagnosed from wind observations. Aerosol-based methods again analyse the result of recent physical and chemical processes, including mixing, advection, aerosol formation, accumulation or hygroscopic growth, and are able to track both MLBH and RLH. They are not able to determine the cause of the change in aerosol vertical characteristics, e.g. whether the tracers were transported as a result of thermal buoyancy or shear-driven turbulence. The RLH can also be assessed based on the height of the capping inversion (CI) in a temperature profile.

For the detection of shallow layers, the near-range capabilities of a ground-based remote sensing profiler are critical while the signal strength (in relation to the noise levels) determines the maximum range observed and data quality within a deep CBL, which can reach several kilometers (3 km, or even higher). Sodars tend to have their strength in the near-range (mostly within the first km) while high-power aerosol research lidars provide high-quality data in greater altitudes and are not very suitable for the assessment of conditions very close to the surface. For lidar systems, there is usually an inverse relation between limitations in the near- and far-range, respectively, because high laser power associated with quality observations at greater altitudes usually goes along with a larger blind-zone near the instrument. For DWL, RWP, ALC, or DIAL, a variety of instrument models is available, with respective range extent capabilities and noise levels. Scanning DWL can reduce the blind zone by adding shallow-angle scan strategies. MWR are very suitable for the assessment of conditions near the ground, given their sensitivity is maximal near the sensor and vertical resolution of their temperature product reduces with increasing altitude. For all systems, studies show that careful processing and detailed quality control are vital to produce high-quality

profile observations. This is particularly critical for measurement uncertainties that propagate to the accuracy of ABL height retrievals.

The morning growth and evening decay of the CBL pose severe challenges to numerical simulations for a range of applications, including air quality, greenhouse gas assessment and numerical weather prediction. When using observations for model evaluation or comparisons, it is crucial to carefully consider the specific uncertainties of the respective measurement used. Also, it is important to understand which atmospheric variable is used for layer detection, as it can introduce systematic biases if e.g. turbulence-derived layer heights are compared to results exploiting aerosol profiles.

Given the different stages of CBL development during morning growth, the continuous monitoring enabled by remote sensing profilers is a clear advantage for the characterization of this period compared to balloon ascends. Profiles from sodar or certain ALC have proven very useful to capture the onset of the CBLH at very low altitudes (< 100 m). Approaches based on high-frequency variations of wind or aerosol are often particularly good at tracking CBLH during morning growth. Turbulence-based results from RWP usually requires longer integration times compared to DWL or ALC that range in the order of minutes. Turbulence- and aerosol-based CBLH during morning growth can be very similar provided appropriate layer attribution is performed. However, several studies report a temporal delay of aerosol-derived CBLH morning growth both relative to temperature-derived CBLH and turbulence-derived growth, with time lags of up to two hours. No clear picture has yet emerged on a potential time lag between the growth of temperature- and turbulence-derived layer heights. Method synergy of high resolution observations (both in time and vertical dimension) is a promising means to better understand and quantify the CBL growth.

Most methods show very good performance during daytime, especially when the CBL is fully developed over the entire ABL. Provided sufficient SNR and careful data processing, CBLH from all retrieval methods can agree within a few hundred metres. A thick entrainment zone (EZ) can result in a weaker delineation at the CBLH, increasing uncertainty in layer detection for all methods. As convective clouds can significantly challenge layer detection, daytime maxima of the layer estimates from temperature-, turbulence-, and aerosol-based methods are most similar in cloud-free conditions. However, also strong shear layers or elevated aerosol layers above the ABL can challenge turbulence-based and aerosol-based algorithms, respectively.

Although CBLH growth rates and maxima are strongly affected by clouds, the majority of ABLH climatology studies to date focus on clear-sky conditions. Cloud cover or even cloud type are considered very rarely. Recent developments in automatic detection algorithms that now consider cloud dynamics are expected to enable more comprehensive assessments in the future. Especially differentiating between boundary layer clouds and those decoupled from the ABL greatly aids interpretation.

The evening transition of the daytime CBL into the nocturnal boundary layer around sunset is directly monitored by turbulence profiles. While turbulence-based layer retrievals and thermodynamic methods are in general agreement at this time of day, aerosol-based MBLH results are particularly uncertain during this time at they try to track the history of recent turbulence activity. Reliable data in the near range, careful processing algorithms and high surface aerosol emission rates increase the likelihood of this transition time to be captured accurately by aerosol profiling methods.

The detection and interpretation of nocturnal layer heights is still prone to significant uncertainty. On average, uncertainty in SBLH detection is estimated around 30-40 %. Since turbulence in the SBL is usually not uniform, the diagnosed layer heights

can differ systematically between thermodynamic, turbulence, or aerosol-based methods. Most methods are challenged when multiple layers are present as the task of layer attribution is considered more uncertain than the simple task of layer detection. Hence at night and early morning, aerosol-based methods are at risk to confuse MBLH and RLH, especially if the composition is similar within the two layers. Turbulence-based layer detection algorithms may be confused by the presence of intermittent turbulence in the RL. Thermodynamic layer detection from MWR profile data is less suitable for the detection of RLH (given lower sensitivity) so that the RL poses less of a problem for the detection of MBLH at night and early morning. The RLH can usually be tracked reliably using thermodynamic retrievals of the CI applied to airborne in-situ sensors or by aerosol-based methods, but also trace gas observations from DIAL or Raman humidity and temperature observations can be exploited. Further investigation is required into the impact of ABL dynamics and atmospheric stability on the relative agreement between SBLH results. At night, instrument synergy between radiometer temperature profiling (IRS, MWR) and aerosol observations from ALC is particularly promising given their respective strengths in observing the SBLH and RLH.

A clear potential is identified for using multiple methods or sensors (*instrument synergy*). These can advance both (i) methodologies and products and (ii) processes studies and applications.

(i) Using the synergy of multiple methods and/or sensors can advance the detection of layer heights and classification procedures:

- Sensors with different range capabilities can be combined to ensure high-quality data are collected along the entire extent of the ABL.

- Multiple sensor types can be combined to retrieve atmospheric variables with different physical information content that can then be used to calculate advanced synergy parameters (such as the bulk Richardson number) feeding into the layer height retrieval (combined by e.g. AI or fuzzy logic).

- Combining layer estimates from a range of methods provides a valuable basis for the assessment of layer height uncertainty, the latter still being a challenging topic due to the lack of an objective reference standard.

- ABL classification schemes are emerging that not only provide layer heights but also incorporate the source (surface-driven, cloud-driven) or nature (buoyancy, shear) of turbulent exchanges or can differentiate between different aerosol types. Where multiple measurements are combined that represent different physical aspects of the ABL, such tools can be particularly powerful.

(ii) Incorporating multiple sensors is extremely valuable for process studies as well as model evaluation.

- Naturally, utilising multiple sensors across an entire measurement network adds spatial information in the horizontal domain, which allows for variations in layer heights to be assessed and interpreted (in relation to e.g., surface forcing, local- or regional circulations, synoptic conditions) but also for transport processes to be better detected (e.g. horizontal advection within the ABL or long-range transport).

– Where observations of multiple atmospheric variables are available simultaneously, they allow for the connections between processes to be explained (e.g. understanding the vertical distribution of aerosols as a result of turbulent mixing processes that form in response to the thermodynamic structure of the ABL).

– Finally, synergy of multiple sensor networks with different types of profilers that operate continuously starts to portray the four-dimensional complexity of ABL dynamics.

It can be concluded that ground-based ABL profile remote sensing is a powerful means to gain high-resolution observations of the atmospheric boundary layer – to date, the most under-sampled part of the atmosphere. The diversity in measurement technology and algorithm variety bears a challenge for the quantification of retrieval uncertainty but should also be considered an advantage for powerful process studies and synergy exploitation of the increasingly rich operational measurement networks.

Code availability.   Not applicable

Data availability.   Not applicable

Code and data availability.   Not applicable.

Author contributions.   SK prepared the manuscript with the following co-author contributions: JABA [Sections 1, 2], MCC [Sections 1, 2, 3], JLGR [Section 1, 2, 4], MJC [Section 1, 2, 4], DC [Sections 2, 3], EJOC [Section 2, 3, 4], MHe [Section 2], MHa [Section 3]. The manuscript is based on an earlier version that was led by JABA. MJP and JABA created Figure 2 and Figure 3. All authors contributed to the manuscript outline. MHa and LAA performed a final revision of the manuscript. AI and DR contributed with funding support through their roles as chairs of the COST Action TOPROF. MHa and DC contributed with funding support through their roles as chairs of the COST Action PROBE.

Competing interests.   The authors declare no conflict of interest.

Acknowledgements.   The authors would like to thank both reviewers for their valuable comments. In particular, we are grateful for the extraordinarily detailed feedback provided by Frank Beyrich which contributed significantly to the quality of this manuscript. This article is based upon work from COST Action CA18235 PROBE, supported by COST (European Cooperation in Science and Technology, www.cost.eu). Support from COST Action ES1303 TOPROF is also acknowledged. SK is funded by DIM-Qi2 (Réseau de recherche Qualité de l'air en Ile-de-France) and Agence National de la Recherche under contract #ANR-20-CE22-0013 (H2C). LAA, JABA, JLGR thank the Spanish Ministry of Economy and Competitiveness (MINECO) for support through project ELPIS (PID2020-120015RB-I00), INTEGRATYON[3] (PID2020.117825GB.C21), the Regional Government of Andalusia through project AEROPRE (P18-RT-3820) and ADAPNE (P20-00136), and the University of Granada, Programa Operativo FEDER Andalucia 2014-2020 through project DEM3TRIOS (A-RNM-430-UGR20) and the Earth System Excellence Units Program. JABA received funding from the Marie Sklodowska-Curie Action Cofund 2016 EU project – Athenea3i under grant agreement no. 754446. MJC is co-funded by national Portuguese funds through FCT - Fundação para a Ciência e Tecnologia, I.P., in the framework of the ICT project with the references UIDB/04683/2020 and UIDP/04683/2020, as well as through TOMAQAPA (PTDC/CTAMET/29678/2017) project.

References

1415 Abril-Gago, J., Guerrero-Rascado, J. L., Costa, M. J., Bravo-Aranda, J. A., Sicard, M., Bermejo-Pantaleón, D., Bortoli, D., Granados-Muñoz, M. J., Rodríguez-Gómez, A., Muñoz-Porcar, C., Comerón, A., Ortiz-Amezcua, P., Salgueiro, V., Jiménez-Martín, M. M., and Alados-Arboledas, L.: Statistical validation of Aeolus L2A particle backscatter coefficient retrievals over ACTRIS/EARLINET stations in the Iberian Peninsula, Atmos. Chem. Phys., pp. 1–51, https://doi.org/10.5194/ACP-2021-388, 2021.

Allabakash, S., Yasodha, P., Bianco, L., Venkatramana Reddy, S., Srinivasulu, P., and Lim, S.: Improved boundary layer height measurement
1420 using a fuzzy logic method: diurnal and seasonal variabilities of the convective boundary layer over a tropical station, J. Geophys. Res. Atmos., 122, 9211–9232, https://doi.org/10.1002/2017JD027615, 2017.

AMS, A. M. S.: American Meteorological Society Glossary of Meteorology, http://glossary.ametsoc.org/, 2017.

Angelini, F., Barnaba, F., Landi, T. C., Caporaso, L., and Gobbi, G. P.: Study of atmospheric aerosols and mixing layer by LIDAR, Radiant. Prot. Dosim. 137, 275–279, https://doi.org/10.1093/rpd/ncp219, 2009.

1425 Angevine, W., Senff, C., and Westwater, E.: Boundary layers/Observational Techniques-Remote, in: Encyclopedia of Atmospheric Sciences, edited by Holton, J. R., pp. 271–279, Academic Press, Oxford, https://doi.org/10.1016/B0-12-227090-8/00089-0, 2003.

Angevine, W. M., White, A. B., and Avery, S. K.: Boundary-layer depth and entrainment zone characterization with a boundary-layer profiler, Boundary-Layer Meteorol., 68, 375–385, https://doi.org/10.1007/BF00706797, 1994.

Ansmann, A., Wandinger, U., Riebesell, M., Weitkamp, C., and Michaelis, W.: Independent measurement of extinction and backscatter
1430 profiles in cirrus clouds by using a combined Raman elastic-backscatter lidar, Appl. Opt., 31, 7113–7131, 1992.

Ao, C. O., Waliser, D. E., Chan, S. K., Li, J.-L., Tian, B., Xie, F., and Mannucci, A. J.: Planetary boundary layer heights from GPS radio occultation refractivity and humidity profiles, J. Geophys. Res. Atmos., 117, https://doi.org/10.1029/2012JD017598, d16117, 2012.

Argentini, S., Viola, A., Sempreviva, A., and Petenko, I.: Summer boundary-layer height at the plateau site of Dome C, Antarctica, Boundary-Layer Meteorol., 115, 409–422, 2005.

1435 Aryee, J. N. A., Amekudzi, L. K., Preko, K., Atiah, W. A., and Danuor, S. K.: Estimation of planetary boundary layer height from radiosonde profiles over West Africa during the AMMA field campaign : Intercomparison of different methods, Sci. Afr. 7, https://doi.org/10.1016/j.sciaf.2019.e00228, 2020.

Baars, H., Ansmann, A., Engelmann, R., and Althausen, D.: Continuous monitoring of the boundary-layer top with lidar, Atmos. Chem. Phys., 8, 7281–7296, https://doi.org/10.5194/acp-8-7281-2008, 2008.

1440 Baars, H., Kanitz, T., Engelmann, R., Althausen, D., Heese, B., Komppula, M., Preißler, J., Tesche, M., Ansmann, A., Wandinger, U., Lim, J.-H., Ahn, J. Y., Stachlewska, I. S., Amiridis, V., Marinou, E., Seifert, P., Hofer, J., Skupin, A., Schneider, F., Bohlmann, S., Foth, A., Bley, S., Pfüller, A., Giannakaki, E., Lihavainen, H., Viisanen, Y., Hooda, R. K., Pereira, S. N., Bortoli, D., Wagner, F., Mattis, I., Janicka, L., Markowicz, K. M., Achtert, P., Artaxo, P., Pauliquevis, T., Souza, R. A. F., Sharma, V. P., van Zyl, P. G., Beukes, J. P., Sun, J., Rohwer, E. G., Deng, R., Mamouri, R.-E., and Zamorano, F.: An overview of the first decade of Polly[NET]: an emerging network of automated
1445 Raman-polarization lidars for continuous aerosol profiling, Atmos. Chem. Phys., 16, 5111–5137, https://doi.org/10.5194/acp-16-5111-2016, 2016.

Ballish, B. A., Kumar, V. K., Ballish, B. A., and Kumar, V. K.: Systematic Differences in Aircraft and Radiosonde Temperatures, Bull. Amer. Meteor. Soc., 89, 1689–1708, https://doi.org/10.1175/2008BAMS2332.1, 2008.

Balsley, B. B., Frehlich, R. G., Jensen, M. L., and Meillier, Y.: High-resolution in situ profiling through the stable boundary layer: Examination of the SBL top in terms of minimum shear, maximum stratification, and turbulence decrease, J. Atmos. Sci., 63, 1291–1307, https://doi.org/10.1175/JAS3671.1, 2006.

Banakh, V. A. and Smalikho, I. N.: Estimation of the turbulence energy dissipation rate from pulsed Doppler lidar data, Atmos. Oceanic Opt., 10, 957–965, 1997.

Banakh, V. A. and Smalikho, I. N.: Lidar observations of atmospheric internal waves in the boundary layer of the atmosphere on the coast of Lake Baikal, Atmos. Meas. Tech., 9, 5239–5248, https://doi.org/10.5194/amt-9-5239-2016, 2016.

Banakh, V. A., Smalikho, I. N., Pichugina, E. L., and Brewer, W. A.: Representativeness of measurements of the dissipation rate of turbulence energy by scanning Doppler lidar, Atmos. Oceanic Opt., 23, 48–54, https://doi.org/10.1134/S1024856010010100, 2010.

Banks, R. F., Tiana-Alsina, J., Rocadenbosch, F., and Baldasano, J. M.: Performance Evaluation of the Boundary-Layer Height from Lidar and the Weather Research and Forecasting Model at an Urban Coastal Site in the North-East Iberian Peninsula, Boundary-Layer Meteorol., 157, 265–292, https://doi.org/10.1007/s10546-015-0056-2, 2015.

Banta, R. M., Senff, C. J., White, A. B., Trainer, M., McNider, R. T., Valente, R. J., Mayor, S. D., Alvarez, R. J., Hardesty, R. M., Parrish, D., and Fehsenfeld, F. C.: Daytime buildup and nighttime transport of urban ozone in the boundary layer during a stagnation episode, J. Geophys. Res. Atmos., 103, 22 519–22 544, https://doi.org/10.1029/98JD01020, 1998.

Banta, R. M., Pichugina, Y. L., and Brewer, W. A.: Turbulent velocity-variance profiles in the stable boundary layer generated by a nocturnal low-level jet, J. Atmos. Sci., 63, 2700–2719, https://doi.org/10.1175/JAS3776.1, 2006.

Banta, R. M., Pichugina, Y. L., Kelley, N. D., Hardesty, R. M., and Brewer, W. A.: Wind Energy Meteorology: Insight into Wind Properties in the Turbine-Rotor Layer of the Atmosphere from High-Resolution Doppler Lidar, Bull. Amer. Meteor. Soc., 94, https://doi.org/10.1175/BAMS-D-11-00057.1, 2013.

Barlow, J., F., Dunbar, T. M., Nemitz, E. G., Wood, C. R., Gallagher, M., Davies, F., O'Connor, E., and Harrison, R. M.: Boundary layer dynamics over London, UK, as observed using Doppler lidar during REPARTEE-II, Atmos. Chem. Phys., 11, 2111—-2125, https://doi.org/10.5194/acp-11-2111-2011, 2011.

Barlow, J., Best, M., Bohnenstengel, S. I., Clark, P., Grimmond, S., Lean, H., Christen, A., Emeis, S., Haeffelin, M., Harman, I. N., Lemonsu, A., Martilli, A., Pardyjak, E., Rotach, M. W., Ballard, S., Boutle, I., Brown, A., Cai, X., Carpentieri, M., Coceal, O., Crawford, B., Di Sabatino, S., Dou, J., Drew, D. R., Edwards, J. M., Fallmann, J., Fortuniak, K., Gornall, J., Gronemeier, T., Halios, C. H., Hertwig, D., Hirano, K., Holtslag, A. A. M., Luo, Z., Mills, G., Nakayoshi, M., Pain, K., Schlünzen, K. H., Smith, S., Soulhac, L., Steeneveld, G.-J., Sun, T., Theeuwes, N. E., Thomson, D., Voogt, J. A., Ward, H. C., Xie, Z.-T., Zhong, J., Barlow, J., Best, M., Bohnenstengel, S. I., Clark, P., Grimmond, S., Lean, H., Christen, A., Emeis, S., Haeffelin, M., Harman, I. N., Lemonsu, A., Martilli, A., Pardyjak, E., Rotach, M. W., Ballard, S., Boutle, I., Brown, A., Cai, X., Carpentieri, M., Coceal, O., Crawford, B., Sabatino, S. D., Dou, J., Drew, D. R., Edwards, J. M., Fallmann, J., Fortuniak, K., Gornall, J., Gronemeier, T., Halios, C. H., Hertwig, D., Hirano, K., Holtslag, A. A. M., Luo, Z., Mills, G., Nakayoshi, M., Pain, K., Schlünzen, K. H., Smith, S., Soulhac, L., Steeneveld, G.-J., Sun, T., Theeuwes, N. E., Thomson, D., Voogt, J. A., Ward, H. C., Xie, Z.-T., and Zhong, J.: Developing a Research Strategy to Better Understand, Observe, and Simulate Urban Atmospheric Processes at Kilometer to Subkilometer Scales, Bull. Amer. Meteor. Soc., 98, ES261–ES264, https://doi.org/10.1175/BAMS-D-17-0106.1, 2017.

Barlow, J. F.: Progress in observing and modelling the urban boundary layer, Urban Clim. 10, 216–240, https://doi.org/10.1016/j.uclim.2014.03.011, 2014.

Barlow, J. F., Halios, C. H., Lane, S. E., and Wood, C. R.: Observations of urban boundary layer structure during a strong urban heat island event, Environ. Fluid Mach. 15, 373–398, https://doi.org/10.1007/s10652-014-9335-6, 2015.

Basha, G. and Ratnam, M. V.: Identification of atmospheric boundary layer height over a tropical station using high-resolution radiosonde refractivity profiles: Comparison with GPS radio occultation measurements, J. Geophys. Res. Atmos., 114, https://doi.org/10.1029/2008JD011692, 2009.

Behrendt, A., Wulfmeyer, V., Bauer, H.-S., Schaberl, T., Di Girolamo, P., Summa, D., Kiemle, C., Ehret, G., Whiteman, D. N., Demoz, B. B., Browell, E. V., Ismail, S., Ferrare, R., Kooi, S., and Wang, J.: Intercomparison of Water Vapor Data Measured with Lidar during IHOP_2002. Part I: Airborne to Ground-Based Lidar Systems and Comparisons with Chilled-Mirror Hygrometer Radiosondes, J. Atmos. Oceanic Technol., 24, 3–21, https://doi.org/10.1175/JTECH1924.1, 2007.

Behrendt, A., Wulfmeyer, V., Hammann, E., Muppa, S., and Pal, S.: Profiles of second-to fourth-order moments of turbulent temperature fluctuations in the convective boundary layer: first measurements with rotational Raman lidar, Atmos. Chem. Phys., 15, 5485–5500, https://doi.org/10.5194/acp-15-5485-2015, 2015.

Behrendt, A., Wulfmeyer, V., Senff, C., Kumar Muppa, S., Späth, F., Lange, D., Kalthoff, N., and Wieser, A.: Observation of sensible and latent heat flux profiles with lidar, Atmos. Meas. Tech., 13, 3221–3233, https://doi.org/10.5194/AMT-13-3221-2020, 2020.

Bennett, L. J., Weckwerth, T. M., Blyth, A. M., Geerts, B., Miao, Q., and Richardson, Y. P.: Observations of the evolution of the nocturnal and convective boundary layers and the structure of open-celled convection on 14 June 2002, Mon. Wea. Rev., 138, 2589–2607, https://doi.org/10.1175/2010MWR3200.1, 2010.

Berg, L. K., Newsom, R. K., and Turner, D. D.: Year-Long Vertical Velocity Statistics Derived from Doppler Lidar Data for the Continental Convective Boundary Layer, J. Appl. Meteor. Climatol., 56, 2441–2454, https://doi.org/10.1175/JAMC-D-16-0359.1, 2017.

Berkes, F., Neis, P., Schultz, M. G., Bundke, U., Rohs, S., Smit, H. G., Wahner, A., Konopka, P., Boulanger, D., Nédélec, P., Thouret, V., and Petzold, A.: In situ temperature measurements in the upper troposphere and lowermost stratosphere from 2 decades of IAGOS long-term routine observation, Atmos. Chem. Phys., 17, 12 495–12 508, https://doi.org/10.5194/acp-17-12495-2017, 2017.

Beyrich, F.: Mixing-height estimation in the convective boundary layer using sodar data, Boundary-Layer Meteorol., 74, 1–18, https://doi.org/10.1007/BF00715708, 1995.

Beyrich, F.: Mixing height estimation from sodar data — A critical discussion, Atmos. Environ., 31, 3941–3953, https://doi.org/10.1016/S1352-2310(97)00231-8, 1997.

Beyrich, F. and Görsdorf, U.: Composing the diurnal cycle of mixing height from simultaneous sodar and wind profiler measurements, Boundary-Layer Meteorol., 76, 387–394, https://doi.org/10.1007/BF00709240, 1995.

Beyrich, F. and Gryning, S.-E.: Estimation of the Entrainment Zone Depth in a Shallow Convective Boundary Layer from Sodar Data, J. Appl. Meteor., 37, 255–268, https://doi.org/10.1175/1520-0450(1998)037<0255:EOTEZD>2.0.CO;2, 1998.

Beyrich, F. and Leps, J. P.: An operational mixing height data set from routine radiosoundings at Lindenberg: Methodology, Meteor. Z., https://doi.org/10.1127/0941-2948/2012/0333, 2012.

Bian, J., Chen, H., Vömel, H., Duan, Y., Xuan, Y., and Lü, D.: Intercomparison of humidity and temperature sensors: GTS1, Vaisala RS80, and CFH, Adv. Atmos. Sci. 28, 139–146, https://doi.org/10.1007/s00376-010-9170-8, 2011.

Bianco, L. and Wilczak, J. M.: Convective Boundary Layer Depth: Improved Measurement by Doppler Radar Wind Profiler Using Fuzzy Logic Methods, J. Atmos. Oceanic Technol., 19, 1745–1758, https://doi.org/10.1175/1520-0426(2002)019<1745:CBLDIM>2.0.CO;2, 2002.

Bianco, L., Wilczak, J. M., and White, A. B.: Convective Boundary Layer Depth Estimation from Wind Profilers: Statistical Comparison between an Automated Algorithm and Expert Estimations, J. Atmos. Oceanic Technol., 25, 1397–1413, https://doi.org/10.1175/2008JTECHA981.1, 2008.

Bianco, L., Friedrich, K., Wilczak, J. M., Hazen, D., Wolfe, D., Delgado, R., Oncley, S. P., and Lundquist, J. K.: Assessing the accuracy of microwave radiometers and radio acoustic sounding systems for wind energy applications, Atmos. Meas. Tech., 10, 1707–1721, https://doi.org/10.5194/amt-10-1707-2017, 2017.

Bianco, L., Muradyan, P., Djalalova, I., Wilczak, J. M., Olson, J. B., Kenyon, J. S., Kotamarthi, R., Lantz, K., Long, C., and Turner, D.: Comparison of Observations and Predictions of Daytime Planetary-Boundary-Layer Heights and Surface Meteorological Variables in the Columbia River Gorge and Basin During the Second Wind Forecast Improvement Project, Boundary-Layer Meteorol., 182, 147–172, https://doi.org/10.1007/s10546-021-00645-x, 2022.

Blumberg, W., Turner, D., Löhnert, U., and Castleberry, S.: Ground-based temperature and humidity profiling using spectral infrared and microwave observations. Part II: Actual retrieval performance in clear-sky and cloudy conditions, J. Appl. Meteor. Climatol., 54, 2305–2319, https://doi.org/10.1175/JAMC-D-15-0005.1, 2015.

Bodeker, G. E., Bojinski, S., Cimini, D., Dirksen, R. J., Haeffelin, M., Hannigan, J. W., Hurst, D. F., Leblanc, T., Madonna, F., Maturilli, M., Mikalsen, A. C., Philipona, R., Reale, T., Seidel, D. J., Tan, D. G. H., Thorne, P. W., Vömel, H., and Wang, J.: Reference Upper-Air Observations for Climate: From Concept to Reality, Bull. Amer. Meteor. Soc., 97, 123–135, https://doi.org/10.1175/BAMS-D-14-00072.1, 2016.

Bodini, N., Lundquist, J. K., and Newsom, R. K.: Estimation of turbulence dissipation rate and its variability from sonic anemometer and wind Doppler lidar during the XPIA field campaign, Atmos. Meas. Tech., 11, 4291–4308, https://doi.org/10.5194/amt-11-4291-2018, 2018.

Bonin, T. A., Blumberg, W. G., Klein, P. M., and Chilson, P. B.: Thermodynamic and Turbulence Characteristics of the Southern Great Plains Nocturnal Boundary Layer Under Differing Turbulent Regimes, Boundary-Layer Meteorol., 157, 401–420, https://doi.org/10.1007/S10546-015-0072-2, 2015.

Bonin, T. A., Newman, J. F., Klein, P. M., Chilson, P. B., and Wharton, S.: Improvement of vertical velocity statistics measured by a Doppler lidar through comparison with sonic anemometer observations, Atmos. Meas. Tech., 9, 5833–5852, https://doi.org/10.5194/amt-9-5833-2016, 2016.

Bonin, T. A., Choukulkar, A., Brewer, W. A., Sandberg, S. P., Weickmann, A. M., Pichugina, Y. L., Banta, R. M., Oncley, S. P., and Wolfe, D. E.: Evaluation of turbulence measurement techniques from a single Doppler lidar, Atmos. Meas. Tech., 10, 3021–3039, https://doi.org/10.5194/amt-10-3021-2017, 2017.

Bonin, T. A., Carroll, B. J., Hardesty, R. M., Brewer, W. A., Hajny, K., Salmon, O. E., and Shepson, P. B.: Doppler Lidar Observations of the Mixing Height in Indianapolis Using an Automated Composite Fuzzy Logic Approach, J. Atmos. Oceanic Technol., 35, 473–490, https://doi.org/10.1175/JTECH-D-17-0159.1, 2018.

Bonin, T. A., Klein, P. M., and Chilson, P. B.: Contrasting Characteristics and Evolution of Southerly Low-Level Jets During Different Boundary-Layer Regimes, Boundary-Layer Meteorol., 174, 179–202, https://doi.org/10.1007/S10546-019-00481-0, 2019.

Bosveld, F. C., Baas, P., Beljaars, A. C., Holtslag, A. A., de Arellano, J. V. G., and van de Wiel, B. J.: Fifty Years of Atmospheric Boundary-Layer Research at Cabauw Serving Weather, Air Quality and Climate, Boundary-Layer Meteorol., 177, 583–612, https://doi.org/10.1007/s10546-020-00541-w, 2020.

1560 Boy, M., Thomson, E. S., Navarro, J. C., Arnalds, O., Batchvarova, E., Bäck, J., Berninger, F., Bilde, M., Dagsson-Waldhauserova, P., Castarède, D., Dalirian, M., De Leeuw, G., Dragosics, M., Duplissy, E. M., Duplissy, J., Ekman, A. M., Fang, K., Gallet, J. C., Glasius, M., Gryning, S. E., Grythe, H., Hansson, H. C., Hansson, M., Isaksson, E., Iversen, T., Jonsdottir, I., Kasurinen, V., Kirkevåg, A., Korhola, A., Krejci, R., Egill Kristjansson, J., Lappalainen, H. K., Lauri, A., Leppäranta, M., Lihavainen, H., Makkonen, R., Massling, A., Meinander, O., Douglas Nilsson, E., Olafsson, H., Pettersson, J. B., Prisle, N. L., Riipinen, I., Roldin, P., Ruppel, M., Salter, M., Sand, M., Seland,
1565 O., Seppä, H., Skov, H., Soares, J., Stohl, A., Ström, J., Svensson, J., Swietlicki, E., Tabakova, K., Thorsteinsson, T., Virkkula, A., Weyhenmeyer, G. A., Wu, Y., Zieger, P., and Kulmala, M.: Interactions between the atmosphere, cryosphere, and ecosystems at northern high latitudes, https://doi.org/10.5194/acp-19-2015-2019, 2019.

Bradley, R. S., Keimig, F. T., and Diaz, H. F.: Recent changes in the North American Arctic boundary layer in winter, J. Geophys. Res. Atmos., 98, 8851–8858, https://doi.org/10.1029/93JD00311, 1993.

1570 Bradley, S.: Atmospheric Acoustic Remote Sensing, Boca Raton: CRC Press., 2007.

Bravo-Aranda, J. A., Titos, G., Granados-Muñoz, M. J., Guerrero-Rascado, J. L., Navas-Guzmán, F., Valenzuela, A., Lyamani, H., Olmo, F. J., Andrey, J., and Alados-Arboledas, L.: Study of mineral dust entrainment in the planetary boundary layer by lidar depolarisation technique, Tellus B, 67, 26 180, https://doi.org/10.3402/tellusb.v67.26180, 2015.

Bravo-Aranda, J. A., de Arruda Moreira, G., Navas-Guzmán, F., Granados-Muñoz, M. J., Guerrero-Rascado, J. L., Pozo-Vázquez, D.,
1575 Arbizu-Barrena, C., Olmo Reyes, F. J., Mallet, M., and Alados Arboledas, L.: A new methodology for PBL height estimations based on lidar depolarization measurements: analysis and comparison against MWR and WRF model-based results, Atmos. Chem. Phys., 17, 6839–6851, https://doi.org/10.5194/acp-17-6839-2017, 2017.

Brotzge, J. A., Wang, J., Thorncroft, C., Joseph, E., Bain, N., Bassill, N., Farruggio, N., Freedman, J., Hemker Jr, K., Johnston, D., et al.: A technical overview of the New York State Mesonet standard network, 37, 1827–1845, 2020.

1580 Cadeddu, M. P., Liljegren, J. C., and Turner, D. D.: The Atmospheric radiation measurement (ARM) program network of microwave radiometers: instrumentation, data, and retrievals, Atmos. Meas. Tech., 6, 2359–2372, https://doi.org/10.5194/amt-6-2359-2013, 2013.

Caicedo, V., Rappenglück, B., Lefer, B., Morris, G., Toledo, D., and Delgado, R.: Comparison of aerosol lidar retrieval methods for boundary layer height detection using ceilometer aerosol backscatter data, Atmos. Meas. Tech., 10, 1609–1622, https://doi.org/10.5194/amt-10-1609-2017, 2017.

1585 Caicedo, V., Rappenglueck, B., Cuchiara, G., Flynn, J., Ferrare, R., Scarino, A. J., Berkoff, T., Senff, C., Langford, A., and Lefer, B.: Bay Breeze and Sea Breeze Circulation Impacts on the Planetary Boundary Layer and Air Quality From an Observed and Modeled DISCOVER-AQ Texas Case Study, J. Geophys. Res. Atmos., 124, 7359–7378, https://doi.org/10.1029/2019JD030523, 2019.

Caicedo, V., Delgado, R., Sakai, R., Knepp, T., Williams, D., Cavender, K., Lefer, B., and Szykman, J.: An Automated Common Algorithm for Planetary Boundary Layer Retrievals Using Aerosol Lidars in Support of the U.S. EPA Photochemical Assessment Monitoring Stations
1590 Program, J. Atmos. Oceanic Technol., 37, 1847–1864, https://doi.org/10.1175/JTECH-D-20-0050.1, 2020.

Canny, J.: A Computational Approach to Edge Detection, IEEE T. Pattern Anal. PAMI-8, 679–698, https://doi.org/10.1109/TPAMI.1986.4767851, 1986.

Caumont, O., Cimini, D., Löhnert, U., Alados-Arboledas, L., Bleisch, R., Buffa, F., Ferrario, M. E., Haefele, A., Huet, T., Madonna, F., and Pace, G.: Assimilation of humidity and temperature observations retrieved from ground-based microwave radiometers into a convective-
1595 scale NWP model, Quart. J. Roy. Meteor. Soc., 142, 2692–2704, https://doi.org/10.1002/qj.2860, 2016.

Chan, K. M. and Wood, R.: The seasonal cycle of planetary boundary layer depth determined using COSMIC radio occultation data, J. Geophys. Res., 118, 422–434, https://doi.org/10.1002/2013JD020147, 2013.

Cimini, D., Hewison, T. J., Martin, L., Güldner, J., Gaffard, C., and Marzano, F. S.: Temperature and humidity profile retrievals from ground-based microwave radiometers during TUC, Meteor. Z., 15, 45–56, https://doi.org/10.1127/0941-2948/2006/0099, 2006.

Cimini, D., Campos, E., Ware, R., Albers, S., Giuliani, G., Oreamuno, J., Joe, P., Koch, S. E., Cober, S., and Westwater, E.: Thermodynamic Atmospheric Profiling During the 2010 Winter Olympics Using Ground-Based Microwave Radiometry, IEEE Trans. Geosci. Remote Sens. 49, 4959–4969, https://doi.org/10.1109/TGRS.2011.2154337, 2011.

Cimini, D., De Angelis, F., Dupont, J.-C., Pal, S., and Haeffelin, M.: Mixing layer height retrievals by multichannel microwave radiometer observations, Atmos. Meas. Tech., 6, 2941–2951, https://doi.org/10.5194/amt-6-2941-2013, 2013.

Cimini, D., Nelson, M., Güldner, J., and Ware, R.: Forecast indices from a ground-based microwave radiometer for operational meteorology, Atmos. Meas. Tech., 8, 315–333, https://doi.org/10.5194/amt-8-315-2015, 2015.

Cimini, D., Haeffelin, M., Kotthaus, S., Löhnert, U., Martinet, P., O'Connor, E., Walden, C., Collaud Coen, M., and Preissler, J.: Towards the profiling of the atmospheric boundary layer at European scale — introducing the COST Action PROBE, Bull. Atmos. Sci. and Technol. pp. 23–42, https://doi.org/10.1007/s42865-020-00003-8, 2020.

CIMO-TECO, W., ed.: GCOS Upper Air Network (GUAN) Radiosonde Observations Past, Present and Future, O3, https://www.wmo.int/pages/prog/www/IMOP/documents/O3_3_Oakley_ExtendedAbstract.pdf, 2018.

Cohen, A. E., Cavallo, S. M., Coniglio, M. C., and Brooks, H. E.: A Review of Planetary Boundary Layer Parameterization Schemes and Their Sensitivity in Simulating Southeastern U.S. Cold Season Severe Weather Environments, Wea. Forecasting, 30, 591–612, https://doi.org/10.1175/WAF-D-14-00105.1, 2015.

Cohn, S. A.: Radar measurements of turbulent eddy dissipation rate in the troposphere: A comparison of techniques, J. Atmos. Oceanic Technol., 12, 85–95, https://doi.org/10.1175/1520-0426(1995)012<0085:RMOTED>2.0.CO;2, 1995.

Cohn, S. A. and Angevine, W. M.: Boundary layer height and entrainment zone thickness measured by lidars and wind-profiling radars, J. Appl. Meteor., 39, 1233–1247, https://doi.org/10.1175/1520-0450(2000)039<1233:BLHAEZ>2.0.CO;2, 2000.

Collaud Coen, M., Praz, C., Haefele, A., Ruffieux, D., Kaufmann, P., and Calpini, B.: Determination and climatology of the planetary boundary layer height above the Swiss plateau by in situ and remote sensing measurements as well as by the COSMO-2 model, Atmos. Chem. Phys., 14, 13 205–13 221, https://doi.org/10.5194/acp-14-13205-2014, 2014.

Compton, J. C., Delgado, R., Berkoff, T. A., Hoff, R. M., Compton, J. C., Delgado, R., Berkoff, T. A., and Hoff, R. M.: Determination of Planetary Boundary Layer Height on Short Spatial and Temporal Scales: A Demonstration of the Covariance Wavelet Transform in Ground-Based Wind Profiler and Lidar Measurements, J. Atmos. Oceanic Technol., 30, 1566–1575, https://doi.org/10.1175/JTECH-D-12-00116.1, 2013.

Da Silva, M. P., Rocadenbosch, F., Tanamachi, R. L., and Saeed, U.: Motivating a Synergistic Mixing-Layer Height Retrieval Method Using Backscatter Lidar Returns and Microwave-Radiometer Temperature Observations, IEEE Trans. Geosci. Remote Sens. 60, https://doi.org/10.1109/TGRS.2022.3158401, 2022.

Dang, R., Yang, Y., Hu, X.-M., Wang, Z., and Zhang, S.: A Review of Techniques for Diagnosing the Atmospheric Boundary Layer Height (ABLH) Using Aerosol Lidar Data, Remote Sens. 11, 1590, https://doi.org/10.3390/rs11131590, 2019.

de Arruda Moreira, G., Guerrero-Rascado, J., Bravo-Aranda, J., Benavent-Oltra, J., Ortiz-Amezcua, P., Róman, R., Bedoya-Velásquez, A., Landulfo, E., and Alados-Arboledas, L.: Study of the planetary boundary layer by microwave radiometer, elastic lidar and Doppler lidar estimations in Southern Iberian Peninsula, Atmos. Res., 213, 185–195, https://doi.org/10.1016/j.atmosres.2018.06.007, 2018.

de Arruda Moreira, G., Guerrero-Rascado, J. L., Benavent-Oltra, J. A., Ortiz-Amezcua, P., Román, R., E. Bedoya-Velásquez, A., Bravo-Aranda, J. A., Olmo Reyes, F. J., Landulfo, E., and Alados-Arboledas, L.: Analyzing the turbulent planetary boundary layer by re-

mote sensing systems: the Doppler wind lidar, aerosol elastic lidar and microwave radiometer, Atmos. Chem. Phys., 19, 1263–1280, https://doi.org/10.5194/acp-19-1263-2019, 2019.

de Arruda Moreira, G., Guerrero-Rascado, J. L., Bravo-Aranda, J. A., Foyo-Moreno, I., Cazorla, A., Alados, I., Lyamani, H., Landulfo, E., and Alados-Arboledas, L.: Study of the planetary boundary layer height in an urban environment using a combination of microwave radiometer and ceilometer, Atmos. Res., p. 104932, https://doi.org/10.1016/j.atmosres.2020.104932, 2020.

de Arruda Moreira, G., Sánchez-Hernández, G., Guerrero-Rascado, J. L., Cazorla, A., and Alados-Arboledas, L.: Estimating the urban atmospheric boundary layer height from remote sensing applying machine learning techniques, Atmos. Res., p. 105962, 2022.

de Bruine, M., Apituley, A., Donovan, D., Klein Baltink, H., and de Haij, M.: Pathfinder: Applying graph theory to consistent tracking of daytime mixed layer height with backscatter lidar, Atmos. Meas. Tech., pp. 1893–1909, https://doi.org/10.5194/amt-10-1893-2017, 2017.

de Haij, M., Wauben, W., and Klein Baltink, H.: Determination of mixing layer height from ceilometer backscatter profiles, Remote Sens. pp. 63 620R–63 620R–12, 2006.

De Wekker, S. F. J. and Kossmann, M.: Convective Boundary Layer Heights Over Mountainous Terrain—A Review of Concepts, Front. Earth Sci. 3, 77, https://doi.org/10.3389/feart.2015.00077, 2015.

Di Girolamo, P., De Rosa, B., Flamant, C., Summa, D., Bousquet, O., Chazette, P., Totems, J., and Cacciani, M.: Water vapor mixing ratio and temperature inter-comparison results in the framework of the Hydrological Cycle in the Mediterranean Experiment—Special Observation Period 1, Bull. Atmos. Sci. and Technol. 1, 113–153, https://doi.org/10.1007/s42865-020-00008-3, 2020.

Di Giuseppe, F., Riccio, A., Caporaso, L., Bonafé, G., Gobbi, G. P., and Angelini, F.: Automatic detection of atmospheric boundary layer height using ceilometer backscatter data assisted by a boundary layer model, Quart. J. Roy. Meteor. Soc., 138, 649–663, https://doi.org/10.1002/qj.964, 2012.

Diémoz, H., Barnaba, F., Magri, T., Pession, G., Dionisi, D., Pittavino, S., Tombolato, I. K. F., Campanelli, M., Della Ceca, L. S., Hervo, M., Di Liberto, L., Ferrero, L., and Gobbi, G. P.: Transport of Po Valley aerosol pollution to the northwestern Alps – Part 1: Phenomenology, Atmos. Chem. Phys., 19, 3065–3095, https://doi.org/10.5194/acp-19-3065-2019, 2019a.

Diémoz, H., Paolo Gobbi, G., Magri, T., Pession, G., Pittavino, S., Tombolato, I. K., Campanelli, M., and Barnaba, F.: Transport of Po Valley aerosol pollution to the northwestern Alps-Part 2: Long-term impact on air quality, Atmos. Chem. Phys., 19, 10 129–10 160, https://doi.org/10.5194/acp-19-10129-2019, 2019b.

Dieudonné, E., Ravetta, F., Pelon, J., Goutail, F., and Pommereau, J.-P.: Linking NO2 surface concentration and integrated content in the urban developed atmospheric boundary layer, Geophys. Res. Lett., 40, 1247–1251, https://doi.org/10.1002/grl.50242, 2013.

Dirksen, R. J., Sommer, M., Immler, F. J., Hurst, D. F., Kivi, R., and Vömel, H.: Reference quality upper-air measurements: GRUAN data processing for the Vaisala RS92 radiosonde, Atmos. Meas. Tech., 7, 4463–4490, https://doi.org/10.5194/amt-7-4463-2014, 2014.

Djalalova, I. V., Turner, D. D., Bianco, L., Wilczak, J. M., Duncan, J., Adler, B., and Gottas, D.: Improving thermodynamic profile retrievals from microwave radiometers by including radio acoustic sounding system (RASS) observations, Atmos. Meas. Tech., 15, 521–537, https://doi.org/10.5194/AMT-15-521-2022, 2022.

Duncan, J. B., Bianco, L., Adler, B., Bell, T., Djalalova, I. V., Riihimaki, L., Sedlar, J., Smith, E. N., Turner, D. D., Wagner, T. J., and Wilczak, J. M.: Evaluating convective planetary boundary layer height estimations resolved by both active and passive remote sensing instruments during the CHEESEHEAD19 field campaign, Atmos. Meas. Tech., 15, 2479–2502, https://doi.org/10.5194/AMT-15-2479-2022, 2022.

Eberhard, W. L., Cupp, R. E., and Healy, K. R.: Doppler Lidar Measurement of Profiles of Turbulence and Momentum Flux, J. Atmos. Oceanic Technol., 6, 809–819, https://doi.org/https://doi.org/10.1175/1520-0426(1989)006<0809:DLMOPO>2.0.CO;2, 1989.

Ecklund, W. L., Carter, D. A., and Balsley, B. B.: A UHF wind profiler for the boundary layer: Brief description and initial results, J. Atmos. Oceanic Technol., 5, 432–441, https://doi.org/10.1175/1520-0426(1988)005<0432:AUWPFT>2.0.CO;2, 1988.

Elie Quentin Bessardon, G., Fosu-Amankwah, K., Petersson, A., and Jane Brooks, B.: Evaluation of Windsond S1H2 performance in Kumasi during the 2016 DACCIWA field campaign, Atmos. Meas. Tech., 12, 1311–1324, https://doi.org/10.5194/AMT-12-1311-2019, 2019.

Emeis, S.: Surface-based remote sensing of the atmospheric boundary layer, vol. 40, Springer Science & Business Media, 2010.

Emeis, S., Schäfer, K., and Münkel, C.: Surface-based remote sensing of the mixing-layer height - A review, Meteor. Z., 17, 621–630, https://doi.org/10.1127/0941-2948/2008/0312, 2008.

Emeis, S., Schäfer, K., and Münkel, C.: Observation of the structure of the urban boundary layer with different ceilometers and validation by RASS data, Meteor. Z., 18, 149–154, https://doi.org/10.1127/0941-2948/2009/0365, 2009.

Engelbart, D. A. M. and Bange, J.: Determination of boundary-layer parameters using wind profiler/RASS and sodar/RASS in the frame of the LITFASS project, Theor. Appl. Climatol. 73, 53–65, https://doi.org/10.1007/s00704-002-0693-5, 2002.

Eresmaa, N., Karppinen, A., Joffre, S., Räsänen, J., and Talvitie, H.: Mixing height determination by ceilometer, Atmos. Chem. Phys., 6, 1485–1493, https://doi.org/10.5194/acp-6-1485-2006, 2006.

Eresmaa, N., Härkönen, J., Joffre, S. M., Schultz, D. M., Karppinen, A., and Kukkonen, J.: A three-step method for estimating the mixing height using ceilometer data from the Helsinki testbed, J. Appl. Meteor. Climatol., 51, 2172–2187, https://doi.org/10.1175/JAMC-D-12-058.1, 2012.

Feltz, W. F. and Mecikalski, J. R.: Monitoring high-temporal-resolution convective stability indices using the ground-based Atmospheric Emitted Radiance Interferometer (AERI) during the 3 May 1999 Oklahoma–Kansas tornado outbreak, Wea. Forecasting, 17, 445–455, https://doi.org/10.1175/1520-0434(2002)017<0445:MHTRCS>2.0.CO;2, 2002.

Feltz, W. F., Smith, W. L., Howell, H. B., Knuteson, R. O., Woolf, H., and Revercomb, H. E.: Near-Continuous Profiling of Temperature, Moisture, and Atmospheric Stability Using the Atmospheric Emitted Radiance Interferometer (AERI), J. Appl. Meteor., 42, 584 – 597, https://doi.org/10.1175/1520-0450(2003)042<0584:NPOTMA>2.0.CO;2, 2003.

Finnigan, J. J., Einaudi, F., and Fua, D.: The interaction between an internal gravity wave and turbulence in the stably-stratified nocturnal boundary layer., J. Atmos. Sci., 41, 2409–2436, https://doi.org/10.1175/1520-0469(1984)041<2409:TIBAIG>2.0.CO;2, 1984.

Flamant, P., Cuesta, J., Denneulin, M.-L., Dabas, A., and Huber, D.: ADM-Aeolus retrieval algorithms for aerosol and cloud products, Tellus A, 60 A, 273–288, https://doi.org/10.1111/J.1600-0870.2007.00287.X, 2016.

Fochesatto, G. J., Drobinski, P., Flamant, C., Guedalia, D., Sarrat, C., Flamant, P. H., and Pelon, J.: Evidence of dynamical coupling between the residual layer and the developing convective boundary layer, Boundary-Layer Meteorol., 99, 451–464, https://doi.org/10.1023/A:1018935129006, 2001.

Foken, T., ed.: Springer Handbook of Atmospheric Measurements, Springer Handbooks, Springer International Publishing, Cham, https://doi.org/10.1007/978-3-030-52171-4, 2021.

Frehlich, R., Meillier, Y., Jensen, M. L., Balsley, B., and Sharman, R.: Measurements of Boundary Layer Profiles in an Urban Environment, J. Appl. Meteor. Climatol., 45, 821–837, https://doi.org/10.1175/JAM2368.1, 2006.

Frehlich, R., Meillier, Y., and Jensen, M. L.: Measurements of Boundary Layer Profiles with In Situ Sensors and Doppler Lidar, J. Atmos. Oceanic Technol., 25, 1328–1340, https://doi.org/10.1175/2007JTECHA963.1, 2008.

Freudenthaler, V., Linné, H., Chaikovski, A., Rabus, D., and Groß, S.: EARLINET lidar quality assurance tools, Atmos. Meas. Tech. Disc., 2018, 1–35, https://doi.org/10.5194/amt-2017-395, 2018.

1710 Fromm, M., Lindsey, D. T., Servranckx, R., Yue, G., Trickl, T., Sica, R., Doucet, P., and Godin-Beekmann, S.: The Untold Story of Pyrocumulonimbus, Bull. Amer. Meteor. Soc., 91, 1193–1210, https://doi.org/10.1175/2010BAMS3004.1, 2010.

Gan, C. M., Wu, Y., Gross, B., and Moshary, F.: Statistical comparison between Hysplit sounding and lidar observation of planetary boundary layer characteristics over New York City, in: Laser Radar Technology and Applications XV, edited by Turner, M. D. and Kamerman, G. W., vol. 7684, p. 76841K, International Society for Optics and Photonics, https://doi.org/10.1117/12.849705, 2010.

1715 Gan, C.-M., Wu, Y., Madhavan, B., Gross, B., and Moshary, F.: Application of active optical sensors to probe the vertical structure of the urban boundary layer and assess anomalies in air quality model PM2.5 forecasts, Atmos. Environ., 45, 6613 – 6621, https://doi.org/10.1016/j.atmosenv.2011.09.013, 2011.

Garratt, J.: Review: the atmospheric boundary layer, Earth-Sci. Rev. 37, 89–134, https://doi.org/10.1016/0012-8252(94)90026-4, 1994.

Geiß, A.: Automated calibration of ceilometer data and its applicability for quantitative aerosol monitoring, Ph.D. thesis, LMU München,
1720 https://edoc.ub.uni-muenchen.de/19930/1/Geiss{_}Alexander.pdf, 2016.

Geiß, A., Wiegner, M., Bonn, B., Schäfer, K., Forkel, R., von Schneidemesser, E., Münkel, C., Chan, K. L., and Nothard, R.: Mixing layer height as an indicator for urban air quality?, Atmos. Meas. Tech., 10, 2969–2988, https://doi.org/10.5194/amt-10-2969-2017, 2017.

Gibert, F., Cuesta, J., Yano, J.-I., Arnault, N., and Flamant, P. H.: On the Correlation between Convective Plume Updrafts and Downdrafts, Lidar Reflectivity and Depolarization Ratio, Boundary-Layer Meteorol., 125, 553–573, https://doi.org/10.1007/s10546-007-9205-6, 2007.

1725 Gibert, F., Xuéref-Rémy, I., Joly, L., Schmidt, M., Cuesta, J., Davis, K. J., Ramonet, M., Flamant, P. H., Parvitte, B., and Zéninari, V.: A Case Study of CO2, CO and Particles Content Evolution in the Suburban Atmospheric Boundary Layer Using a 2-μm Doppler DIAL, a 1-μm Backscatter Lidar and an Array of In-situ Sensors, Boundary-Layer Meteorol., 128, 381–401, https://doi.org/10.1007/s10546-008-9296-8, 2008.

Görsdorf, U. and Lehmann, V.: Enhanced Accuracy of RASS-Measured Temperatures Due to an Improved Range Correction, J. Atmos.
1730 Oceanic Technol., 17, 406–416, https://doi.org/10.1175/1520-0426(2000)017<0406:EAORMT>2.0.CO;2, 2000.

Gottschall, J., Courtney, M. S., Wagner, R., Jørgensen, H. E., and Antoniou, I.: Lidar profilers in the context of wind energy - a verification procedure for traceable measurements, Wind Energy, 15, 147–159, https://doi.org/10.1002/we.518, 2012.

Granados-Muñoz, M., Navas-Guzmán, F., Bravo-Aranda, J., Guerrero-Rascado, J., Lyamani, H., Fernández-Gálvez, J., and Alados-Arboledas, L.: Automatic determination of the planetary boundary layer height using Lidar: One-year analysis over southeastern Spain, J.
1735 Geophys. Res. Atmos., 117, https://doi.org/10.1029/2012JD017524, 2012.

Gryning, S.-E. and Batchvarova, E.: Parametrization of the depth of the entrainment zone above the daytime mixed layer, Quart. J. Roy. Meteor. Soc., 120, 47–58, https://doi.org/10.1002/qj.49712051505, 1994.

Guerrero-Rascado, J. L., Olmo, F. J., Avilés-Rodríguez, I., Navas-Guzmán, F., Pérez-Ramírez, D., Lyamani, H., and Arboledas, L. A.: Extreme saharan dust event over the southern Iberian peninsula in September 2007: Active and passive remote sensing from surface and
1740 satellite, Atmos. Chem. Phys., 9, 8453–8469, https://doi.org/10.5194/ACP-9-8453-2009, 2009.

Guimarães, Ye, Batista, Barbosa, Ribeiro, Medeiros, Souza, and Martin: Vertical Profiles of Ozone Concentration Collected by an Unmanned Aerial Vehicle and the Mixing of the Nighttime Boundary Layer over an Amazonian Urban Area, Atmosphere, 10, 599, https://doi.org/10.3390/atmos10100599, 2019.

Güldner, J.: A model-based approach to adjust microwave observations for operational applications: results of a campaign at Munich Airport
1745 in winter 2011/2012, Atmos. Meas. Tech., 6, 2879–2891, https://doi.org/10.5194/amt-6-2879-2013, 2013.

Guo, J., Miao, Y., Zhang, Y., Liu, H., Li, Z., Zhang, W., He, J., Lou, M., Yan, Y., Bian, L., and Zhai, P.: The climatology of planetary boundary layer height in China derived from radiosonde and reanalysis data, Atmos. Chem. Phys., 16, 13 309–13 319, https://doi.org/10.5194/acp-16-13309-2016, 2016.

Haeffelin, M., Angelini, F., Morille, Y., Martucci, G., Frey, S., Gobbi, G., Lolli, S., O'dowd, C., Sauvage, L., Xueref-Rémy, I., et al.: Evaluation of mixing-height retrievals from automatic profiling lidars and ceilometers in view of future integrated networks in Europe, Boundary-Layer Meteorol., 143, 49–75, https://doi.org/10.1007/s10546-011-9643-z, 2012.

Haid, M., Gohm, A., Umek, L., Ward, H. C., Muschinski, T., Lehner, L., and Rotach, M. W.: Foehn–cold pool interactions in the Inn Valley during PIANO IOP2, Quart. J. Roy. Meteor. Soc., 146, 1232–1263, https://doi.org/10.1002/qj.3735, 2020.

Halios, C. H. and Barlow, J. F.: Observations of the Morning Development of the Urban Boundary Layer Over London, UK, Taken During the ACTUAL Project, Boundary-Layer Meteorol., pp. 1–28, https://doi.org/10.1007/s10546-017-0300-z, 2017.

Haman, C. L., Lefer, B., Morris, G. A., Haman, C. L., Lefer, B., and Morris, G. A.: Seasonal Variability in the Diurnal Evolution of the Boundary Layer in a Near-Coastal Urban Environment, J. Atmos. Oceanic Technol., 29, 697–710, https://doi.org/10.1175/JTECH-D-11-00114.1, 2012.

Han, S., Bian, H., Tie, X., Xie, Y., Sun, M., and Liu, A.: Impact of nocturnal planetary boundary layer on urban air pollutants: Measurements from a 250-m tower over Tianjin, China, J. HAZARD. MATER. 162, 264–269, https://doi.org/10.1016/J.JHAZMAT.2008.05.056, 2009.

Hanna, S. R.: The thickness of the planetary boundary layer, Atmos. Environ., 3, 519–536, 1969.

Harvey, N. J., Hogan, R. J., and Dacre, H. F.: A method to diagnose boundary-layer type using Doppler lidar, Quart. J. Roy. Meteor. Soc., 139, 1681–1693, https://doi.org/10.1002/qj.2068, 2013.

Harvey, N. J., Hogan, R. J., and Dacre, H. F.: Evaluation of boundary-layer type in a weather forecast model utilizing long-term Doppler lidar observations, Quart. J. Roy. Meteor. Soc., 141, 1345–1353, https://doi.org/10.1002/qj.2444, 2015.

Heese, B., Flentje, H., Althausen, D., Ansmann, A., and Frey, S.: Ceilometer lidar comparison: backscatter coefficient retrieval and signal-to-noise ratio determination, Atmos. Meas. Tech., 3, 1763–1770, https://doi.org/10.5194/amt-3-1763-2010, 2010.

Heffter, J. L.: Transport Layer Depth Calculations, in: 2nd Joint Conference on Applications of Air Pollution Modelling, New Orleans, LA, USA, pp. 787–791, American Meteorological Society, 45 Beacon St., Boston, MA, USA, 1980.

Helbig, M., Gerken, T., Beamesderfer, E. R., Baldocchi, D. D., Banerjee, T., Biraud, S. C., Brown, W. O., Brunsell, N. A., Burakowski, E. A., Burns, S. P., Butterworth, B. J., Chan, W. S., Davis, K. J., Desai, A. R., Fuentes, J. D., Hollinger, D. Y., Kljun, N., Mauder, M., Novick, K. A., Perkins, J. M., Rahn, D. A., Rey-Sanchez, C., Santanello, J. A., Scott, R. L., Seyednasrollah, B., Stoy, P. C., Sullivan, R. C., de Arellano, J. V.-G., Wharton, S., Yi, C., and Richardson, A. D.: Integrating continuous atmospheric boundary layer and tower-based flux measurements to advance understanding of land-atmosphere interactions, Agric. For. Meteor., 307, 108 509, https://doi.org/10.1016/J.AGRFORMET.2021.108509, 2021.

Helmis, C., Sgouros, G., Tombrou, M., Schäfer, K., Münkel, C., Bossioli, E., and Dandou, A.: A comparative study and evaluation of mixing-height estimation based on sodar-RASS, ceilometer data and numerical model simulations, Boundary-Layer Meteorol., pp. 1–20, https://doi.org/10.1007/s10546-012-9743-4, 2012.

Hennemuth, B. and Lammert, A.: Determination of the atmospheric boundary layer height from radiosonde and lidar backscatter, Boundary-Layer Meteorol., https://doi.org/10.1007/s10546-005-9035-3, 2006.

Hervo, M., Poltera, Y., and Haefele, A.: An empirical method to correct for temperature dependent variations in the overlap function of CHM15k ceilometers, Atmos. Meas. Tech., 9, 2947–2959, https://doi.org/10.5194/amt-9-2947-2016, 2016.

Hirsikko, A., O'Connor, E. J., Komppula, M., Korhonen, K., Pfüller, A., Giannakaki, E., Wood, C. R., Bauer-Pfundstein, M., Poikonen, A., Karppinen, T., Lonka, H., Kurri, M., Heinonen, J., Moisseev, D., Asmi, E., Aaltonen, V., Nordbo, A., Rodriguez, E., Lihavainen, H., Laaksonen, A., Lehtinen, K. E. J., Laurila, T., Petäjä, T., Kulmala, M., and Viisanen, Y.: Observing wind, aerosol particles, cloud and precipitation: Finland's new ground-based remote-sensing network, Atmos. Meas. Tech., 7, 1351–1375, https://doi.org/10.5194/amt-7-1351-2014, 2014.

Ho, S.-p., Peng, L., Anthes, R. A., Kuo, Y.-H., and Lin, H.-C.: Marine Boundary Layer Heights and Their Longitudinal, Diurnal, and Interseasonal Variability in the Southeastern Pacific Using COSMIC, CALIOP, and Radiosonde Data, J. Climate, 28, 2856–2872, https://doi.org/10.1175/JCLI-D-14-00238.1, 2015.

Ho, S.-P., Zhou, X., Shao, X., Zhang, B., Adhikari, L., Kireev, S., He, Y., Yoe, J. G., Xia-Serafino, W., and Lynch, E.: Initial assessment of the COSMIC-2/FORMOSAT-7 neutral atmosphere data quality in NESDIS/STAR using in situ and satellite data, Remote Sens. 12, 4099, 2020.

Hogan, R. J., Grant, A. L., Illingworth, A. J., Pearson, G. N., and O'Connor, E. J.: Vertical velocity variance and skewness in clear and cloud-topped boundary layers as revealed by Doppler lidar, Quart. J. Roy. Meteor. Soc., 135, 635–643, https://doi.org/10.1002/qj.413, 2009.

Holtslag, A. and Nieuwstadt, F.: Scaling the atmospheric boundary layer, Boundary-Layer Meteorol., 36, 201–209, https://doi.org/10.1007/BF00117468, 1986.

Holzworth, G. C.: Estimates of mean maximum mixing depths in the contiguous United States, Mon. Wea. Rev., 92, 235–242, https://doi.org/10.1175/1520-0493(1964)092<0235:EOMMMD>2.3.CO;2, 1964.

Hooper, W. P. and Eloranta, E. W.: Lidar measurements of wind in the planetary boundary layer: the method, accuracy and results from joint measurements with radiosonde and kytoon, J. Climate Appl. Meteor., 25, 990–1001, https://doi.org/10.1175/1520-0450(1986)025<0990:LMOWIT>2.0.CO;2, 1986.

Hopkin, E., Illingworth, A. J., Charlton-Perez, C., Westbrook, C. D., and Ballard, S.: A robust automated technique for operational calibration of ceilometers using the integrated backscatter from totally attenuated liquid clouds, Atmos. Meas. Tech., 12, 4131–4147, https://doi.org/10.5194/amt-12-4131-2019, 2019.

Hu, X. M., Klein, P. M., Xue, M., Lundquist, J. K., Zhang, F., and Qi, Y.: Impact of low-level jets on the nocturnal urban heat island intensity in Oklahoma city, J. Appl. Meteor. Climatol., 52, 1779–1802, https://doi.org/10.1175/JAMC-D-12-0256.1, 2013.

Huang, M., Gao, Z., Miao, S., Chen, F., LeMone, M. A., Li, J., Hu, F., and Wang, L.: Estimate of Boundary-Layer Depth Over Beijing, China, Using Doppler Lidar Data During SURF-2015, Boundary-Layer Meteorol., 162, 503–52, https://doi.org/10.1007/s10546-016-0205-2, 2017.

Huang, T., Yim, S. H. L., Yang, Y., Lee, O. S. M., Lam, D. H. Y., Cheng, J. C. H., and Guo, J.: Observation of turbulent mixing characteristics in the typical daytime cloud-topped boundary layer over Hong Kong in 2019, Remote Sens. 12, 1533, https://doi.org/10.3390/RS12091533, 2020.

Illingworth, A. J., Cimini, D., Gaffard, C., Haeffelin, M., Lehmann, V., Löhnert, U., O'Connor, E. J., and Ruffieux, D.: Exploiting existing ground-based remote sensing networks to improve high-resolution weather forecasts, Bull. Amer. Meteor. Soc., 96, 2107–2125, https://doi.org/10.1175/BAMS-D-13-00283.1, 2015.

Illingworth, A. J., Cimini, D., Haefele, A., Haeffelin, M., Hervo, M., Kotthaus, S., Löhnert, U., Martinet, P., Mattis, I., O'Connor, E., et al.: How Can Existing Ground-Based Profiling Instruments Improve European Weather Forecasts?, Bull. Amer. Meteor. Soc., 100, 605–619, https://doi.org/10.1175/BAMS-D-17-0231.1, 2019.

Johansson, C. and Bergström, H.: An auxiliary tool to determine the height of the boundary layer, Boundary-Layer Meteorol., 115, 423–432, https://doi.org/10.1007/s10546-004-1424-5, 2005.

Jordan, N. S., Hoff, R. M., and Bacmeister, J. T.: Validation of Goddard Earth Observing System-version 5 MERRA planetary boundary layer heights using CALIPSO, J. Geophys. Res. Atmos., 115, https://doi.org/10.1029/2009JD013777, 2010.

Kavaya, M. J. and Suni, P. J. M.: Continuous wave coherent laser radar: calculation of measurement location and volume, Appl. Opt., 30, 2634–2642, 1991.

Keller, C. A., Huwald, H., Vollmer, M. K., Wenger, A., Hill, M., Parlange, M. B., and Reimann, S.: Fiber optic distributed temperature sensing for the determination of the nocturnal atmospheric boundary layer height, Atmos. Meas. Tech., 4, 143–149, https://doi.org/10.5194/amt-4-143-2011, 2011.

Ketterer, C., Zieger, P., Bukowiecki, N., Collaud Coen, M., Maier, O., Ruffieux, D., and Weingartner, E.: Investigation of the Planetary Boundary Layer in the Swiss Alps Using Remote Sensing and In Situ Measurements, Boundary-Layer Meteorol., 151, 317–334, https://doi.org/10.1007/s10546-013-9897-8, 2014.

Klein, A., Ancellet, G., Ravetta, F., Thomas, J. L., and Pazmino, A.: Characterizing the seasonal cycle and vertical structure of ozone in Paris, France using four years of ground based LIDAR measurements in the lowermost troposphere, Atmos. Environ., 167, 603–615, https://doi.org/10.1016/J.ATMOSENV.2017.08.016, 2017.

Klein, A., Ravetta, F., Thomas, J. L., Ancellet, G., Augustin, P., Wilson, R., Dieudonné, E., Fourmentin, M., Delbarre, H., and Pelon, J.: Influence of vertical mixing and nighttime transport on surface ozone variability in the morning in Paris and the surrounding region, Atmos. Environ., 197, 92–102, https://doi.org/10.1016/j.atmosenv.2018.10.009, 2019.

Knepp, T. N., Szykman, J. J., Long, R., Duvall, R. M., Krug, J., Beaver, M., Cavender, K., Kronmiller, K., Wheeler, M., Delgado, R., et al.: Assessment of mixed-layer height estimation from single-wavelength ceilometer profiles, Atmos. Meas. Tech., 10, 3963, https://doi.org/10.5194/amt-2017-127, 2017.

Knuteson, R., Revercomb, H., Best, F., Ciganovich, N., Dedecker, R., Dirkx, T., Ellington, S., Feltz, W., Garcia, R., Howell, H., et al.: Atmospheric emitted radiance interferometer. Part I: Instrument design, J. Atmos. Oceanic Technol., 21, 1763–1776, https://doi.org/10.1175/JTECH-1662.1, 2004a.

Knuteson, R., Revercomb, H., Best, F., Ciganovich, N., Dedecker, R., Dirkx, T., Ellington, S., Feltz, W., Garcia, R., Howell, H., et al.: Atmospheric emitted radiance interferometer. Part II: Instrument performance, J. Atmos. Oceanic Technol., 21, 1777–1789, https://doi.org/10.1175/JTECH-1663.1, 2004b.

Kokkalis, P., Alexiou, D., Papayannis, A., Rocadenbosch, F., Soupiona, O., Raptis, P. I., Mylonaki, M., Tzanis, C. G., and Christodoulakis, J.: Application and Testing of the Extended-Kalman-Filtering Technique for Determining the Planetary Boundary-Layer Height over Athens, Greece, Boundary-Layer Meteorol., 176, 125–147, https://doi.org/10.1007/s10546-020-00514-z, 2020.

Kotthaus, S. and Grimmond, C. S. B.: Atmospheric boundary-layer characteristics from ceilometer measurements. Part 1: A new method to track mixed layer height and classify clouds, Quart. J. Roy. Meteor. Soc., 144, 1525–1538, https://doi.org/10.1002/qj.3299, 2018a.

Kotthaus, S. and Grimmond, C. S. B.: Atmospheric boundary-layer characteristics from ceilometer measurements. Part 2: Application to London's urban boundary layer, Quart. J. Roy. Meteor. Soc., 144, 1511–1524, https://doi.org/10.1002/qj.3298, 2018b.

Kotthaus, S., O'Connor, E., Münkel, C., Charlton-Perez, C., Haeffelin, M., Gabey, A. M., and Grimmond, C. S. B.: Recommendations for processing atmospheric attenuated backscatter profiles from Vaisala CL31 ceilometers, Atmos. Meas. Tech., 9, 3769–3791, https://doi.org/10.5194/amt-9-3769-2016, 2016.

Kotthaus, S., Halios, C. H., Barlow, J. F., and Grimmond, C.: Volume for pollution dispersion: London's atmospheric boundary layer during ClearfLo observed with two ground-based lidar types, Atmos. Environ., https://doi.org/10.1016/J.ATMOSENV.2018.06.042, 2018.

1860 Kotthaus, S., Haeffelin, M., Drouin, M.-A., Dupont, J.-C., Grimmond, S., Haefele, A., Hervo, M., Poltera, Y., and Wiegner, M.: Tailored Algorithms for the Detection of the Atmospheric Boundary Layer Height from Common Automatic Lidars and Ceilometers (ALC), Remote Sens. https://doi.org/10.3390/rs12193259, 2020.

Kouznetsov, R. D.: The summertime ABL structure over an antarctic oasis with a vertical Doppler sodar, Meteor. Z., 18, 163–167, https://doi.org/10.1127/0941-2948/2009/0369, 2009.

1865 Kramar, V. F., Baykova, E., Kallistratova, M., Kouznetsov, R., and Kulichkov, S.: Ground-Based Remote Sensing of the ABL Structure in Moscow and Its Use to Estimate Pollutant Surface Emission Rates, J. Appl. Meteor. Climatol., 53, 1272–1281, https://doi.org/10.1175/JAMC-D-13-010.1, 2014.

Krishnamurthy, R., Newsom, R. K., Berg, L. K., Xiao, H., Ma, P. L., and Turner, D. D.: On the estimation of boundary layer heights: A machine learning approach, Atmos. Meas. Tech., 14, 4403–4424, https://doi.org/10.5194/AMT-14-4403-2021, 2021.

1870 Lammert, A. and Bösenberg, J.: Determination of the convective boundary-layer height with laser remote sensing, Boundary-Layer Meteorol., 119, 159–170, https://doi.org/10.1007/s10546-005-9020-x, 2006.

Lange, D., Tiana-Alsina, J., Saeed, U., Tomas, S., and Rocadenbosch, F.: Atmospheric boundary layer height monitoring using a Kalman filter and backscatter lidar returns, IEEE Trans. Geosci. Remote Sens. 52, 4717–4728, https://doi.org/10.1109/TGRS.2013.2284110, 2013.

Lareau, N. P. and Clements, C. B.: Environmental controls on pyrocumulus and pyrocumulonimbus initiation and development, Atmos.
1875 Chem. Phys., 16, 4005–4022, https://doi.org/10.5194/acp-16-4005-2016, 2016.

Lauvaux, T., Miles, N. L., Deng, A., Richardson, S. J., Cambaliza, M. O., Davis, K. J., Gaudet, B., Gurney, K. R., Huang, J., O'Keefe, D., Song, Y., Karion, A., Oda, T., Patarasuk, R., Razlivanov, I., Sarmiento, D., Shepson, P., Sweeney, C., Turnbull, J., and Wu, K.: High-resolution atmospheric inversion of urban CO_2 emissions during the dormant season of the Indianapolis Flux Experiment (INFLUX), J. Geophys. Res. Atmos., 121, 5213–5236, https://doi.org/10.1002/2015JD024473, 2016.

1880 Lee, J., Hong, J. W., Lee, K., Hong, J., Velasco, E., Lim, Y. J., Lee, J. B., Nam, K., and Park, J.: Ceilometer Monitoring of Boundary-Layer Height and Its Application in Evaluating the Dilution Effect on Air Pollution, Boundary-Layer Meteorol., 172, 435–455, https://doi.org/10.1007/s10546-019-00452-5, 2019.

Lehmann, V. and Teschke, G.: Advanced intermittent clutter filtering for radar wind profiler: signal separation through a Gabor frame expansion and its statistics, Ann. Geophys. 26, 759–783, https://doi.org/10.5194/angeo-26-759-2008, 2008.

1885 Lehning, M., Richner, H., and Kok, G. L.: Transport of air pollutants from the boundary layer to the free troposphere over complex terrain, Phys. Chem. Earth, 23, 667 – 672, https://doi.org/10.1016/S0079-1946(98)00108-6, 1998.

LeMone, M. A., Tewari, M., Chen, F., and Dudhia, J.: Objectively determined fair-weather CBL depths in the ARW-WRF model and their comparison to CASES-97 observations, Mon. Wea. Rev., 141, 30–54, https://doi.org/10.1175/MWR-D-12-00106.1, 2013.

Lemone, M. A., Tewari, M., Chen, F., and Dudhia, J.: Objectively determined fair-weather NBL features in ARW-WRF and their comparison
1890 to CASES-97 observations, Mon. Wea. Rev., 142, 2709–2732, https://doi.org/10.1175/MWR-D-13-00358.1, 2014.

Lenschow, D. H., Wulfmeyer, V., and Senff, C.: Measuring Second- through Fourth-Order Moments in Noisy Data, J. Atmos. Oceanic Technol., 17, 1330–1347, https://doi.org/https://doi.org/10.1175/1520-0426(2000)017<1330:MSTFOM>2.0.CO;2, 2000.

Lewis, J. R., Welton, E. J., Molod, A. M., and Joseph, E.: Improved boundary layer depth retrievals from MPLNET, J. Geophys. Res. Atmos., 118, 9870–9879, https://doi.org/10.1002/jgrd.50570, 2013.

1895   Li, H., Yang, Y., Hu, X.-m., Huang, Z., and Wang, G.: Evaluation of retrieval methods of daytime convective boundary layer height based on Lidar data, J. Geophys. Res., https://doi.org/10.1002/2016JD025620, 2017.

Liljegren, J. C., Boukabara, S. A., Cady-Pereira, K., and Clough, S. A.: The effect of the half-width of the 22-GHz water vapor line on retrievals of temperature and water vapor profiles with a 12-channel microwave radiometer, IEEE Trans. Geosci. Remote Sens. 43, 1102–1108, https://doi.org/10.1109/TGRS.2004.839593, 2005.

1900   Liu, B., Ma, Y., Gong, W., Zhang, M., and Yang, J.: Determination of boundary layer top on the basis of the characteristics of atmospheric particles, Atmos. Environ., 178, 140–147, https://doi.org/10.1016/J.ATMOSENV.2018.01.054, 2018.

Liu, B., Ma, Y., Guo, J., Gong, W., Zhang, Y., Mao, F., Li, J., Guo, X., and Shi, Y.: Boundary layer heights as derived from ground-based radar wind profiler in Beijing, IEEE Trans. Geosci. Remote Sens. 57, 8095–8104, https://doi.org/10.1109/TGRS.2019.2918301, 2019a.

Liu, B., Guo, J., Gong, W., Shi, L., Zhang, Y., and Ma, Y.: Characteristics and performance of wind profiles as observed by the radar wind
1905   profiler network of China, Atmos. Meas. Tech., 13, 4589–4600, https://doi.org/10.5194/AMT-13-4589-2020, 2020.

Liu, J., Huang, J., Chen, B., Zhou, T., Yan, H., Jin, H., Huang, Z., and Zhang, B.: Comparisons of PBL heights derived from CALIPSO and ECMWF reanalysis data over China, J. Quant. Spectrosc. Ra; 153, 102 – 112, https://doi.org/10.1016/j.jqsrt.2014.10.011, 2015a.

Liu, L., Sun, X.-j., Liu, X.-c., Gao, T.-c., and Zhao, S.-j.: Comparison of Cloud Base Height Derived from a Ground-Based Infrared Cloud Measurement and Two Ceilometers, Adv. Meteorol. 2015, 1–8, https://doi.org/10.1155/2015/853861, 2015b.

1910   Liu, S. and Liang, X. Z.: Observed diurnal cycle climatology of planetary boundary layer height, J. Climate, 23, 5790–5809, https://doi.org/10.1175/2010JCLI3552.1, 2010.

Liu, Z., Barlow, J. F., Chan, P.-W., Fung, J., Li, Y., Ren, C., Mak, H., and Ng, E.: A Review of Progress and Applications of Pulsed Doppler Wind LiDARs, Remote Sens. 11, 2522, https://doi.org/10.3390/rs11212522, 2019b.

Löhnert, U. and Maier, O.: Operational profiling of temperature using ground-based microwave radiometry at Payerne: prospects and chal-
1915   lenges, Atmos. Meas. Tech., 5, 1121–1134, https://doi.org/10.5194/amt-5-1121-2012, 2012.

Lothon, M., Lenschow, D. H., and Mayor, S. D.: Coherence and Scale of Vertical Velocity in the Convective Boundary Layer from a Doppler Lidar, Boundary-Layer Meteorol., 121, 521–536, https://doi.org/10.1007/s10546-006-9077-1, 2006.

Lotteraner, C. and Piringer, M.: Mixing-Height Time Series from Operational Ceilometer Aerosol-Layer Heights, Boundary-Layer Meteorol., 161, 265–287, https://doi.org/10.1007/s10546-016-0169-2, 2016.

1920   Löhnert, U., Turner, D. D., and Crewell, S.: Ground-Based Temperature and Humidity Profiling Using Spectral Infrared and Microwave Observations. Part I: Simulated Retrieval Performance in Clear-Sky Conditions, J. Appl. Meteor. Climatol., 48, 1017–1032, https://doi.org/10.1175/2008JAMC2060.1, 2009.

Madonna, F., Kivi, R., Dupont, J. C., Ingleby, B., Fujiwara, M., Romanens, G., Hernandez, M., Calbet, X., Rosoldi, M., Giunta, A., Karppinen, T., Iwabuchi, M., Hoshino, S., Von Rohden, C., and William Thorne, P.: Use of automatic radiosonde launchers to measure temper-
1925   ature and humidity profiles from the GRUAN perspective, Atmos. Meas. Tech., 13, 3621–3649, https://doi.org/10.5194/AMT-13-3621-2020, 2020.

Madonna, F., Tramutola, E., Souleymane, S. Y., Serva, F., Proto, M., Rosoldi, M., Gagliardi, S., Amato, F., Marra, F., Fassò, A., Gardiner, T., and Thorne, P. W.: The New Radiosounding HARMonization (RHARM) Data Set of Homogenized Radiosounding Temperature, Humidity, and Wind Profiles With Uncertainties, J. Geophys. Res. Atmos., 127, e2021JD035 220, https://doi.org/10.1029/2021JD035220,
1930   2022.

Mahrt, L.: Boundary-layer moisture regimes, Quart. J. Roy. Meteor. Soc., 117, 151–176, https://doi.org/10.1002/QJ.49711749708, 1991.

Mahrt, L., Heald, R. C., Lenschow, D. H., Stankov, B. B., and Troen, I. B.: An observational study of the structure of the nocturnal boundary layer, Boundary-Layer Meteorol., 17, 247–264, https://doi.org/10.1007/BF00117983, 1979.

Manninen, A., Marke, T., Tuononen, M., and O'Connor, E.: Atmospheric boundary layer classification with Doppler lidar, J. Geophys. Res. Atmos., 123, 8172–8189, https://doi.org/10.1029/2017JD028169, 2018.

Manninen, A. J., O'Connor, E. J., Vakkari, V., and Petäjä, T.: A generalised background correction algorithm for a Halo Doppler lidar and its application to data from Finland, Atmos. Meas. Tech., 9, 817–827, https://doi.org/10.5194/amt-9-817-2016, 2016.

Marke, T., Crewell, S., Schemann, V., Schween, J. H., and Tuononen, M.: Long-Term Observations and High-Resolution Modeling of Midlatitude Nocturnal Boundary Layer Processes Connected to Low-Level Jets, J. Appl. Meteor. Climatol., 57, 1155 – 1170, https://doi.org/10.1175/JAMC-D-17-0341.1, 2018.

Markowicz, K. M., Flatau, P. J., Kardas, A. E., Remiszewska, J., Stelmaszczyk, K., Woeste, L., Markowicz, K. M., Flatau, P. J., Kardas, A. E., Remiszewska, J., Stelmaszczyk, K., and Woeste, L.: Ceilometer Retrieval of the Boundary Layer Vertical Aerosol Extinction Structure, J. Atmos. Oceanic Technol., 25, 928–944, https://doi.org/10.1175/2007JTECHA1016.1, 2008.

Marsik, F. J., Fischer, K. W., McDonald, T. D., Samson, P. J., Marsik, F. J., Fischer, K. W., McDonald, T. D., and Samson, P. J.: Comparison of Methods for Estimating Mixing Height Used during the 1992 Atlanta Field Intensive, J. Appl. Meteor., 34, 1802–1814, https://doi.org/10.1175/1520-0450(1995)034<1802:COMFEM>2.0.CO;2, 1995.

Martinet, P., Cimini, D., Burnet, F., Ménétrier, B., Michel, Y., and Unger, V.: Improvement of numerical weather prediction model analysis during fog conditions through the assimilation of ground-based microwave radiometer observations: a 1D-Var study, Atmos. Meas. Tech., 13, 6593–6611, https://doi.org/10.5194/amt-13-6593-2020, 2020.

Martucci, G., Matthey, R., Mitev, V., and Richner, H.: Comparison between backscatter lidar and radiosonde measurements of the diurnal and nocturnal stratification in the lower troposphere, J. Atmos. Oceanic Technol., 24, 1231–1244, https://doi.org/10.1175/JTECH2036.1, 2007.

Martucci, G., Matthey, R., Mitev, V., and Richner, H.: Frequency of Boundary-Layer-Top Fluctuations in Convective and Stable Conditions Using Laser Remote Sensing, Boundary-Layer Meteorol., 135, 313–331, https://doi.org/10.1007/s10546-010-9474-3, 2010a.

Martucci, G., Milroy, C., and O'Dowd, C. D.: Detection of Cloud-Base Height Using Jenoptik CHM15K and Vaisala CL31 Ceilometers, J. Atmos. Oceanic Technol., 27, 305–318, https://doi.org/10.1175/2009JTECHA1326.1, 2010b.

Mather, J. H. and Voyles, J. W.: The ARM Climate Research Facility: A Review of Structure and Capabilities, Bull. Amer. Meteor. Soc., 94, 377–392, https://doi.org/10.1175/BAMS-D-11-00218.1, 2013.

Menut, L., Flamant, C., Pelon, J., and Flamant, P. H.: Urban boundary-layer height determination from lidar measurements over the Paris area, Appl. Opt., 38, 945, https://doi.org/10.1364/AO.38.000945, 1999.

Millán, L., Lebsock, M., Fishbein, E., Kalmus, P., and Teixeira, J.: Quantifying Marine Boundary Layer Water Vapor beneath Low Clouds with Near-Infrared and Microwave Imagery, J. Appl. Meteor. Climatol., 55, 213–225, https://doi.org/10.1175/JAMC-D-15-0143.1, 2016.

Milroy, C., Martucci, G., Lolli, S., Loaec, S., Sauvage, L., Xueref-Remy, I., Lavrič, J. V., Ciais, P., Feist, D. G., Biavati, G., and O'Dowd, C. D.: An assessment of pseudo-operational ground-based light detection and ranging sensors to determine the boundary-layer structure in the coastal atmosphere, Adv. Meteorol. 2012, 1–19, https://doi.org/10.1155/2012/929080, 2012.

Min, J. S., Park, M. S., Chae, J. H., and Kang, M.: Integrated System for Atmospheric Boundary Layer Height Estimation (ISABLE) using a ceilometer and microwave radiometer, Atmos. Meas. Tech., 13, 6965–6987, https://doi.org/10.5194/AMT-13-6965-2020, 2020.

Moigne, P. L., Legain, D., Lagarde, F., Potes, M., Tzanos, D., Moulin, E., Barrié, J., Salgado, R., Messiaen, G., Fiandrino, A., et al.: Evaluation of the lake model FLake over a coastal lagoon during the THAUMEX field campaign, Tellus A, 65, 20 951, https://doi.org/10.3402/tellusa.v65i0.20951, 2013.

Molod, A., Salmun, H., and Dempsey, M.: Estimating Planetary Boundary Layer Heights from NOAA Profiler Network Wind Profiler Data, J. Atmos. Oceanic Technol., 32, 1545–1561, https://doi.org/10.1175/JTECH-D-14-00155.1, 2015.

Molod, A., Salmun, H., and Marquardt Collow, A. B.: Annual Cycle of Planetary Boundary Layer Heights Estimated From Wind Profiler Network Data, J. Geophys. Res. Atmos., 124, 6207–6221, https://doi.org/10.1029/2018JD030102, 2019.

Moreira, G. d. A., Marques, M., Nakaema, W., de CA Moreira, A., and Landulfo, E.: Detecting the planetary boundary layer height from low-level jet with Doppler lidar measurements, in: Lidar Technologies, Techniques, and Measurements for Atmospheric Remote Sensing XI, vol. 9645, p. 96450F, International Society for Optics and Photonics, https://doi.org/10.1117/12.2195278, 2015.

Morille, Y., Haeffelin, M., Drobinski, P., and Pelon, J.: STRAT: An automated algorithm to retrieve the vertical structure of the atmosphere from single-channel lidar data, J. Atmos. Oceanic Technol., 24, 761–775, https://doi.org/10.1175/JTECH2008.1, 2007.

Mues, A., Rupakheti, M., Münkel, C., Lauer, A., Bozem, H., Hoor, P., Butler, T., and Lawrence, M. G.: Investigation of the mixing layer height derived from ceilometer measurements in the Kathmandu Valley and implications for local air quality, Atmos. Chem. Phys., 17, 8157–8176, https://doi.org/10.5194/acp-17-8157-2017, 2017.

Münkel, C.: Mixing height determination with lidar ceilometers–results from Helsinki Testbed, Meteor. Z., 16, 451–459, https://doi.org/10.1127/0941-2948/2007/0221, 2007.

Münkel, C.: Combining gradient and profile fit method for an advanced ceilometer-based boundary layer height detection algorithm, in: 18th International Symposium for the Advancement of Boundary-Layer Remote Sensing, edited by ISARS2016, p. 8 June, 2016.

Neisser, J., Adam, W., Beyrich, F., Leiterer, U., and Steinhagen, H.: Atmospheric boundary layer monitoring at the Meteorological Observatory Lindenberg as a part of the "Lindenberg Column": Facilities and selected results, Meteor. Z., 11, 241–253, https://doi.org/10.1127/0941-2948/2002/0011-0241, 2002.

Newsom, R. K., Turner, D. D., Lehtinen, R., Münkel, C., Kallio, J., and Roininen, R.: Evaluation of a Compact Broadband Differential Absorption Lidar for Routine Water Vapor Profiling in the Atmospheric Boundary Layer, J. Atmos. Oceanic Technol., 37, 47–65, https://doi.org/10.1175/JTECH-D-18-0102.1, 2020.

Nielsen-Gammon, J. W., Powell, C. L., Mahoney, M. J., Angevine, W. M., Senff, C., White, A., Berkowitz, C., Doran, C., and Knupp, K.: Multisensor estimation of mixing heights over a coastal city, J. Appl. Meteor. Climatol., 47, 27–43, https://doi.org/10.1175/2007JAMC1503.1, 2008.

Nieuwstadt, F. and Duynkerke, P.: Turbulence in the atmospheric boundary layer, Atmos. Res., 40, 111–142, https://doi.org/10.1016/0169-8095(95)00034-8, 1996.

O'Connor, E. J., Illingworth, A. J., and Hogan, R. J.: A Technique for Autocalibration of Cloud Lidar, J. Atmos. Oceanic Technol., 21, 777–786, 2004.

O'Connor, E. J., Illingworth, A. J., Brooks, I. M., Westbrook, C. D., Hogan, R. J., Davies, F., and Brooks, B. J.: A Method for Estimating the Turbulent Kinetic Energy Dissipation Rate from a Vertically Pointing Doppler Lidar, and Independent Evaluation from Balloon-Borne In Situ Measurements, J. Atmos. Oceanic Technol., 27, 1652–1664, https://doi.org/10.1175/2010JTECHA1455.1, 2010.

Pal, S., Xueref-Remy, I., Ammoura, L., Chazette, P., Gibert, F., Royer, P., Dieudonné, E., Dupont, J. C., Haeffelin, M., Lac, C., Lopez, M., Morille, Y., and Ravetta, F.: Spatio-temporal variability of the atmospheric boundary layer depth over the Paris agglomeration: An

2005   assessment of the impact of the urban heat island intensity, Atmos. Environ., 63, 261–275, https://doi.org/10.1016/j.atmosenv.2012.09.046, 2012.

Pal, S., Haeffelin, M., and Batchvarova, E.: Exploring a geophysical process-based attribution technique for the determination of the atmospheric boundary layer depth using aerosol lidar and near-surface meteorological measurements, J. Geophys. Res. Atmos., 118, 9277–9295, https://doi.org/10.1002/jgrd.50710, 2013.

2010   Palmén, E. H. and Newton, C. W.: Atmospheric circulation systems: their structure and physical interpretation, vol. 13, Academic press, 1969.

Pandolfi, M., Martucci, G., Querol, X., Alastuey, A., Wilsenack, F., Frey, S., O'Dowd, C. D., and Dall'Osto, M.: Continuous atmospheric boundary layer observations in the coastal urban area of Barcelona during SAPUSS, Atmos. Chem. Phys., 13, 4983–4996, https://doi.org/10.5194/acp-13-4983-2013, 2013.

2015   Pappalardo, G., Amodeo, A., Apituley, A., Comeron, A., Freudenthaler, V., Linné, H., Ansmann, A., Bösenberg, J., D'Amico, G., Mattis, I., Mona, L., Wandinger, U., Amiridis, V., Alados-Arboledas, L., Nicolae, D., and Wiegner, M.: EARLINET: Towards an advanced sustainable European aerosol lidar network, Atmos. Meas. Tech., 7, 2389–2409, https://doi.org/10.5194/AMT-7-2389-2014, 2014.

Parikh, N. and Parikh, J.: Systematic tracking of boundary layer aerosols with laser radar, Opt. Laser Technol. 34, 177–185, https://doi.org/10.1016/S0030-3992(01)00107-4, 2002.

2020   Park, M.-S., Park, S.-H., Chae, J.-H., Choi, M.-H., Song, Y., Kang, M., and Roh, J.-W.: High-resolution urban observation network for user-specific meteorological information service in the Seoul Metropolitan Area, South Korea, Atmos. Meas. Tech., 10, 1575–1594, https://doi.org/10.5194/amt-10-1575-2017, 2017.

Päschke, E., Leinweber, R., and Lehmann, V.: An assessment of the performance of a 1.5 μm Doppler lidar for operational vertical wind profiling based on a 1-year trial, Atmos. Meas. Tech., 8, 2251–2266, https://doi.org/doi:10.5194/amt-8-2251-2015, 2015.

2025   Pattantyús-Ábrahám, M., Mattis, I., Begbie, R., Bravo-Aranda, J., Brettle, M., Cermak, J., Drouin, M.-A., Geiß, A., Görsdorf, U., Haefele, A., Haeffelin, M., Hervo, M., Komínková, K., Leinweber, R., Münkel, C., Pönitz, K., Vande Hey, J., Wagner, F., and Wiegner, M.: The dataset of the CeiLinEx 2015 Ceilometer-Inter-comparison Experiment, Version v001, https://doi.org/10.5676/DWD/CEILINEX2015, 2017.

Pearson, G., Davies, F., and Collier, C.: Remote sensing of the tropical rain forest boundary layer using pulsed Doppler lidar, Atmos. Chem. Phys., 10, 5891–5901, https://doi.org/10.5194/acp-10-5891-2010, 2010.

2030   Peña, A., Gryning, S., and Hasager, C. B.: Measurements and modelling of the wind speed profile in the marine atmospheric boundary layer, Boundary-Layer Meteorol., 129, 479–495, 2008.

Peña, A., Floors, R., Sathe, A., Gryning, S. E., Wagner, R., Courtney, M. S., Larsén, X. G., Hahmann, A. N., and Hasager, C. B.: Ten Years of Boundary-Layer and Wind-Power Meteorology at Høvsøre, Denmark, Boundary-Layer Meteorol., 158, 1–26, https://doi.org/10.1007/S10546-015-0079-8/FIGURES/9, 2016.

2035   Peng, J., Grimmond, C., Fu, X., Chang, Y., Zhang, G., Guo, J., Tang, C., GAO, J., Xu, X., Tan, J., Peng, J., Grimmond, C., Fu, X., Chang, Y., Zhang, G., Guo, J., Tang, C., GAO, J., Xu, X., and Tan, J.: Ceilometer based analysis of Shanghai's boundary layer height (under rain and fog free conditions), J. Atmos. Oceanic Technol., https://doi.org/10.1175/JTECH-D-16-0132.1, 2017.

Pentikäinen, P., O'Connor, E. J., Manninen, A. J., and Ortiz-Amezcua, P.: Methodology for deriving the telescope focus function and its uncertainty for a heterodyne pulsed Doppler lidar, Atmos. Meas. Tech., 13, 2849–2863, https://doi.org/10.5194/amt-13-2849-2020, 2020.

2040   Petetin, H., Jeoffrion, M., Sauvage, B., Athier, G., Blot, R., Boulanger, D., Clark, H., Cousin, J. M., Gheusi, F., Nedelec, P., Steinbacher, M., and Thouret, V.: Representativeness of the IAGOS airborne measurements in the lower troposphere, Elementa, 6, https://doi.org/10.1525/elementa.280, 2018.

Pichugina, Y. L. and Banta, R. M.: Stable boundary layer depth from high-resolution measurements of the mean wind profile, J. Appl. Meteor. Climatol., 49, 20–35, https://doi.org/10.1175/2009JAMC2168.1, 2010.

2045 Pichugina, Y. L., Tucker, S. C., Banta, R. M., Brewer, W. A., Kelley, N. D., Jonkman, B. J., and Newsom, R. K.: Horizontal-velocity and variance measurements in the stable boundary layer using Doppler lidar: Sensitivity to averaging procedures, J. Atmos. Oceanic Technol., 25, 1307–1327, https://journals.ametsoc.org/view/journals/atot/25/8/2008jtecha988_1.xml, 2008.

Pichugina, Y. L., Banta, R. M., Brewer, W. A., Sandberg, S. P., and Hardesty, R. M.: Doppler Lidar–Based Wind-Profile Measurement System for Offshore Wind-Energy and Other Marine Boundary Layer Applications, J. Appl. Meteor. Climatol., 51, https://doi.org/10.1175/JAMC-
2050 D-11-040.1, 2012.

Piironen, A. K. and Eloranta, E. W.: Convective boundary layer mean depths and cloud geometrical properties obtained from volume imaging lidar data, J. Geophys. Res. Atmos., 100, 25 569–25 576, 1995.

Piters, A. J. M., Boersma, K. F., Kroon, M., Hains, J. C., Van Roozendael, M., Wittrock, F., Abuhassan, N., Adams, C., Akrami, M., Allaart, M. A. F., Apituley, A., Beirle, S., Bergwerff, J. B., Berkhout, A. J. C., Brunner, D., Cede, A., Chong, J., Clémer, K., Fayt, C., Frieß, U.,
2055 Gast, L. F. L., Gil-Ojeda, M., Goutail, F., Graves, R., Griesfeller, A., Großmann, K., Hemerijckx, G., Hendrick, F., Henzing, B., Herman, J., Hermans, C., Hoexum, M., van der Hoff, G. R., Irie, H., Johnston, P. V., Kanaya, Y., Kim, Y. J., Klein Baltink, H., Kreher, K., de Leeuw, G., Leigh, R., Merlaud, A., Moerman, M. M., Monks, P. S., Mount, G. H., Navarro-Comas, M., Oetjen, H., Pazmino, A., Perez-Camacho, M., Peters, E., du Piesanie, A., Pinardi, G., Puentedura, O., Richter, A., Roscoe, H. K., Schönhardt, A., Schwarzenbach, B., Shaiganfar, R., Sluis, W., Spinei, E., Stolk, A. P., Strong, K., Swart, D. P. J., Takashima, H., Vlemmix, T., Vrekoussis, M., Wagner, T., Whyte, C., Wilson,
2060 K. M., Yela, M., Yilmaz, S., Zieger, P., and Zhou, Y.: The Cabauw Intercomparison campaign for Nitrogen Dioxide measuring Instruments (CINDI): design, execution, and early results, Atmos. Meas. Tech., 5, 457–485, https://doi.org/10.5194/amt-5-457-2012, 2012.

Poltera, Y., Martucci, G., Collaud Coen, M., Hervo, M., Emmenegger, L., Henne, S., Brunner, D., and Haefele, A.: PathfinderTURB: an automatic boundary layer algorithm. Development, validation and application to study the impact on in-situ measurements at the Jungfraujoch, Atmos. Chem. Phys., pp. 1–34, https://doi.org/10.5194/acp-17-10051-2017, 2017.

2065 Pospichal, B., Küchler, N., Löhnert, U., and Güldner, J.: J-CAL (Joint microwave calibration) - Recommendations for operation and calibration of Microwave Radiometers (MWR) within a network, http://www.toprof.imaa.cnr.it/images/toprof/pubs/TOPROF_MWR_recommendations_20160315.pdf, 2016.

Rahn, D. A. and Mitchell, C. J.: Diurnal Climatology of the Boundary Layer in Southern California Using AMDAR Temperature and Wind Profiles, J. Appl. Meteor. Climatol., 55, 1123–1137, https://doi.org/10.1175/JAMC-D-15-0234.1, 2016.

2070 Ramon, J., Lledó, L., Pérez-Zanón, N., Soret, A., and Doblas-Reyes, F. J.: The Tall Tower Dataset: a unique initiative to boost wind energy research, Eearth Syst. Sci. Data, 12, 429–439, https://doi.org/10.5194/essd-12-429-2020, 2020.

Ravetta, F. and Ancellet, G.: Compact airborne lidar for tropospheric ozone: description and field measurements, Appl. Opt., 37, 5509–5521, https://doi.org/10.1364/AO.37.005509, 1998.

Reitebuch, O., Strassburger, A., Emeis, S., and Kuttler, W.: Nocturnal secondary ozone concentration maxima analysed by sodar observations
2075 and surface measurements, Atmos. Environ., 34, 4315–4329, https://doi.org/10.1016/S1352-2310(00)00185-0, 2000.

Renju, R., Raju, C. S., Mishra, M. K., Mathew, N., Rajeev, K., and Moorthy, K. K.: Atmospheric Boundary Layer Characterization Using Multiyear Ground-Based Microwave Radiometric Observations Over a Tropical Coastal Station, IEEE Trans. Geosci. Remote Sens. 55, 6877–6882, https://doi.org/10.1109/TGRS.2017.2735626, 2017.

Rieutord, T., Aubert, S., and Machado, T.: Deriving boundary layer height from aerosol lidar using machine learning: KABL and ADABL
2080 algorithms, Atmos. Meas. Tech., 14, 4335–4353, https://doi.org/10.5194/amt-14-4335-2021, 2021.

Robinson, I., Jack, J. W., Rae, C. F., and Moncrieff, J. B.: A robust optical parametric oscillator and receiver telescope for differential absorption lidar of greenhouse gases, Proc. SPIE, 9645, 9645 – 9645 – 7, https://doi.org/10.1117/12.2197251, 2015.

Rose, T., Crewell, S., Löhnert, U., and Simmer, C.: A network suitable microwave radiometer for operational monitoring of the cloudy atmosphere, Atmos. Res., 75, 183 – 200, https://doi.org/https://doi.org/10.1016/j.atmosres.2004.12.005, cLIWA-NET: Observation and Modelling of Liquid Water Clouds, 2005.

Rotach, M. W. and Zardi, D.: On the boundary-layer structure over highly complex terrain: Key findings from MAP, Quart. J. Roy. Meteor. Soc., 133, 937–948, https://doi.org/10.1002/QJ.71, 2007.

Ruffieux, D.: Evaluation of WMO-CBS Wind Profiler Survey, https://www.wmo.int/pages/prog/www/OSY/Meetings/ICT-IOS8/documents/ICT-IOS8-INF-4-Wind-profiler-survey.pdf, 2014.

Rye, B. J. and Hardesty, R. M.: Discrete spectral peak estimation in incoherent backscatter heterodyne lidar. I: Spectral accumulation and the Cramer-Rao lower bound, IEEE Trans. Geosci. Remote Sens. 31, 16–27, https://doi.org/10.1109/36.210440, 1993.

Rüfenacht, R., Haefele, A., Pospichal, B., Cimini, D., Bircher-Adrot, S., Turp, M., and Sugier, J.: EUMETNET opens to microwave radiometers for operational thermodynamical profiling in Europe, Bull. Atmos. Sci. and Technol. 2, 231–261, https://doi.org/10.1007/s42865-021-00033-w, 2021.

Saeed, U., Rocadenbosch, F., and Crewell, S.: Adaptive estimation of the stable boundary layer height using combined lidar and microwave radiometer observations, IEEE Trans. Geosci. Remote Sens. 54, 6895–6906, https://doi.org/10.1109/TGRS.2016.2586298, 2016.

Sathe, A. and Mann, J.: A review of turbulence measurements using ground-based wind lidars, Atmos. Meas. Tech., 6, 3147–3167, https://doi.org/10.5194/amt-6-3147-2013, 2013.

Sathe, A., Mann, J., Vasiljevic, N., and Lea, G.: A six-beam method to measure turbulence statistics using ground-based wind lidars, Atmos. Meas. Tech., 8, 729–740, https://doi.org/10.5194/amt-8-729-2015, 2015.

Sawyer, V. and Li, Z.: Detection, variations and intercomparison of the planetary boundary layer depth from radiosonde, lidar and infrared spectrometer, Atmos. Environ., 79, 518–528, https://doi.org/10.1016/j.atmosenv.2013.07.019, 2013.

Scarino, A. J., Obland, M. D., Fast, J. D., Burton, S. P., Ferrare, R. A., Hostetler, C. A., Berg, L. K., Lefer, B., Haman, C., Hair, J. W., Rogers, R. R., Butler, C., Cook, A. L., Harper, D. B., and Northwest, Pacific and Sciences, Atmospheric and Consultants, Trinity and Rouge, Baton: Comparison of mixed layer heights from airborne high spectral resolution lidar, ground-based measurements, and the WRF-Chem model during CalNex and CARES, Atmos. Chem. Phys., pp. 5547–5560, https://doi.org/10.5194/acp-14-5547-2014, 2014.

Schäfer, K., Emeis, S. M., Rauch, A., Münkel, C., and Vogt, S.: Determination of the mixing layer height from ceilometer backscatter profiles, in: Remote Sensing of Clouds and the Atmosphere XI, edited by Comeron, A., Carleer, M. R., Picard, R. H., and Sifakis, N. I., pp. 248–259, International Society for Optics and Photonics, https://doi.org/10.1117/12.565592, 2004.

Schmid, P. and Niyogi, D.: A Method for Estimating Planetary Boundary Layer Heights and Its Application over the ARM Southern Great Plains Site, J. Atmos. Oceanic Technol., 29, 316–322, https://doi.org/10.1175/JTECH-D-11-00118.1, 2012.

Schreiner, W. S., Weiss, J., Anthes, R. A., Braun, J., Chu, V., Fong, J., Hunt, D., Kuo, Y.-H., Meehan, T., Serafino, W., et al.: COSMIC-2 radio occultation constellation: First results, Geophys. Res. Lett., 47, e2019GL086 841, 2020.

Schween, J. H., Hirsikko, A., Löhnert, U., and Crewell, S.: Mixing-layer height retrieval with ceilometer and Doppler lidar: from case studies to long-term assessment, Atmos. Meas. Tech., pp. 3685–3704, https://doi.org/10.5194/amt-7-3685-2014, 2014.

Seibert, P., Beyrich, F., Gryning, S., Joffre, S., Rasmussen, A., and Tercier, P.: Mixing layer depth determination for dispersion modelling, in: COST Action 710-Final Report. Harmonisation of the pre-processing of meteorological data for atmospheric dispersion models., edited

by Fisher, B., Erbrink, J., Finardi, S., Jeannet, P., Jore, S., Morselli, M., Pechinger, U., Seibert, P., and Thomson, D., L-2985 Luxembourg: European Commission, EUR 18195 EN, 1998.

2120 Seibert, P., Beyrich, F., Gryning, S.-E., Joffre, S., Rasmussen, A., and Tercier, P.: Review and intercomparison of operational methods for the determination of the mixing height, Atmos. Environ., 34, 1001 – 1027, https://doi.org/10.1016/S1352-2310(99)00349-0, 2000.

Seidel, D. J., Ao, C. O., and Li, K.: Estimating climatological planetary boundary layer heights from radiosonde observations: Comparison of methods and uncertainty analysis, J. Geophys. Res. Atmos., 115, n/a–n/a, https://doi.org/10.1029/2009JD013680, d16113, 2010.

Seidel, D. J., Zhang, Y., Beljaars, A., Golaz, J.-C., Jacobson, A. R., and Medeiros, B.: Climatology of the planetary boundary layer over the
2125 continental United States and Europe, J. Geophys. Res., 117, D17 106, https://doi.org/10.1029/2012JD018143, 2012.

Serafin, S., Adler, B., Cuxart, J., De Wekker, S. F., Gohm, A., Grisogono, B., Kalthoff, N., Kirshbaum, D. J., Rotach, M. W., Schmidli, J., Stiperski, I., Večenaj, Ž., and Zardi, D.: Exchange Processes in the Atmospheric Boundary Layer Over Mountainous Terrain, Atmosphere, 9, 102, https://doi.org/10.3390/ATMOS9030102, 2018.

Shi, Z., Vu, T., Kotthaus, S., Harrison, R. M., Grimmond, S., Yue, S., Zhu, T., Lee, J., Han, Y., Demuzere, M., Dunmore, R. E., Ren, L., Liu,
2130 D., Wang, Y., Wild, O., Allan, J., Acton, W. J., Barlow, J., Barratt, B., Beddows, D., Bloss, W. J., Calzolai, G., Carruthers, D., Carslaw, D. C., Chan, Q., Chatzidiakou, L., Chen, Y., Crilley, L., Coe, H., Dai, T., Doherty, R., Duan, F., Fu, P., Ge, B., Ge, M., Guan, D., Hamilton, J. F., He, K., Heal, M., Heard, D., Hewitt, C. N., Hollaway, M., Hu, M., Ji, D., Jiang, X., Jones, R., Kalberer, M., Kelly, F. J., Kramer, L., Langford, B., Lin, C., Lewis, A. C., Li, J., Li, W., Liu, H., Liu, J., Loh, M., Lu, K., Lucarelli, F., Mann, G., McFiggans, G., Miller, M. R., Mills, G., Monk, P., Nemitz, E., O'Connor, E., Ouyang, B., Palmer, P. I., Percival, C., Popoola, O., Reeves, C., Rickard, A. R.,
2135 Shao, L., Shi, G., Spracklen, D., Stevenson, D., Sun, Y., Sun, Z., Tao, S., Tong, S., Wang, Q., Wang, W., Wang, X., Wang, X., Wang, Z., Wei, L., Whalley, L., Wu, X., Wu, Z., Xie, P., Yang, F., Zhang, Q., Zhang, Y., Zhang, Y., and Zheng, M.: Introduction to the special issue "In-depth study of air pollution sources and processes within Beijing and its surrounding region (APHH-Beijing)", Atmos. Chem. Phys., 19, 7519–7546, https://doi.org/10.5194/acp-19-7519-2019, 2019.

Shimizu, A., Nishizawa, T., Jin, Y., Kim, S.-W., Wang, Z., Batdorj, D., and Sugimoto, N.: Evolution of a lidar network for tropospheric
2140 aerosol detection in East Asia, oe, 56, 1 – 12, https://doi.org/10.1117/1.OE.56.3.031219, 2016.

Shrestha, B., Brotzge, J., Wang, J., Bain, N., Thorncroft, C., Joseph, E., Freedman, J., and Perez, S.: Overview and Applications of the New York State Mesonet Profiler Network, J. Appl. Meteor. Climatol., 60, 1591–1611, 2021.

Sicard, M., Pérez, C., Rocadenbosch, F., Baldasano, J., and García-Vizcaino, D.: Mixed-layer depth determination in the Barcelona coastal area from regular lidar measurements: methods, results and limitations, Boundary-Layer Meteorol., 119, 135–157,
2145 https://doi.org/10.1007/s10546-005-9005-9, 2006.

Simeonov, V., Larcheveque, G., Quaglia, P., Van Den Bergh, H., and Calpini, B.: Influence of the photomultiplier tube spatial uniformity on lidar signals, Appl. Opt., 38, 5186–5190, https://doi.org/10.1364/AO.38.005186, 1999.

Sinclair, V. A., Ritvanen, J., Urbancic, G., Statnaia, I., Batrak, Y., Moisseev, D., and Kurppa, M.: Boundary-layer height and surface stability at Hyytiala, Finland, in ERA5 and observations, Atmos. Meas. Tech., 15, 3075–3103, https://doi.org/10.5194/AMT-15-3075-2022, 2022.

2150 Singal, S. P.: Acoustic Remote Sensing Applications, Springer Berlin Heidelberg, 1997.

Singh, N., Solanki, R., Ojha, N., Janssen, R. H. H., and Pozzer, A.: Boundary layer evolution over the central Himalayas from radio wind profiler and model simulations, Atmos. Chem. Phys., pp. 10 559–10 572, https://doi.org/10.5194/acp-16-10559-2016, 2016.

Smalikho, I. N. and Banakh, V. A.: Measurements of wind turbulence parameters by a conically scanning coherent Doppler lidar in the atmospheric boundary layer, Atmos. Meas. Tech., 10, 4191–4208, https://doi.org/10.5194/amt-10-4191-2017, 2017.

Smith, E. N., Greene, B. R., Bell, T. M., Blumberg, W. G., Wakefield, R., Reif, D., Niu, Q., Wang, Q., and Turner, D. D.: Evaluation and Applications of Multi-Instrument Boundary-Layer Thermodynamic Retrievals, Boundary-Layer Meteorol., 181, 95–123, https://doi.org/10.1007/S10546-021-00640-2, 2021.

Solheim, F., Godwin, J. R., Westwater, E. R., Han, Y., Keihm, S. J., Marsh, K., and Ware, R.: Radiometric profiling of temperature, water vapor and cloud liquid water using various inversion methods, Radio Sci. 33, 393–404, https://doi.org/10.1029/97RS03656, 1998.

Spirig, C., Guenther, A., Greenberg, J. P., Calanca, P., and Tarvainen, V.: Tethered balloon measurements of biogenic volatile organic compounds at a Boreal forest site, Atmos. Chem. Phys., 4, 215–229, https://doi.org/10.5194/acp-4-215-2004, 2004.

Stachlewska, I. S., Piądłowski, M., Migacz, S., Szkop, A., Zielińska, A. J., and Swaczyna, P. L.: Ceilometer observations of the boundary layer over Warsaw, Poland, ACTA Geophys. 60, 1386–1412, https://doi.org/10.2478/s11600-012-0054-4, 2012.

Steeneveld, G. J., van de Wiel, B. J., and Holtslag, A. A.: Diagnostic equations for the stable boundary layer height: Evaluation and dimensional analysis, J. Appl. Meteor. Climatol., 46, 212–225, https://doi.org/10.1175/JAM2454.1, 2007.

Steyn, D. G., Baldi, M., and Hoff, R. M.: The Detection of Mixed Layer Depth and Entrainment Zone Thickness from Lidar Backscatter Profiles, J. Atmos. Oceanic Technol., 16, 953–959, https://doi.org/10.1175/1520-0426(1999)016<0953:TDOMLD>2.0.CO;2, 1999.

Stirnberg, R., Cermak, J., Kotthaus, S., Haeffelin, M., Andersen, H., Fuchs, J., Kim, M., Petit, J. E., and Favez, O.: Meteorology-driven variability of air pollution (PM1) revealed with explainable machine learning, Atmos. Chem. Phys., 21, 3919–3948, https://doi.org/10.5194/acp-21-3919-2021, 2021.

Stohl, A., Forster, C., Frank, A., Seibert, P., and Wotawa, G.: Technical note: The Lagrangian particle dispersion model FLEXPART version 6.2, Atmos. Chem. Phys., 5, 2461–2474, https://doi.org/10.5194/ACP-5-2461-2005, 2005.

Straume, A., Rennie, M., Isaksen, L., de Kloe, J., Marseille, G.-J., Stoffelen, A., Flament, T., Stieglitz, H., Dabas, A., Huber, D., Reitebuch, O., Lemmerz, C., Lux, O., Marksteiner, U., Weiler, F., Witschas, B., Meringer, M., Schmidt, K., Nikolaus, I., Geiss, A., Flamant, P., Kanitz, T., Wernham, D., von Bismarck, J., Bley, S., Fehr, T., Floberghagen, R., and Parinello, T.: ESA's Space-Based Doppler Wind Lidar Mission Aeolus – First Wind and Aerosol Product Assessment Results, EPJ Web of Conf., 237, 01 007, https://doi.org/10.1051/EPJCONF/202023701007, 2020.

Stull, R.: An Introduction to Boundary Layer Meteorology, Atmospheric and Oceanographic Sciences Library, Springer Netherlands, 1988.

Su, T., Li, Z., Li, C., Li, J., Han, W., Shen, C., Tan, W., Wei, J., and Guo, J.: The significant impact of aerosol vertical structure on lower atmosphere stability and its critical role in aerosol-planetary boundary layer (PBL) interactions, Atmos. Chem. Phys., 20, 3713–3724, https://doi.org/10.5194/ACP-20-3713-2020, 2020.

Sujatha, P., Mahalakshmi, D. V., Ramiz, A., Rao, P. V. N., and Naidu, C. V.: Ventilation coefficient and boundary layer height impact on urban air quality, Cog. Environ. Sci. 2, https://doi.org/10.1080/23311843.2015.1125284, 2016.

Sørensen, J., Rasmussen, A., and Svensmark, H.: Forecast of atmospheric boundary-layer height utilised for ETEX real-time dispersion modelling, Phys. Chem. Earth, 21, 435–439, https://doi.org/10.1016/S0079-1946(97)81138-X, ocean and Atmosphere, 1996.

Tang, G., Zhang, J., Zhu, X., Song, T., Münkel, C., Hu, B., Schäfer, K., Liu, Z., Zhang, J., Wang, L., Xin, J., Suppan, P., and Wang, Y.: Mixing layer height and its implications for air pollution over Beijing, China, Atmos. Chem. Phys., 16, 2459–2475, https://doi.org/10.5194/acp-16-2459-2016, 2016.

Tangborn, A., Demoz, B., Carroll, B. J., Santanello, J., and Anderson, J. L.: Assimilation of lidar planetary boundary layer height observations, Atmos. Meas. Tech., 14, 1099–1110, https://doi.org/10.5194/amt-14-1099-2021, 2021.

Tennekes, H.: A Model for the Dynamics of the Inversion Above a Convective Boundary Layer, J. Atmos. Sci., 30, 558–567, https://doi.org/10.1175/1520-0469(1973)030<0558:AMFTDO>2.0.CO;2, 1973.

Teschke, G. and Lehmann, V.: Mean wind vector estimation using the velocity–azimuth display (VAD) method: an explicit algebraic solution, Atmos. Meas. Tech., 10, 3265–3271, https://doi.org/10.5194/amt-10-3265-2017, 2017.

Theeuwes, N. E., Barlow, J. F., Teuling, A. J., Grimmond, C. S. B., and Kotthaus, S.: Persistent cloud cover over mega-cities linked to surface heat release, npj Clim. Atmos. Sci. 2, 1–15, https://doi.org/10.1038/s41612-019-0072-x, 2019.

Thobois, L., Freedman, J., Royer, P., Brotzge, J., and Joseph, E.: Validation and deployment of the first Lidar based weather observation network in New York State: The NYS MesoNet Project, EPJ Web Conf., 176, 09 010, https://doi.org/10.1051/epjconf/201817609010, 2018.

Thorne, P. W., Madonna, F., Schulz, J., Oakley, T., Ingleby, B., Rosoldi, M., Tramutola, E., Arola, A., Buschmann, M., Mikalsen, A. C., Davy, R., Voces, C., Kreher, K., De Maziere, M., and Pappalardo, G.: Making better sense of the mosaic of environmental measurement networks: a system-of-systems approach and quantitative assessment, Geosci. Instrum. Meth. 6, 453–472, https://doi.org/10.5194/gi-6-453-2017, 2017.

Toledo, D., Córdoba-Jabonero, C., and Gil-Ojeda, M.: Cluster Analysis: A New Approach Applied to Lidar Measurements for Atmospheric Boundary Layer Height Estimation, J. Atmos. Oceanic Technol., 31, 422–436, https://doi.org/10.1175/JTECH-D-12-00253.1, 2014.

Toledo, D., Córdoba-Jabonero, C., Adame, J. A., De La Morena, B., and Gil-Ojeda, M.: Estimation of the atmospheric boundary layer height during different atmospheric conditions: a comparison on reliability of several methods applied to lidar measurements, Int. J. Remote Sens. 38, 3203–3218, https://doi.org/10.1080/01431161.2017.1292068, 2017.

Tonttila, J., O'Connor, E. J., Hellsten, A., Hirsikko, A., O'Dowd, C., Järvinen, H., and Räisänen, P.: Turbulent structure and scaling of the inertial subrange in a stratocumulus-topped boundary layer observed by a Doppler lidar, Atmos. Chem. Phys., 15, 5873–5885, https://doi.org/10.5194/acp-15-5873-2015, 2015.

Träumner, K., Kottmeier, C., Corsmeier, U., and Wieser, A.: Convective Boundary-Layer Entrainment: Short Review and Progress using Doppler Lidar, Boundary-Layer Meteorol., 141, 369–391, https://doi.org/10.1007/s10546-011-9657-6, 2011.

Tsaknakis, G., Papayannis, A., Kokkalis, P., Amiridis, V., Kambezidis, H. D., Mamouri, R. E., Georgoussis, G., and Avdikos, G.: Inter-comparison of lidar and ceilometer retrievals for aerosol and Planetary Boundary Layer profiling over Athens, Greece, Atmos. Meas. Tech., 4, 1261–1273, https://doi.org/10.5194/amt-4-1261-2011, 2011.

Tucker, S. C., Senff, C. J., Weickmann, A. M., Brewer, W. A., Banta, R. M., Sandberg, S. P., Law, D. C., and Hardesty, R. M.: Doppler lidar estimation of mixing height using turbulence, shear, and aerosol profiles, J. Atmos. Oceanic Technol., 26, 673–688, https://doi.org/10.1175/2008JTECHA1157.1, 2009.

Tuononen, M., O'Connor, E. J., Sinclair, V. A., and Vakkari, V.: Low-level jets over Utö, Finland, based on Doppler lidar observations, J. Appl. Meteor. Climatol., 56, 2577–2594, https://doi.org/doi:10.1175/JAMC-D-16-0411.1, 2017.

Turner, D. and Löhnert, U.: Information content and uncertainties in thermodynamic profiles and liquid cloud properties retrieved from the ground-based Atmospheric Emitted Radiance Interferometer (AERI), J. Appl. Meteor. Climatol., 53, 752–771, https://doi.org/10.1175/JAMC-D-13-0126.1, 2014.

Turner, D. D. and Blumberg, W. G.: Improvements to the AERIoe thermodynamic profile retrieval algorithm, IEEE J. Sel. Top. Appl. 12, 1339–1354, https://doi.org/10.1109/JSTARS.2018.2874968, 2018.

Turner, D. D. and Löhnert, U.: Ground-based temperature and humidity profiling: combining active and passive remote sensors, Atmos. Meas. Tech., 14, 3033–3048, https://doi.org/10.5194/amt-14-3033-2021, 2021.

Vajda, A., Tuomenvirta, H., Jokinen, P., Luomaranta, A., Makkonen, L., Tikanmäki, M., Groenemeijer, P., Saarikivi, P., Michaelides, S., Papadakis, M., Tymvios, F., and Athanasatos, S.: Probabilities of adverse weather affecting transport in Europe: Climatology and scenarios up to the 2050s, Clin. Epigenetics, https://doi.org/10.2/JQUERY.MIN.JS, 2011.

Vakkari, V., O'Connor, E. J., Nisantzi, A., Mamouri, R. E., and Hadjimitsis, D. G.: Low-level mixing height detection in coastal locations with a scanning Doppler lidar, Atmos. Meas. Tech., 8, 1875–1885, https://doi.org/10.5194/amt-8-1875-2015, 2015.

Vakkari, V., Manninen, A. J., O'Connor, E. J., Schween, J. H., van Zyl, P. G., and Marinou, E.: A novel post-processing algorithm for Halo Doppler lidars, Atmos. Meas. Tech., 12, 839–852, https://doi.org/10.5194/amt-12-839-2019, 2019.

Vivone, G., D'Amico, G., Summa, D., Lolli, S., Amodeo, A., Bortoli, D., and Pappalardo, G.: Atmospheric boundary layer height estimation from aerosol lidar: A new approach based on morphological image processing techniques, Atmos. Chem. Phys., 21, 4249–4265, https://doi.org/10.5194/ACP-21-4249-2021, 2021.

Vogelezang, D. H. P. and Holtslag, A. A. M.: Evaluation and model impacts of alternative boundary-layer height formulations, Boundary-Layer Meteorol., 81, 245–269, https://doi.org/10.1007/BF02430331, 1996.

von Engeln, A. and Teixeira, J.: A planetary boundary layer height climatology derived from ECMWF reanalysis data, J. Climate, 26, 6575–6590, https://doi.org/10.1175/JCLI-D-12-00385.1, 2013.

von Engeln, A., Teixeira, J., Wickert, J., and Buehler, S. A.: Using CHAMP radio occultation data to determine the top altitude of the Planetary Boundary Layer, Geophys. Res. Lett., 32, https://doi.org/10.1029/2004GL022168, 2005.

Wærsted, E. G., Haeffelin, M., Dupont, J. C., Delanoë, J., and Dubuisson, P.: Radiation in fog: Quantification of the impact on fog liquid water based on ground-based remote sensing, Atmos. Chem. Phys., 17, 10 811–10 835, https://doi.org/10.5194/ACP-17-10811-2017, 2017.

Wagner, T. J., Feltz, W. F., and Ackerman, S. A.: The temporal evolution of convective indices in storm-producing environments, Wea. Forecasting, 23, 786–794, https://doi.org/10.1175/2008WAF2007046.1, 2008.

Wagner, T. J., Klein, P. M., and Turner, D. D.: A new generation of ground-based mobile platforms for active and passive profiling of the boundary layer, Bull. Amer. Meteor. Soc., 100, 137–153, https://doi.org/10.1175/BAMS-D-17-0165.1, 2019.

Wang, D., Stachlewska, I. S., Song, X., Heese, B., and Nemuc, A.: Variability of the Boundary Layer Over an Urban Continental Site Based on 10 Years of Active Remote Sensing Observations in Warsaw, Remote Sens. 12, 340, https://doi.org/10.3390/rs12020340, 2020.

Wang, X. Y. and Wang, K. C.: Estimation of atmospheric mixing layer height from radiosonde data, Atmos. Meas. Tech., 7, 1701–1709, https://doi.org/10.5194/amt-7-1701-2014, 2014.

Wang, Z., Cao, X., Zhang, L., Notholt, J., Zhou, B., Liu, R., and Zhang, B.: Lidar measurement of planetary boundary layer height and comparison with microwave profiling radiometer observation, Atmos. Meas. Tech., 5, 1965, https://doi.org/10.5194/amt-5-1965-2012, 2012.

Weckwerth, T. M., Weber, K. J., Turner, D. D., and Spuler, S. M.: Validation of a water vapor micropulse differential absorption lidar (DIAL), J. Atmos. Oceanic Technol., 33, 2353–2372, https://doi.org/10.1175/JTECH-D-16-0119.1, 2016.

Weitkamp, C.: LiDAR: introduction, in: Laser remote sensing, pp. 19–54, CRC Press, 2005.

Welton, E. J., Stewart, S. A., Lewis, J. R., Belcher, L. R., Campbell, J. R., and Lolli, S.: Status of the NASA Micro Pulse Lidar Network (MPLNET): overview of the network and future plans, new version 3 data products, and the polarized MPL, EPJ Web of Conf., 176, 09 003, https://doi.org/10.1051/EPJCONF/201817609003, 2018.

Westwater, E. R., Crewell, S., and Mätzler, C.: A review of surface-based microwave and millimeter-wave radiometric remote sensing of the troposphere, URSI Radio Sci. Bull. 2004, 59–80, https://doi.org/10.23919/URSIRSB.2004.7909438, 2004.

White, A.: Mixing depth detection using 915-MHz radar reflectivity data, in: Eighth Symposium on Observations and Instrumentation. 8th Symposium on Meteorological Observations and Instrumentation, Anaheim, CA. American Meteorological Society, Boston MA, pp. 248–250, 1993.

Wiegner, M. and Geiß, A.: Aerosol profiling with the Jenoptik ceilometer CHM15kx, Atmos. Meas. Tech., 5, 1953–1964, https://doi.org/10.5194/amt-5-1953-2012, 2012.

Wiegner, M., Emeis, S., Freudenthaler, V., Heese, B., Junkermann, W., Münkel, C., Schäfer, K., Seefeldner, M., and Vogt, S.: Mixing layer height over Munich, Germany: Variability and comparisons of different methodologies, J. Geophys. Res. Atmos., 111, https://doi.org/10.1029/2005JD006593, 2006.

Wilczak, J. M., Cancillo, M. L., and King, C. W.: A wind profiler climatology of boundary layer structure above the boreal forest, J. Geophys. Res. Atmos., 102, 29 083–29 100, https://doi.org/10.1029/97JD02315, 1997.

Wildmann, N., Bodini, N., Lundquist, J. K., Bariteau, L., and Wagner, J.: Estimation of turbulence dissipation rate from Doppler wind lidars and in situ instrumentation for the Perdigão 2017 campaign, Atmos. Meas. Tech., 12, 6401–6423, https://doi.org/10.5194/amt-12-6401-2019, 2019.

WMO: GCOS, 144. Guide to the GCOS Surface Network (GSN) and GCOS Upper-Air Network (GUAN) World Meteorological Organization (WMO), Tech. Rep. GCOS–144, WMO/TD 1558, WMO/TD, https://library.wmo.int/doc_num.php?explnum_id=3855, 2010.

WMO: The GCOS Reference Upper-Air Network (GRUAN): Guide, http://library.wmo.int/pmb_ged/gcos_171.pdf, 2013.

WMO: Workshop on the Review of the GCOS Surface Network (GSN), GCOS Upper-Air Network (GUAN) and related atmospheric networks, https://library.wmo.int/opac/doc_num.php?explnum_id=4013, 2014.

WMO: WMO Global Observing System Upper-air observations, http://www.wmo.int/pages/prog/www/OSY/Gos-components.html#upper, 2017.

Wood, R.: Stratocumulus clouds, Mon. Wea. Rev., 140, 2373–2423, https://doi.org/10.1175/MWR-D-11-00121.1, 2012.

Wulfmeyer, V., Pal, S., Turner, D. D., and Wagner, E.: Can Water Vapour Raman Lidar Resolve Profiles of Turbulent Variables in the Convective Boundary Layer?, Boundary-Layer Meteorol., 136, 253–284, https://doi.org/10.1007/s10546-010-9494-z, 2010.

Wulfmeyer, V., Hardesty, R. M., Turner, D. D., Behrendt, A., Cadeddu, M. P., Di Girolamo, P., Schlüssel, P., Van Baelen, J., and Zus, F.: A review of the remote sensing of lower tropospheric thermodynamic profiles and its indispensable role for the understanding and the simulation of water and energy cycles, Rev. Geophys. 53, 819–895, https://doi.org/10.1002/2014RG000476, 2015.

Xie, F., Wu, D. L., Ao, C. O., Mannucci, A. J., and Kursinski, E. R.: Advances and limitations of atmospheric boundary layer observations with GPS occultation over southeast Pacific Ocean, Atmos. Chem. Phys., 12, 903–918, https://doi.org/10.5194/acp-12-903-2012, 2012.

Yang, S., Petersen, G. N., von Löwis, S., Preißler, J., and Finger, D. C.: Determination of eddy dissipation rate by Doppler lidar in Reykjavik, Iceland, Meteor. Appl., 27, e1951, https://doi.org/10.1002/met.1951, 2020.

Yang, T., Wang, Z., Zhang, W., Gbaguidi, A., Sugimoto, N., Wang, X., Matsui, I., and Sun, Y.: Technical note: Boundary layer height determination from lidar for improving air pollution episode modeling: development of new algorithm and evaluation, Atmos. Chem. Phys., 17, 6215–6225, https://doi.org/10.5194/acp-17-6215-2017, 2017.

Yim, S. H. L.: Development of a 3D Real-Time Atmospheric Monitoring System (3DREAMS) Using Doppler LiDARs and Applications for Long-Term Analysis and Hot-and-Polluted Episodes, Remote Sens. 12, 1036, https://doi.org/10.3390/rs12061036, 2020.

Zhang, H., Zhang, X., Li, Q., Cai, X., Fan, S., Song, Y., Hu, F., Che, H., Quan, J., Kang, L., and Zhu, T.: Research Progress on Estimation of the Atmospheric Boundary Layer Height, 34, 482–498, https://doi.org/10.1007/S13351-020-9910-3, 2020.

Zhang, W., Guo, J., Miao, Y., Liu, H., Zhang, Y., Li, Z., and Zhai, P.: Planetary boundary layer height from CALIOP compared to radiosonde over China, Atmos. Chem. Phys., 16, 9951–9963, https://doi.org/10.5194/acp-16-9951-2016, 2016.

2305   Zhang, Y. and Klein, S. A.: Mechanisms affecting the transition from shallow to deep convection over land: Inferences from observations of the diurnal cycle collected at the ARM Southern Great Plains site, J. Atmos. Sci., 67, 2943–2959, https://doi.org/10.1175/2010JAS3366.1, 2010.

Zilitinkevich, S. and Baklanov, A.: Calculation of the height of the stable boundary layer in practical applications, Boundary-Layer Meteorol., 105, 389–409, 2002.